Detection Of Sepsis Biomarkers Using Microfluidics

Detection Of Sepsis Biomarkers Using Microfluidics

By Sreekant Damodara

A thesis submitted to the School of Graduate Studies

In partial fulfilment of the requirements for the degree of

Doctor of Philosophy in Mechanical Engineering

DOCTOR OF PHILOSOPHY (2020)

Graduate Program in

McMaster University, Hamilton, Ontario, Canada

TITLE: Detection of sepsis biomarkers using microfluidics

AUTHOR: Sreekant Damodara

SUPERVISOR: Dr. P. Ravi Selvaganapathy

PAGES: xxi, 192

Lay abstract

Sepsis is a major reason for hospitalization and cause of death in hospitals worldwide. Its treatment is highly time sensitive with each hour of delay in diagnosis causing a significant increase in chances of death. Due to the wide range of symptoms that can be caused by sepsis, its diagnosis uses a scoring method that relies on the expertise of the onsite doctors and nurses increasing their workload. A more objective system for detection requires the measurement of the quantities of different biomarkers in blood. Biomarkers are proteins present in plasma that change in quantity due to the body's reaction to sepsis. Several of these biomarkers have been identified and studied for their use in both diagnosing the presence of sepsis and in predicting the outcome with the current treatment plan. In this PhD study, we chose two of these biomarkers – circulating free DNA (cfDNA) and protein C and developed low-cost techniques for rapidly measuring their concentration in blood plasma. To do this, we made microfluidic devices with techniques that use low-cost materials such as plastic sheets and threads. The device for the measurement of protein C required separating it from many other proteins in plasma. We showed that a device fabricated from stacked plastic sheets and integrated with agarose gels could be used for the measurement of protein C in plasma with sufficient resolution to help with treating septic patients at a cost of less $5 per device. Similarly, we showed that a device that integrated threads with plastic sheets could be used for measuring the quantity of cfDNA in plasma in a portable format within 15 minutes. Overall, we developed tools for rapid measurement of two biomarkers of sepsis using low cost device that cost under $5 to run and could led to improving the quality of care for sepsis patients.

Abstract

Sepsis is a “life-threatening organ dysfunction caused by a dysregulated host response to infection” that has a widespread impact on human life around the world. It affects more than 1.5 million people, killing at least 250,000 each year in the US alone and affects 90,000 people annually, with estimated mortality rates of up to 30% in Canada. Our understanding of the different biochemical pathways that in the progression of sepsis has improved patient care for sepsis patients. One part of patient care is the use of biomarkers for patient prognosis that draws on the full range of relevant and available information to model the possible outcomes for an individual. Numerous biomarkers have been studied for patient prognosis that includes Procalcitonin (PCT), C-reactive protein (CRP), TNF-α, cfDNA, protein C and PAI 1. Using a panel of multiple biomarkers provided more accuracy in patient prognosis than using individual biomarkers and one such panel that was proposed used cfDNA, protein C, platelet count, creatinine, Glasgow Coma Scale [GCS] score, and lactate. Commercial, low cost POC techniques were available for the measurement of all biomarkers besides cfDNA and protein C. The objective of this doctoral thesis was chosen to develop low cost, microfluidic devices for the measurement of protein C and cfDNA using nonspecific fluorescence dyes that would enable the eventual integration of the systems and improve patient prognosis. The measurement of protein C in plasma required the separation of protein C from interfering proteins in plasma. This was done through the development of a two-stage separation process that included the development of tunable agarose isoelectric gates for separating proteins using their isoelectric point and the miniaturization of immobilized metal affinity chromatography and its extension to Barium for the selective binding of proteins using their chemical affinity. This was performed in a xurographically fabricated chip to reduce costs and enable the use of geometric focusing of the electric field to enable the operation of the device at a lower applied voltage. The challenges faced with cfDNA were different due to the

different characteristics of the material and less interference from plasma. The requirement was to measure the total cfDNA content with minimal cost in comparison to currently available techniques. This was achieved through the development of thread microfluidic devices that showed the use of thread for automated aliquoting of samples by controlling length and twists of the thread. Preconcentration and use of external apparatus was avoided by showing that thread could be used to amplify fluorescence response to a range that was sufficient for the measurement of cfDNA in sepsis patients. A portable fluorescence imaging setup was developed for this purpose and was used in demonstration for the measurement of cfDNA in plasma with sufficient resolution. In conclusion, we developed technologies for rapid and low-cost measurement of protein C and cfDNA using xurographic and thread-based microfluidics that may serve as valuable in improving patient prognosis.

Acknowledgements

Firstly, I would like to express my gratitude to my supervisor, Dr. Ravi Selvaganapathy for his guidance in helping me navigate through the intricacies of the projects, in exposing me to new ideas and providing me the freedom to pursue my own ideas. The time spent in the laboratory and in the meetings have been instrumental to helping me understand myself and my future directions.

I am deeply grateful to my committee members, Dr. Alison E. Fox-Robichaud and Dr. Raja Ghosh, for taking the time to provide me with guidance and insights over the course of the PhD. The discussions helped me have a more comprehensive and well-rounded perspective on projects.

I would also like to thank To Dr. Patricia C. Liaw, Dr. Dhruva J. Dwivedi, and Jaskirat Arora for aiding and helping me better understand the clinical side of the projects over the duration of the program. I would like to extend my sincere thanks to Dr. Yujie Zhu, for her help with brainstorming the use of threads and in aiding me through laying the groundwork for using threads in sensing

Finally, I would like to express my gratitude to my family for their unwavering love, support, and belief in me. To my friends and lab mates, for your friendship, understanding and patience which helped make this a more enjoyable and memorable journey, thank you.

Table of Contents

List of figures and tables

FIGURES

Chapter 1:

Chapter 2:

Chapter 3:

Chapter 4:

Chapter 5:

TABLES

CHAPTER 1

List of abbreviations

1-D/2-D/3-D – One/Two/Three Dimensional

A1PI - Alpha 1-proteinase inhibitor

aPC – activated protein C

AUC - area under the ROC curve

BSA- Bovine serum albumin

CE – Capillary Electrophoresis

cfDNA – cell free deoxyribonucleic acid

COC - cyclic olefin copolymer

CRP - C-reactive protein

dd/RT/q PCR - digital droplet/ real time/ quick polymerase chain reaction

dIEF/ cIEF – digital/ capillary isoelectric focusing

DIGE – Difference gel electrophoresis

DSLR - Digital single-lens reflex camera

GCS – Glasgow Coma Scale

GLA - γ-carboxyglutamic acid domain

hPC – human protein C

ICU – Intensive care unit

IEF – Isoelectric focusing

IET -Isoelectric trapping

IL – Interleukin

IMAC - immobilized metal affinity chromatography

LED – Light emitting diode

LOD – Limit of detection

PAGE - Polyacrylamide gel electrophoresis

PAI - Plasminogen activator inhibitor

PCT – Procalcitonin

PDMS - Polydimethylsiloxane

PET - Polyethylene Terephthalate

pI – Isoelectric point

PLA – Polylactic acid

POC – Point of Care

ROC - Receiver Operating Characteristic

SDS - Sodium dodecyl sulfate

SOFA - Sequential Organ Failure Assessment

TNFα - Tumor necrosis factor-alpha

UV - Ultraviolet

Tpi/ tpcm – Twists per inch/ per centimetre

μTAS – micro total analysis systems

Declaration of academic achievement

Sreekant Damodara contributed to formulating the concepts, the writing, experimental design, conducting of experiments, literature research, data analysis, interpretation of results, and figure generation for all chapters of the thesis.

Ponnambalam R. Selvaganapathy contributed to formulating the concepts, experimental design, interpretation of results, and revision of the manuscripts for all chapters of the thesis.

Alison E. Fox-Robichaud provided inputs on the formulating the concept, experimental protocols, and revision of the manuscripts for chapters 1,2,3, and 5 of the thesis.

Patricia C. Liaw provided protein C, inputs on biomarkers and protein behavior and provided inputs for the revision of the manuscripts for chapters 2,3, and 5 of the thesis.

Dhruva J. Dwivedi provided protein C samples and provided inputs on biomarkers and protein behavior for chapters 2 and 3 of the thesis

Yujie Zhu contributed to formulating the concept and experimental design for chapter 4 of the thesis

Jaskirat Arora provided cfDNA samples and provided inputs on experimentation and manuscript revisions for chapter 5 of the thesis

Chapter 1: Introduction

Chapter Preface

Sepsis is a medical emergency with widespread impacts on human life around the world. As a result of our growing understanding of the pathophysiology of sepsis and the numerous factors involved, we have been making major progress in reducing the mortality due it. A large part of our progress stems from understanding the different biochemical pathways that seem to be essential to the progression of sepsis and using this knowledge to better understand how to treat patients with sepsis. A logical progression of this progress is the development of techniques to measure the concentrations of these biomarkers and use that to quantify the efficacy of our treatment plans. Current laboratory scale techniques are expensive and require trained personnel to operate because of which, there is limited use of biomarker detection for constant monitoring of patient status. Microfluidic devices show immense potential in reducing the cost of diagnostic care improving the standard of care by enabling more frequent biomarker detection. Development of thread, paper and plastic devices reduces the cost of fabrication while improving the potential to scale up the manufacturing of devices. Additionally, the biomarkers needed span from genomic material to various cytokines and proteins. Currently, these biomarkers are measured using targeted measurement and detection techniques which are difficult to integrate.

In this chapter, An overview of the pathophysiology of sepsis, a few of the biomarkers that have been recognized for their role in the pathophysiology and their potential use in diagnosis or prognosis of patients was introduced. The detection methods for these biomarkers are explored with a particular emphasis on technologies that can be used for bedside, rapid care in a low-cost manner. Then, an overview of different microfluidic technologies that can be used for the fabrication of such devices are explored and their advantages and drawbacks are presented. In the chapters that follow, technologies developed for the detection of biomarkers – cell free DNA and protein C are presented

and shown to meet the necessary requirements for detection in plasma at a resolution needed for prognosis while using fluorescence imaging which can be eventually integrated into a single device.

1. Sepsis pathophysiology

Sepsis is “a life-threatening organ dysfunction caused by a dysregulated host response to infection” [1]. It is the 13th leading cause of death in Canada [2] and affects 90,000 people annually, with estimated mortality rates of up to 30% [3]. Based on data from the Institute for Clinical evaluative Sciences (ICES), the economic burden of sepsis in Canada is more than $1.5 billion annually [4]. As a result, sepsis has been widely studied and numerous theories have been proposed regrading the multiple factors that play a role and their relative importance. However, due to the complexity of sepsis and the wide variety of symptoms presented, the pathological process leading to the development of multiple organ dysfunction is still not completely understood.

Our current understanding of sepsis revolves the interplay between the inflammatory response to an infection and the coagulation cascade which is further exacerbated by other factors such as a cytokine storm and apoptotic cell death. The first response to an infection is the activation of innate immune cells such as macrophages, monocytes among others which result in the activation of intracellular signal transduction pathways which initiates the release of proinflammatory cytokines TNFα, IL-1, and IL-6 and inflammasomes such as IL-1β and IL-18. Cytokines are often produced in a cascade as the release of one cytokine stimulates its target cells to make additional cytokines. A potentially fatal immune response consisting of a positive feedback loop between cytokines and immune cells is termed as a cytokine storm [5]. While inflammation is useful to localize the effects of infection, an extreme inflammatory response causes vascular congestion, endothelial injury, and overstimulation of the coagulation system. One of the effects of the increase in proinflammatory cytokines is the upregulation of tissue factor production. Tissue factor causes a systemic activation of the coagulation

cascade which causes an increase in the production of thrombin and platelet activation ultimately leading to an increase in the formation of microthrombi and disseminated intravascular coagulation (DIC) which can cause tissue hypoxia and organ dysfunction [6].

The coagulation cascade in a healthy human exists in a state of balance between coagulation and fibrinolysis [7]. However, during sepsis, the excess release of tissue factor due to inflammatory cytokines in combination with release of other important procoagulants including plasminogen activator inhibitor, platelet activating factor, and von Willebrand's factor amplifies the procoagulant response. Simultaneously, there is a depression in the anticoagulant responses of protein C and thrombin. A schematic of the interaction between different components in the coagulation cascade is presented in Fig. 1. Protein C is converted to activated protein C by thrombomodulin which is activated by thrombin. Activated protein C in combination with activated protein S inhibits the procoagulant effects of factors Va and factor VIIIa. It also has an anti-inflammatory response by inhibiting the effects of TNFα, IL-1β, and IL-6. However, as sepsis has a large inflammatory response, these proteins are consumed, and the balance is broken resulting in a runaway coagulation cascade and production of large amounts of thrombin [8]. Thrombin converts soluble fibrinogen to insoluble fibrin which clumps with platelets to form clots. Excessive formation of these clots may result in them acting as emboli that block the microvasculature throughout the body. This is further exacerbated by the release of plasminogen activator inhibitor - 1 (procoagulant) that inhibits the release of tissue plasminogen activator that activates plasmin which is responsible for breaking down fibrin breaking down the fibrinolytic pathway and hence, swaying the balance between coagulation and fibrinolysis further towards runway coagulation [7].

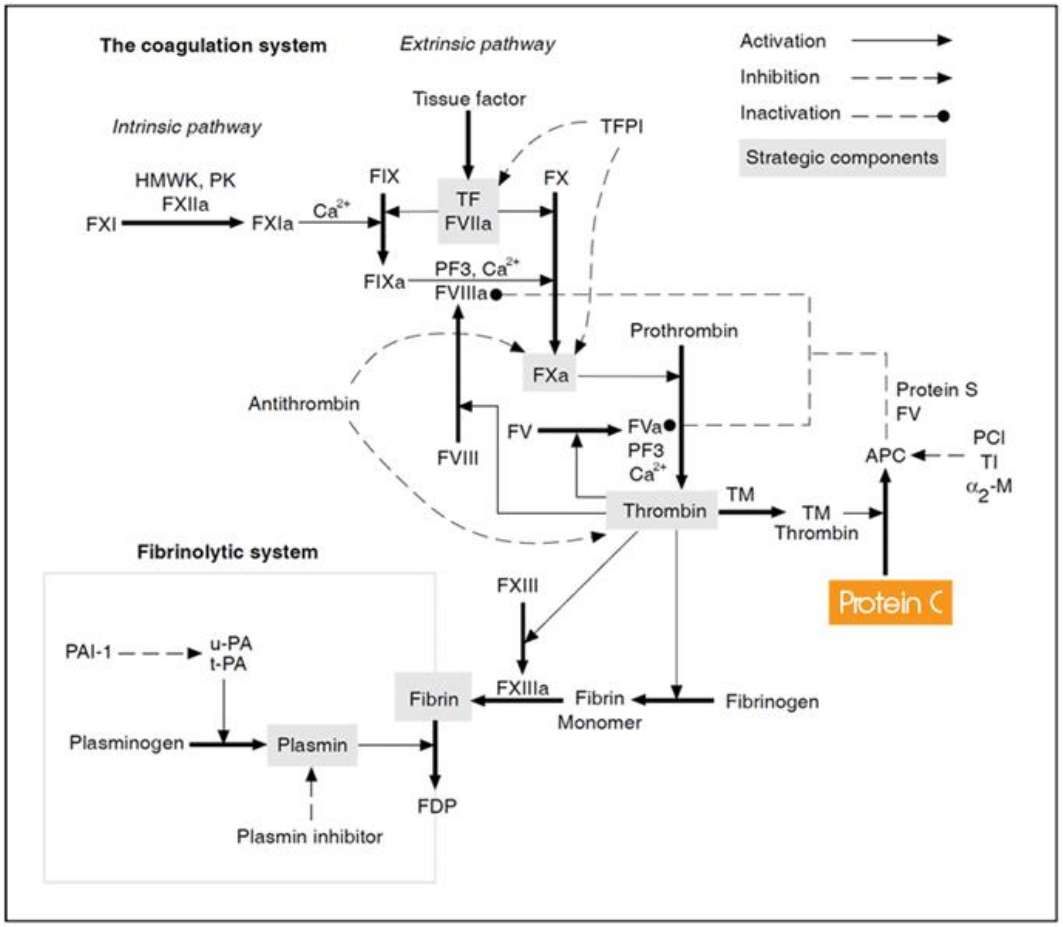

Figure 1 Schematic showing the major components and interaction of the coagulation cascade and fibrinolytic system [9]

In addition, any cell death during the progression of sepsis results in the release of molecules from dead or damaged host cells such as cell free DNA, ATP and mitochondrial DNA, which can bind to receptors on monocytes and macrophages increasing the inflammatory response further propagating the sepsis response [6]. In addition, neutrophils release extracellular traps known as NETs through another death mechanism (NETosis)[10]. NETosis releases extracellular chromatin wrapped around histones and numerous granular proteins and enzymes. Citrullination of these histones in the presence of peptidyl arginine deiminase-4 releases cfDNA into the circulation to engulf invading microbes resulting in an increase in plasma concentration of cfDNA. Other components such histones mediate

extensive cellular damage in endothelial cells aggravating the hemostatic imbalance and amplifying the inflammatory response by inducing cytokine production [11].

2. Sepsis Biomarkers

As a result, of the complex pathophysiology of sepsis and the resulting wide variety of symptoms presented, diagnosing sepsis is exceptionally challenging.

2.1 Current diagnostic and prognosis methodologies

The current system for identifying and assessing patients with sepsis was chosen by performing a multivariable regression analysis with 21 bedside and laboratory criteria using the electronic health records of 1.3 million encounters at 12 community and academic hospitals [1]. Their predictive ability was tested, and it was found that SOFA (Sequential Organ Failure Assessment) and Logistic Organ Dysfunction System were found to have the highest predictive power, of which SOFA is the scoring system in predominant use. SOFA grades the functioning of various organ systems on a scale of 1- 4 using a number of parameters. These parameters are partial pressure of oxygen (Respiration), Platelet count (Coagulation), Bilirubin levels (Liver function), Blood pressure, dopamine/ epinephrine/ norepinephrine dosage (Cardiovascular system), Glasgow coma scale (Nervous system), Creatinine and urine output (Renal system). The scaling of each of these parameters is shown in Table 1. A higher SOFA score is correlated with an increased probability of mortality. A SOFA score of greater than 2 was identified as organ dysfunction

Table 1 Sequential Organ Failure Assessment - SOFA (Adapted from [1] *)*

System	Score				
Parameter	0	1	2	3	4
Respiration					
Ratio of arterial oxygen partial pressure to fractional inspired oxygen in mm of Hg	≥ 400 (53.3 kPa)	< 400 (53.3 kPa)	< 300 (40 kPa)	< 200 (26.7 kPa) with support	< 100 (13.13 kPa) with support
Coagulation					
Platelet count, $x10^3/\mu L$	≥ 150	< 150	< 100	< 50	< 20
Liver					
Bilirubin, mg/dL	< 1.2	1.2 - 1.9	2.0 - 5.9	6.0 - 11.9	> 12.0
Cardiovascular					
Mean arterial pressure (MAP)	≥ 70mm of Hg	< 70mm of Hg	Need dosage of Dopamine < 5	Need dosage of Dopamine 5.1 - 15 or epinephrine ≤ 0.1 or norepinephrine ≤ 0.1	Need dosage of Dopamine > 15 or epinephrine > 0.1 or norepinephrine > 0.1
Central nervous system					
Glasgow Coma Scale	15	13 -14	10 - 12	6 - 9	< 6
Renal					
Creatinine, mg/dL	< 1.2	1.2 - 1.9	2.0 - 3.4	3.5 - 4.9	> 5

However, since parts of SOFA such as creatinine and bilirubin level require laboratory testing, and have a delayed response to organ dysfunction, a rapid test for screening possible sepsis patients was suggested. The suggested protocol was in the form of quickSOFA (qSOFA). It contained three clinical variables - Glasgow Coma Scale score of 13 or less (altered mentation), systolic blood pressure of 100 mmHg or less, and respiratory rate 22 /min or greater. It was reported that any 2 of 3 of these had a similar predictive validity to SOFA outside the ICU. The report suggested that exhibiting altered

mentation with one of the other two criteria be used as a screening tool and be followed up by the testing needed for a positive qSOFA. This is less robust than the criteria set by a SOFA of greater than 2, particularly in the ICU and was suggested only as an external screening tool.

In addition to detecting the host response to an infection, blood cultures are used to confirm the presence of an invasive infection. However, this takes 2 – 14 days and has a low yield. As a result, the host response is assumed to be due to an infection in the early stages of diagnosis [12].

To reduce the limitations of current clinical scoring methods and improve the insight into host response based on the differential impact of the individual components in the scoring system, experimental scoring methods have been suggested. One such scoring system uses six factors - cfDNA, protein C, platelet count, creatinine, Glasgow Coma Scale [GCS] score, and lactate. This was shown to have a stronger predictive power than SOFA [13]. The increase in predictive power is due to two reasons. One is the use of weights determined by observed data instead of equal weights like in SOFA. The other is the use of biomarkers identified to play a key role in our present understanding of sepsis. Numerous biomarkers have been identified that could play a role in diagnosis or prognosis for sepsis which are described in chapter.

2.2 Overview of biomarkers

A recent review describes 258 biomarkers that have been identified as biomarkers for sepsis. Of these 258, 26 biomarkers have been evaluated in studies with over 300 patients [14]. Due to the wide variation in symptoms for sepsis, biomarkers include proinflammatory biomarkers such as C-reactive proteins, endothelial proteins such as angiopoietins, cell surface receptors such as CD64 and cfDNA, cytokines such as TNF-α and immunomodulatory biomarkers such as lymphocyte count and neutrophil behaviour [15]. Some of the most investigated biomarkers among these are Lactate, Procalcitonin (PCT), C-reactive protein (CRP), TNF-α, CD64, IL – 6, PAI 1 [1,15–17]. Furthermore,

the use of a panel of biomarkers improved the accuracy of biomarkers for prognosis and diagnosis of sepsis for which additional biomarkers like protein C were found to be of interest.

Biomarkers and biomarker panels can be used either for diagnostics to identify the presence of a disease in a patient or for prognostics to identify the likely outcome of the disease. Diagnosis classifies patients into groups defined by disease and pathology. This provides clinicians the means to organise and interpret patient symptoms and test results which can then be used for decision making. This is a dichotomous result which does not fully account for disease severity. However, the underlying disease is a continuous distribution of probability for future outcomes, and this is better reflected in prognosis. Prognosis draws on the full range of relevant and available information to model the possible outcomes for an individual. As a result, it is currently used after initial diagnosis to provide effective treatment based in individual requirements [18]. Of the listed biomarkers, Lactate, CD64 and IL – 6 have been studied for their use, either by themselves or as a panel for diagnostics while Procalcitonin (PCT), C-reactive protein (CRP), TNF-α, cfDNA, protein C and PAI 1 have been found to useful for prognostics [14,15].

However, the use of biomarkers in hospitals for diagnosis or prognosis of patients has been limited due to the time needed to run assays for measuring their concentration, the instrumentation/running cost of each assay and the inability to combine the measurement of multiple biomarkers in a single format. The current standard for benchtop assays of biomarkers uses immunoassay kits that are widely available [-CRP 19,-Procalcitonin 20,21]. The most common immunoassay performed is a sandwich immunoassay. A sandwich immunoassay consists of a capture probe that is bonded to the surface using either adhesion or functionalization of the surface. The probe can be either an antibody specific to the biomarker or an aptamer designed to bind specifically to the biomarker. The sample is then flowed over the capture antibodies to allow binding of the biomarker to the capture probe. This is

followed by using a detection antibody/aptamer that binds to the antigen forming a sandwich. The detection antibody is bound to a detector depending on the method of detection used. This can be a fluorophore, a nanoparticle causing a color change or any of the other detection methods. These steps are interspersed by wash steps to remove excess reagent and steps to passivate the remaining surface of the device. This is done to reduce nonspecific binding with the other proteins in solution. Numerous techniques have been developed to further increase the signal obtained from the immunoassay. A simplified schematic of an immunoassay with the capture and detection probes is shown in Fig. 2. Step i shows the capture of the analyte using a capture antibody. Step ii shows the binding of the detection antibody to the analyte following which the fluorescent marker binds to the detection antibody in step 3.

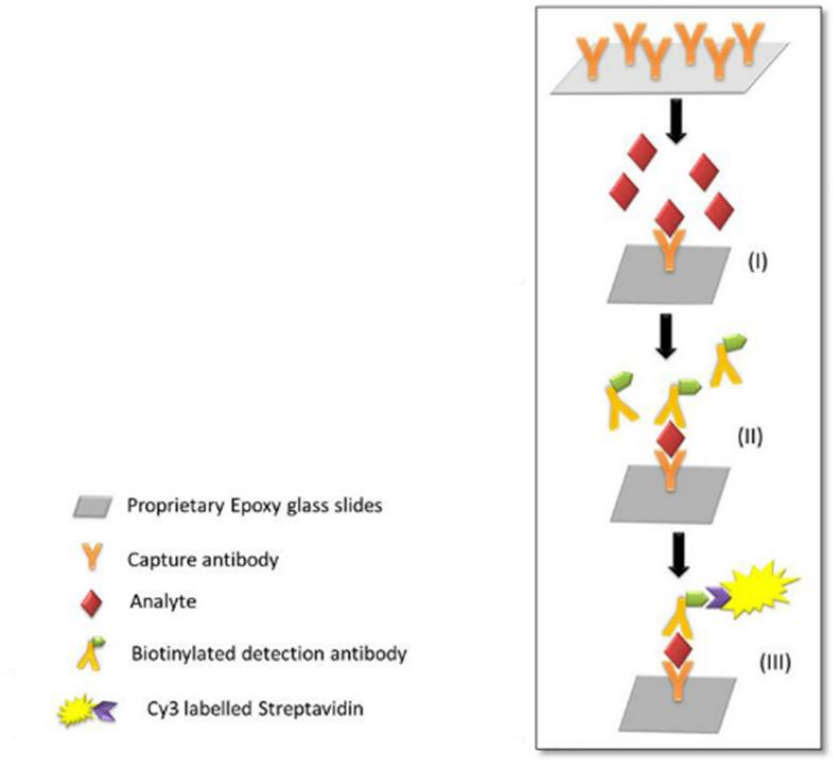

Figure 2 Schematic of a simplified sandwich immunoassay and detection using fluorescence. [22].

However, while laboratory scale processes are widely available, the commercially available kits are slow taking upwards of 4 hours to complete [23], require the use of expensive reagents and need trained personnel to perform each of the steps manually. This makes them ineffectual for use as bedside diagnostic techniques. There are also no integrated laboratory scale techniques available for measuring the concentrations of multiple biomarkers simultaneously. The measurement of multiple biomarkers has been shown improve the accuracy of prognosis and would be required for the successful development of a POC device for sepsis. Additionally, the POC device would need to be a low-cost and minimize the number and complexity of steps needed such that personnel who have received minimal training can operate the device. This is best achieved using microfluidics which can enable the integration of multiple steps and the simultaneous detection of multiple analytes in a low cost, easy to use format. The microfluidic devices that have been developed for the measurement of different biomarkers are described in section 2.3. The microfluidic methods available for the detection of Lactate, Procalcitonin, C-reactive protein and TNF-α and cfDNA are described in sections 2.3.1-2.3.5 respectively. The challenges in measurement of protein C are described in detail in section 2.3.6 as there were very few microfluidic devices targeted at protein C.

2.3 Microfluidic devices for detection of sepsis biomarkers

Microfluidics is the study and manipulation of fluids at a submillimeter length scale. The effects of scaling down offer compelling advantages in the development of diagnostic devices. The combined effects of reducing sample volume, lower cost of production and integration of multiple steps and biomarkers in a single chip streamlines complex assay protocols results in the reduction of cost and increases the usability of diagnostic tests. This has led to the development of a class of microfluidic devices called miniaturized (micro) total analysis systems (μTAS) [24] aimed at reducing the cost of diagnostic devices in resource poor regions and simplifying their usability to be used by untrained

personnel. μTAS have been developed for several bacterial and viral diseases with known biomarkers [25]. Microfluidic devices to improve the rate of detection of blood cultures for sepsis have been developed. However, the use of these POC methods vary based on the source of infection, with different methods available for bacterial, fungal and viral infections [12,26].

Different formats of capture and detection of biomarkers have been developed specifically to target each biomarker of sepsis that result from the host response to an infection as they have a wide range of properties and native concentrations. The physiological role, the range of measurement and devices developed are described. The efficacy of a biomarker in providing information for the diagnosis or prognosis of sepsis is described by using the Receiver Operating Characteristic (ROC) which is a graphical representation of the trade off between the false negative (sensitivity) and false positive rates (1 – specificity). The accuracy of a test is measured by the area under the ROC curve (AUC). A higher AUC represents a better biomarker. Additionally, the optimal sensitivity and specificity was mentioned where available.

2.3.1 Lactate

Lactate is produced in tissues when the body experiences inadequate perfusion of oxygen. It is formed from the anaerobic oxidation of pyruvate to produce ATP. It can be produced during heavy exercise, seizures and numerous other instances that can cause inadequate oxygen delivery, disproportionate oxygen demand or inadequate oxygen utilization. It can thus be used as a marker for strained cellular metabolism [27]. Sepsis patients with lactate levels of more than 4 mmol/L had an in-hospital mortality of 28.4%. One of the methods developed for the use of lactate as a biomarker involved the introduction of external lactase and studying the clearing time. An increase in concentration of blood lactate of more than 0.6 mmol/L 60 minutes after the start time of external lactate infusion was 53% sensitive and 90% specific with an odds ratio of 14.2 ($p=0.042$) for 28- day mortality [28].

Microfluidic detection of lactate is the simplest of the listed biomarkers as it has been measured for determining the status of acid-base homeostasis in the human body for a long time [27]. As a result, the protocol for measurement is well established and scales down well. This led to the development of commercial point of care testing equipment [29] which has been tested for practical use as a point of care device [30]. The device has a turnaround time of 13 seconds per experimental run and measures lactate concentration in the range of 0.3 – 20 mmol/L.

2.3.2 Procalcitonin (PCT)

Procalcitonin is a protein with a molecular weight of 13kDa which is a precursor to calcitonin which is essential to maintaining calcium homeostasis. Typically, procalcitonin is only produced in the thyroid but is produced by other tissues when an infection is present. This results in a large increase in procalcitonin within 4 hours and peaks in 12-48 hours. However, it is highly nonspecific and changes in concentration to any infection or inflammation. As a result, it has found to be of better use as a monitoring tool. PCT guided treatments have reported reduced duration of antibiotics, length of ICU stay, increase of antibiotic free days and lowered cost of antibiotics [31]. Serum concentration of PCT in healthy individuals is below 0.1 ng/mL [15] and increases to above 2 ng/mL in case of sepsis . PCT has a sensitivity of 77% and a specificity of 79% in diagnosing sepsis with a cutoff at 2 ng/mL. It has an AUC of 0.878 [32].

Procalcitonin has been measured on a microfluidic device using immunofluorescence with an evanescent wave to improve sensitivity [33]. Murine monoclonal antibodies specific to procalcitonin were prepared used for a sandwich immunoassay. The fluorescence emitted was captured using a photomultiplier, and the slope of the liner range of the fluorescence signal in V/sec was proportional to the analyte concentration and used as the measurement. Using this, a limit of detection of 0.02 ng/mL and a range of 0-9 ng/mL in whole blood was obtained with an experimental time of 9 minutes.

Additionally, numerous devices have been developed using variations of immunoassay developed by BRAHMS GmbH with resolutions of 0.02 ng/mL to 0.5 ng/mL [33–35]. An electrochemical magneto-immunoassay showed detection of 0.02 ng/mL of procalcitonin with 25 µL of sample in 15 minutes [36]. However, the use of specifically produced antibodies makes these assays expensive for regular use.

2.3.3 C-reactive protein (CRP)

C-reactive protein is synthesised and released by the liver and is a part of a nonspecific acute-phase response of the body to inflammation, infection and tissue damage. It binds to polysaccharides and peptido-polysaccharides in bacteria, fungi and parasites in the presence of calcium and plays an active role in their clearance. As a result, the CRP levels which are present in a range of 0.3-1.7 µg/mL in healthy individuals to over 10 µg/mL in patients with inflammation and infection [37]. The cut-off for sepsis has been recommended to be over 50 µg/mL with a sensitivity of 98.5% and a specificity of 75% [38]. The AUC for CRP is 0.811 [32].

ELISA has also been used in the detection of C-reactive protein using antibodies produced in a mouse paired with gold nanoparticles [39]. The device was a paper microfluidic assay in vertical flow assay format and sequential steps were arranged by using pressed paper to control flow rates. The color change due to capturing of the gold nanoparticles in the test region was used to measure concentration and resultant device had a limit of detection of 0.005 µg/mL in buffered samples with a range of up to 5 µg/mL. An experimental time of 15 minutes was used between sample input and detection. However, mouse produced antibodies are expensive and are limited in supply, an alternative was the use of aptamers designed to be specific to CRP [40]. Using aptamers paired magnetic beads microfluidic devices have been designed using PDMS with external pumping for sensing with 5µL of sample with a limit of detection of 0.0125 µg/mL within 30 minutes. A simpler version of the

device without a micromixer was shown to have a similar LOD but operating with 62 µL of sample [41]. These devices used a luminometer to measure the intensity of emitted light from tagged CRP that bound to the aptamers. Label free detection was shown using cyclic voltammetry and electrochemical impedance spectroscopy with antibodies from a goat [42]. The device used a nanoelectrode array with anti-CRP antibodies immobilized on the surface. The resulting device had a limit of detection of 11 ng/mL with a range of up to 5 µg/mL with an experimental time of a few minutes. However, the use of CRP specific antibodies and aptamers increases the operating costs of the devices which worsens their applicability as a bedside test for sepsis.

2.3.4 Tumor necrosis factor-alpha (TNF-α)

TNF-α is a cytokine that acts as a mediator of the inflammatory response. It is released by macrophages within 30 minutes of infection causing an increase in concentration during sepsis. The plasma concentration in healthy individuals is usually below 10 pg/mL [43]. This rises to between 20-100 pg/mL in sepsis [44]. The AUC of TNF-α is 0.835 [32].

TNF-α detection in plasma was shown performing an immunoassay in a cyclic olefin copolymer (COP) microdevice [45]. An inkjet printer was used for deposition of discrete drops of mouse antibodies specific to TNF-α and a pipette was used for deposition of other reagents into a surrounding microchannel. A sandwich assay carried out using this platform with plasma showed a LOD of 0.46 pg/mL and a range of 0-32 pg/mL in 5 hours. A second platform for using ELISA to detect TNF-α was fabricated in PDMS and consisted of two parallel networks linked by a controllable valve [44]. The valves were used to control the release of functionalised beads for detection which in combination with multiple wash steps was used to reduce nonspecific adsorption to PDMS and improve sensitivity. The resultant device was shown to detect TNF-α in serum at concentrations of 25-500 pg/mL in under 30 minutes. Another technique for detection used surface immunofluorescence [46]. It consisted of a

silicon chip etched to form capillary channels through which 0.3μL of sample and detection antibodies were pumped using capillary forces and active evaporation using a Peltier element. A PDMS block coated with capture antibodies from a goat was manually placed in conformal contact with the capillaries to form a grid that enables rapid detection. The resultant device was shown to have a sensitivity ranging from 10 to 50 pg/mL in 12 minutes depending on the flow rate of the analyte in the device. A solid phase assay for measurement of TNF-α was demonstrated using a magnetic bead-based proximity ligation assay in a COP chip [43]. The technique consists of binding, ligation, and amplification by qPCR of paired oligonucleotides/goat antibodies to detect specific proteins. This resulted in a portable device that could measure TNF-α in a range of 12.5-100 pg/mL in plasma.

2.3.5 cell free DNA (cfDNA)

cfDNA molecules are transient fragments of DNA released from neutrophils, eosinophils and macrophages as a result of either apoptosis or necrosis [31,47]. They are present in minimal levels in healthy humans as they are regularly cleared by phagocytosis. However, in septic patients, there is rapid cellular death and increased necrosis. Furthermore, Neutrophils release extracellular traps (NETs) via a death mechanism, known as NETosis. This releases the extracellular chromatin that is wrapped around histones and numerous granular proteins and enzymes. The Citrullination of these histones by peptidyl arginine deiminase-4 relaxes and releases cfDNA into the circulation to engulf invading microbes. As a result, the cfDNA concentration was found to be a prognostic indicator for overall morbidity and mortality, as cfDNA content in surviving patients (1.16 ± 0.13 μg/mL) was similar to that of healthy volunteers (0.93 ± 0.76 μg/mL) ($p = 0.426$), while that of non-survivors (4.65 ± 0.48 μg/mL) was notably higher [48]. cfDNA with a cut-off of 2.35 ng/μL has a sensitivity of 88% and a specificity of 94% for predicting ICU mortality [47] and an AUC of 0.84 for hospital mortality [49] .

Isolation of cfDNA has been performed using many different techniques. Solid phase isolation was performed leveraging the nonspecific absorption of DNA to silica. Silica channels, silica immobilized in sol-gels and poly- (ethylene glycol) have all been demonstrated before [50,51]. However, these methods are limited by uneven bead distribution and use of solutions that inhibit amplification. Other methods include the use of a functionalized surface to bind to cfDNA. 3-aminopropyltrietboxysilane (APTES) and 3-[2-(2-aminoethylamino)-ethylamino]-propyluimethoxysilane (AEEA) have both been found to have been used to bind to cfDNA [52]. However, the recovery efficiency in blood is 27-40%, and it attracts other negative species in solution. Dimethyl dithiobispropionimidate (DTBP) is another amine binding nonchaotropic reagent that has been used to bind to cfDNA with a greater recovery but has similar limitations [53]. Solid phase separation of cfDNA is limited by the need to functionalize the surface or use complicated fabrication methods to trap silica/chaotropic agents in the microfluidic device and can only be used for fixed quantities before being saturated [54]. Liquid phase separations simplify the fabrication of the device and use an electric field or chemical agents to trap cfDNA. Furthermore, they can be designed for continuous separation. This was demonstrated by designing a multiphase channel with a mixture of three organic components: phenol, chloroform, and isoamyl alcohol acting to separate DNA from a protein-DNA mixture with a yield of more than 92% [54]. However, the extension of this technique to cfDNA is yet to be demonstrated. Electrophoretic concentration of cfDNA has been demonstrated using agarose gel to alter the mobility of DNA in an electric field and increase the concentration prior to measurement using fluorescence [48]. However, these methods of isolation and measurement still require complex and expensive external hardware for controlling fluid flow, manipulating the electric field and measurement.

2.3.6 Protein C

Protein C is a vitamin K dependant protein zymogen present in plasma that plays an active role in the coagulation cascade and inflammatory response. As described in the earlier section on sepsis pathology, Protein C breaks down in the presence of thrombin and thrombomodulin to form activated protein C which inhibits the procoagulant effects of factors Va and factor VIIIa impeding the coagulation cascade. In addition, it also has an anti-inflammatory response by inhibiting the effects of TNFα, IL-1β, and IL-6. However, as there is only an initial concentration of protein C of 3.9-5.9 µg/mL in plasma [7], it is rapidly consumed during sepsis resulting in a decrease in concentration. This decrease was found to be meaningful in predicting the outcome of the patient. It was reported that protein C in plasma reduced from 0.61-1.33 U/mL in healthy individuals to 0.41±0.22 U/mL in non survivors of sepsis and 0.53±0.24 U/ml in survivors. Additionally, non survivors had a sustained decrease in protein C values after 7 days to below 0.37 U/mL (1.8 µg/mL assuming an average protein C concentration of 4.5 µg/mL) while the protein C in survivors increased to 0.7±0.22 U/mL [55]. Protein C has an AUC of 0.64 on its own but increases to 0.92 when combined with cfDNA.

Protein C detection in microfluidic devices has been demonstrated only using a two-step sandwich immunoassay with antibodies sourced from a mouse[56]. This results in a prohibitively high cost for using protein C as a constantly monitored biomarker. The high cost and complexity of separation is potentially due to the similarity in properties between protein C and other proteins in the coagulation cascade. Other than the use of an immunoassay, the primary method for separating protein C leverages the presence of a γ-carboxyglutamic acid domain (GLA) domain in its composition and the resulting affinity to barium. Dropwise addition of 1M barium chloride to a solution with 0.2M sodium citrate and the sample results in the formation of precipitate. Centrifugation of this precipitate formed a pellet which can be resuspended in a solution with 0.2M ethylenediaminetetraacetic acid to extract the

bound proteins, all of which contain a GLA domain [57]. There a limited number of GLA domain containing proteins in plasma. These are coagulation factors II (prothrombin), VII, IX, X, proteins C, S and Z in plasma [57–59]. These were then separated from protein C using a combination of ammonium sulfate fractionation, DEAE-Sephadex chromatography, dextran sulfate agarose chromatography, preparative polyacrylamide gel electrophoresis [60] or other similar sample preparation processes that requires multiple steps [61,62]. An alternative separation method that was more recently described was the use of immobilized metal affinity chromatography (IMAC) that would leverage the presence of a large number of histidine groups in protein C and was used to show its separation from Cohn fraction Iva [63,64] and transgenic milk [65]. However, IMAC was only used as one of a series of steps for isolation of protein C.

Current benchtop measurement of protein C primarily uses immunoassays [61,66] or functional assays following the isolation of protein C. This was done by isolating protein C using one of the methods described above following which the protein C was activated to form aPC. The increase in clotting time due to the addition of aPC was used to quantify it [66,67]. Alternatively, a chromogenic assay was performed to measure the color change produced when added to a selective chromogenic substrate [68].

As a result, microfluidic tools for rapid and low-cost measurement of protein C are unavailable despite the possibly high utility of protein C in improving the quality of care for sepsis patients.

2.3.7 Multi protein panels

In addition to detection of individual biomarkers, devices have been developed for parallel detection of a panel of biomarkers. Panels have been shown to improve the accuracy of prognosis and provide a more comprehensive overview of the state of the patients. One such device was fabricated in epoxy resin with capture antibodies printed on the surface using a contact spotter [22]. Nonspecific binding

was reduced using BSA to block the remaining surface. An optimized format for a binding inhibition assay for CRP and miniaturized surface immunoassay was used with magnetic nanoparticles to improve sensitivity. The resulting device was incubated with the protein samples for 2.5 hours to obtain a LOD of 1.2 pg/mL for IL- 6 and 0.13 µg/mL of CRP in addition to S-100 and E-Selectin which are other suggested biomarkers for sepsis. The biomarkers were chosen as different sub groups of the panel were shown to have a higher specificity and sensitivity to diagnosing prenatal sepsis at different time points [69]. A prior version of this chip in a similar format without magnetic nanoparticles was tested with a panel of IL-6, IL-8, IL-10, TNF-α, and PCT resulting in LOD's of 15 pg/mL, 26 pg/mL, 65 pg/mL, 40 pg/mL, 0.078 ng/mL and 3 µg/mL respectively in 2.5 hours [23]. A microfluidic device that integrates preparation steps using similar protocols was later demonstrated. This device was tested with PCT, IL-6 and CRP. The device tested with 4% human albumin had LOD's of 0.34 ng/mL, 0.27 ng/mL and 0.9 µg/mL. When the device was tested for measurement of IL-6 in plasma, it was found to have an LOD of 0.6 ng/mL. However, the effectiveness of this panel for the diagnosis or prognosis of sepsis was not evaluated.

A panel consisting of cfDNA, protein C, platelet count, creatinine, Glasgow Coma Scale [GCS] score, and lactate proposed earlier has been reported to have a high accuracy in predicting patient outcome [13]. The panel had an AUC for predicting a "single" mortality outcome for each patient in 28 days of 0.903 compared to SOFA which has an AUC of 0.86 in similar conditions. Of these, lactate, platelet count and creatinine have commercially available technologies for rapid measurement, Glasgow Coma Scale is a qualitative scoring tool and requires rapid development of microfluidic devices for cfDNA and protein C. While cfDNA has techniques available for measurement, they require complex external hardware for measurement which makes these methods hard to use for bedside assays. A simplified technique that is low cost and senses in a range of 1-5 µg/mL would improve usability for

diagnosis. Protein C is currently only measurable using expensive immunoassays or multi-staged processes that render it inconvenient for diagnostics. An alternative method for measuring protein C concentration in a single step while not being expensive is necessary for the use of protein C as a biomarker. Furthermore, the current techniques used for the measurement of cfDNA and protein C are not suitable to be integrated into a single device that could be used for the measurement of both biomarkers. The development of devices for the measurement of protein C and cfDNA that use a common method of detection while maintaining a low cost and run time would pave the way for the use of a new panel of biomarkers that could rapidly assess the status of a sepsis patient with higher accuracy than current biomarkers.

3. Fabrication techniques for low-cost biomarker separation

The development of devices for low cost and rapid diagnosis of biomarkers required an assessment of different fabrication methods available in microfabrication and an analysis of the strengths and limitations of each of these methods which are summarized in this section. As the requirements for the materials used in the measurement of cfDNA and protein C are different, an analysis is provided at the end of each section detailing the limitations of using the fabrication method for measurement of cfDNA and protein C. The goal for the device measuring cfDNA is lowering the complexity of the device while retaining the sensitivity in the range of 1 – 5 µg/mL. In addition, using the device with a portable detection method required a compact size and low depth while storing a large volume of fluid. These were the main criteria for cfDNA measurement. The goal for the protein C measurement device was the ability to fabricate multiple individual 2D layers which then needed to be integrated, in addition to minimizing surface adsorption, electrical and thermal insulation, low cost and rapid prototyping. Due to the need for low cost, silicon based micromanufacturing and photolithographic fabrication techniques were excluded from consideration.

3.1 Polydimethylsiloxane (PDMS)

Soft lithography using PDMS is currently the most widely used method for fabrication of microfluidic devices. This is due to the many favourable characteristics of PDMS for rapid prototyping such as its high transparency, ease of fabrication, replication of nanoscale characteristics, excellent biocompatibility and low autofluorescence. The fabrication method used for PDMS microdevices is illustrated in Fig. 3 and shows the major steps in fabrication. A mold with the required design is first prepared using a different fabrication method and the resolution of which determines the final resolution of the device. PDMS which is sold with two different components – base elastomer and curing agent, are mixed in a ratio of 10:1 and degassed to remove trapped air bubbles. The combined mixture is deposited in the mold and allowed to cure at 80 °C for two hours or at room temperature for over 24 hours to allow the two components to copolymerize forming a flexible polymer which can then be extracted from the mold. The resulting PDMS block can then be integrated with another patterned PDMS block, a plain PDMS membrane or glass slides using plasma treatment, wet bonding, or other bonding processes [70]. The tremendous amount of research performed using PDMS has resulted in a comprehensive characterization of the material[71] and a wide variety of bonding methods, surface treatments and functionalization methods being available to alter the device to meet different requirements [72].

However, despite these advantages, PDMS is unsuitable for the measurement of protein C and cfDNA. This is due to the hydrophobicity of PDMS which would require the use of additional pumps to flow samples through the device. This also increases the absorption of proteins to the walls reducing the specificity of the device without additional surface treatment. PDMS also has a low surface energy which in combination with flexibility of PDMS device and reduces stability of gels integrated in PDMS. This was found to be necessity for detection of protein C.

3.2 Other polymers

Thermoplastic polymers, including polycarbonate, polyimide, COC, and PMMA have been used in the fabrication of microdevices using hot embossing with a mold. Injection molding is a well-established fabrication process for polymers in high volume production due to its fast process time and high replication accuracy. The polymer is fed into a chamber and melted (200–350 °C depending on the melting temperature of polymer). It is then injected into the mold cavity and cooled to form a replica. This has been demonstrated with both thermosetting and thermoplastic polymers. COC and COP have been extensively used for low-cost microfluidic devices due to ease of transition to injection molding. However, despite the ease of use of injection molding and hot embossing, they are not suitable for the current application. This is primarily due to the use of a relatively high cost for the mold material to ensure it can withstand the high temperature process.

3.3 Paper microfluidics

Patterned paper microfluidic technology was first popularized in 2007 [73] and has since found widespread use for its ease of fabrication and low cost. The porosity and hydrophilicity of paper results in the capillary flow of fluids through the device which makes it an attractive substrate for portable microfluidic applications without the need for external pumps. The growth of paper microfluidic devices led to an array of patterning tools and applications for the technology. Broadly, they can be classified as (i) Photolithography, (ii) Surface functionalization, (iii) Wax patterning/printing, (iv) Plotting, and (v) Laser cutting. Except for plotting and laser cutting where the sections of the substrate were physically separated, the mechanism for manipulating fluid flow in paper was through the creation of difference of hydrophobicity between channels (hydrophilic) and boundaries (hydrophobic). Photo-lithography which was the first method proposed for patterning using a hydrophobic photoresist to pattern the walls of the channel into the paper[73]; Surface

functionalization was used to create barriers in paper. The chemical modification of sections of paper to make those sections hydrophobic was performed using alkyl ketene dimer (AKD) [74] which was added to the -OH groups in cellulose through an esterification reaction. Similarly, Trimethoxyoctadecylsilane (TMOS) reacts with -OH groups in cellulose to create hydrophobic regions and has been used to make paper based sensors by making a patterned mask soaked in TMOS and bringing it in contact with paper and being allowed to evaporate [75]. Wax printing which was proposed as a low-cost alternative to photolithography. Parafilm was one of the earliest materials used to pattern paper using a heated metal stamp[76]. A similar method that combined a printing head with stamping technology for paper devices was also demonstrated for multiplexed design fabrication more recently [77]. Screen printing [78] and manual wax and PDMS drawing [79] were also demonstrated but suffer from far lower reliability and lack of scalability. The most popularly used method for wax/inkjet patterning uses a modified inkjet printer to print patterns using a wax based ink [80].

Plotting or paper cutting which was a promising method of fabrication as no chemicals were needed to define channels for fluid flow, and hence was independent of flow characteristics of wax, polymers and solvents. This improved the precision in manufacturing channels. However, due to the reduction of material, the mechanical stability of the paper was reduced, and the device requires additional support which increased costs [81]. However, the cutting action sometimes induced warping or tearing of the paper, which necessitated the use of a backing material [81]. Sensors have been fabricated by craft cutting nitrocellulose with a polyester backing [82]. Laser cutting using a computer-controlled CO_2 laser was similar to using a craft cutter and could cut through the paper in a single pass without the need for a backing material. However, this increased the cost of fabrication [83]. Laser cutters have also been used to fabricate laser-ablated hollow channels that were partially attached to the bulk

filter paper sheet in a single step which eliminated the removal of unused, excess material [84]. A summary of the different methods of fabrication is shown in Fig. 3

Despite the potential for using paper microfluidic devices in the development of low-cost diagnostic devices, they were found to not be suitable for this application due to a number of reasons. The choice of materials for paper microfluidic devices was limited, primarily being cellulose and cellulose derived materials, which have limited chemical compatibility. Secondly, the thickness of paper microfluidic devices was limited, resulting in a wider distribution of sample volume. This would reduce the limit of detection of the device when used with optical detection methods. Thirdly, paper microfluidic devices have a low wet strength which makes the integration of multiple patterned paper layers with gels challenging. This was necessary requirement for protein C measurement.

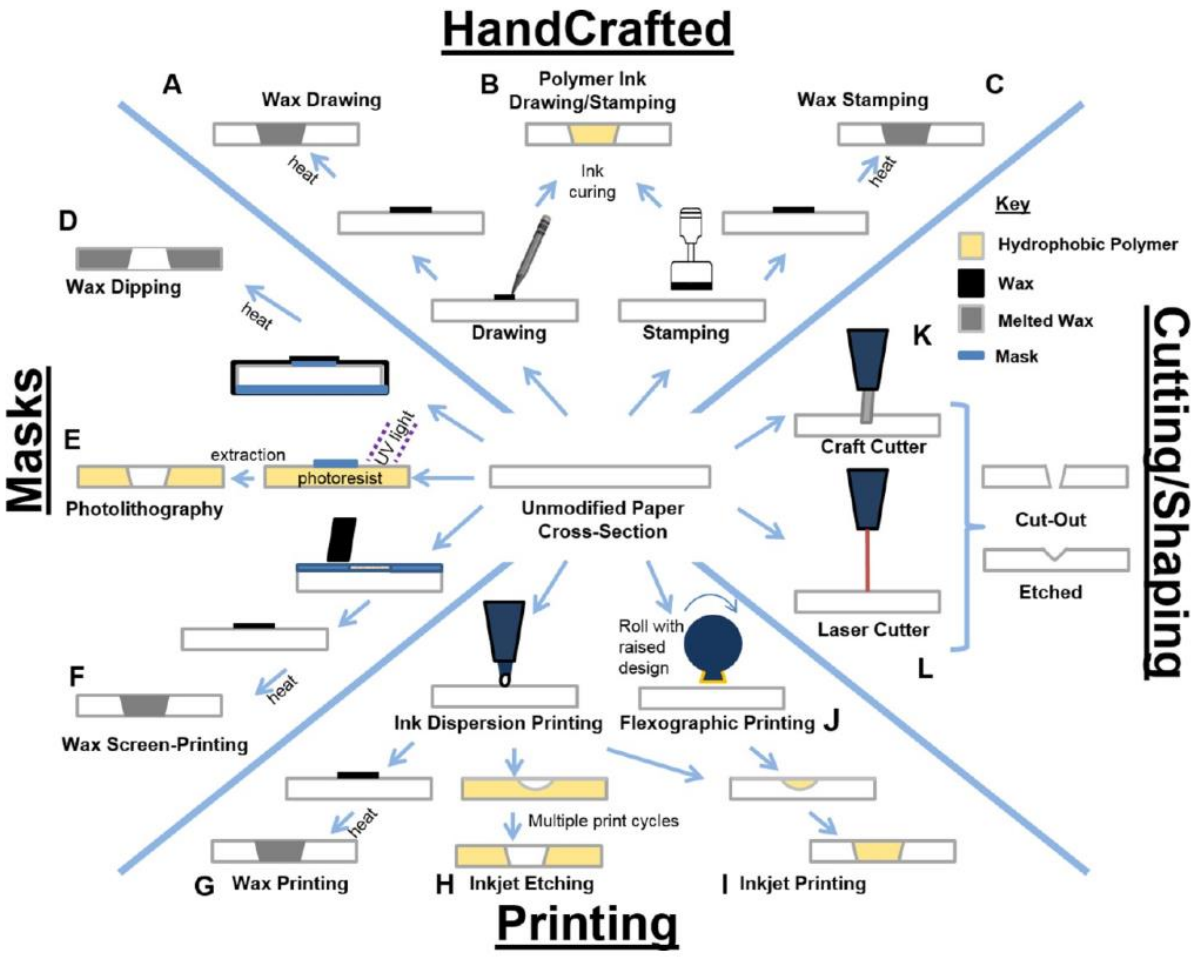

Figure 3Overview of different fabrication techniques for paper microfluidic devices[85]

3.4 Thread microfluidics

Thread microfluidics was proposed shortly after paper microfluidic devices by two different groups. [86,87]. The proposition for thread microfluidic devices was based on having similar advantages of low cost and ease of fabrication while having a wider range of materials to choose from, better wet strength and pre-established chemical modification toolkit from the fabric industry. However, this was at the cost of increased complexity of fluid flow. The increased complexity of fluid flow was most apparent in the number of variables that could be tuned to alter rate of fluid flow and volume stored in a length of thread. Numerous studies were performed analysing these parameters including theoretical analysis of the effects of twists per inch (tpi) of the thread [88], effects of knots on fluid

resistance, Laplace pressure [89], deformation of the thread when twisting [90] and the effects of integrating strings of multiple materials with different surface energy in the thread [91]. In addition, active flow control was demonstrated using electrophoretic forces [92] that were dependant on the material of thread, temperature based valves [93] and the external deposition of a hydrophilic material [94].

Fluid flow in threads was controlled using techniques dependant on the format of the device. These can broadly be classified as 1-D and 2-D devices. 1-D devices are those in which there is no variation of flow along the width or height. The simplest format used threads weaved into a plastic frame and intertwining of threads was used to induce fluid mixing [86,87]. A valve in a 1-D thread was demonstrated by patterning the thread using plasma treatment to make a hydrophobic cotton thread hydrophilic across its length except in a specific region of the thread. Fluid could then be passed through the thread from either inlet into a second thread which was moved to switch and transfer flow between the inlets of the first thread or stop flow entirely by moving the second thread to the hydrophobic blocked region of the first thread [95]. Knots have also been used to direct flow in threads by controlling flow resistance in threads [88]. These are illustrated in Fig. 4(a)(b). 2-D thread device patterning is more analogous to paper microfluidic devices and is derived from a similar ideology of shaping hydrophilic regions to act as channels surrounded by hydrophobic section of thread. This has been demonstrated using photolithography [96] wax patterning [97], Intertwining/weaving hydrophobic strings around hydrophilic strings to form channels [98][99]. The intertwining of strings with different properties is unique to threads and is only possible due to the wide variety of materials available for thread microfluidic devices and the different surface treatments available for those materials. These devices are shown in Fig. 4(c)(d).

Thread microfluidic devices have been demonstrated using a variety of materials such as cotton, wool [100], silk [98], nylon, polyester, stainless steel [101], gold microwires [102] and suture threads [103]. Cotton is the most commonly used material of choice due to its low cost and compatibility with a wide range of testing reagents evidenced by the large number of paper microfluidic devices which share the same backbone material – cellulose [104]. However, the morphology of cotton thread and non-uniformities in it introduce large variations in flow rate and pore size which prevents its use in applications which requires reliable mobility of particles that could be entrapped [105]. Composite threads consisting of a blend of polyester and cotton are available on the market and enable tuning the wicking and absorption rate to the required preferences [106].

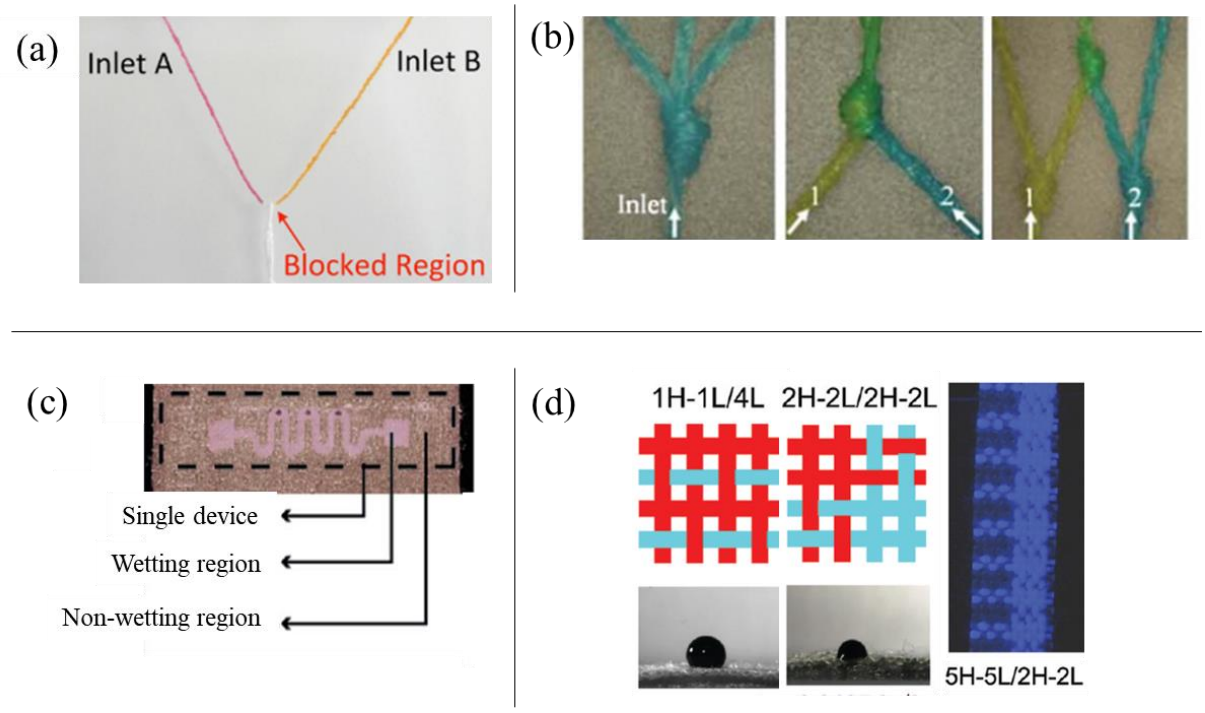

Figure 4 Patterning of (a)(b) 1-D and (c)(d) 2-D threads.a) Valve using hydrophobic sections of the thread [95] *(b) Knots used for controlled mixing of solutions* [88] *(c) Device fabricated on silk with hydrophilic strings weaved around hydrophobic strings* [98]*(d) Polyester fabric patterned using hydrophobic (L) and hydrophilic (H) strings in different proportions to obtain different wetting characteristics* [99]

Thread microfluidic presents many advantages compared to other similar technologies such as the wide variety of material choices to minimize background fluorescence, low cost of fabrication, high wet strength, ease of integration with other materials, and controllable porosity. As a result, it would be ideal for fabrication of a POC device for the measurement of cfDNA. The porosity and larger volume of sample stored in each length of thread would theoretically improve the optical signal obtained compared to a paper microfluidic device while retaining the low cost. The wider variety of materials available would enable choosing a material that is compatible for the required application. However, the complexity of the 3D structure within the thread would result in a complicated electrical field distribution making this a more challenging fabrication technique for use in applications that require a known gradient in electric field.

3.5 Xurography

Xurography is an inexpensive microfabrication technique patterning of complex shapes in films. First proposed by Bartholomeusz et al., in 2006 [107], the technique uses a cutting plotter to cut out shapes in plastics which are then layered together using adhesive films to make microfluidic devices. It enables the integration of different materials into a single device using inexpensive materials [108], rapid fabrication, and simple processing. Additionally, this method enables the integration of electrodes by cutting and physically adhering metal films into microfluidic devices to reduce the cost of fabrication of devices [109].

Xurography can broadly be classified into 2 discrete steps as illustrated in Fig. 5. The first is a patterning step where a cutting plotter is used to physically carve a pattern into a thin sheet (Fig. 5a). This is followed by an adhesion step where these films are aligned and adhered together by the application of an external pressure (Fig. 5b). The patterning of xurographic films is controlled by a range of parameters including the angle of the cutting blade, the vertical and horizontal cutting force

applied, the thickness of the blade, depth of cut and cutting speed among others [110]. These parameters need to be individually assigned based on the choice of material and thickness of the film. Furthermore, as xurography is a mechanical process, a wide variety of materials can be processed using these methods, this includes polyethylene terephthalate (PET), polyester, polyimide and polycarbonate, acrylic among others. In comparison to laser cutting, xurography has more uniform physical properties as the material is unaffected by heat, is more portable and has a lower cost of fabrication while laser cutting has a higher resolution of cutting. The adhesion of sheets together has been demonstrated with the use of pressure sensitive and UV sensitive adhesives. A wide range of adhesives are available which can broadly be classified based on their backbone as acrylic, rubber, and silicone adhesives resulting in an array of properties including tape thickness, material properties, surface energy, cost and availability [111].

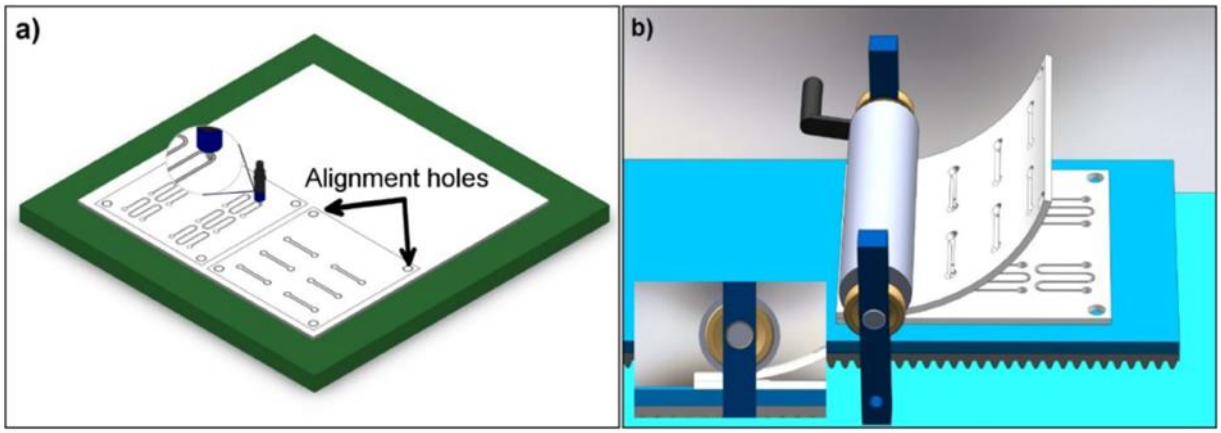

Figure 5 Schematic of the two steps of xurography (a) Cutting a pattern using a plotter (b) Aligning and adhering the individual layers together [108].

Xurography would be the ideal method of fabrication for the detection of protein C due to several reasons. Firstly, the ability to pattern individual layers would result in a simple structure that could be used to focus the electric field in specific regions of the device. Secondly, the use of plastics like PET which have a low zeta potential and protein adsorption would reduce electroendosmosis of agarose

and protein loss during measurement. Finally, the ease of integration with other materials such as agarose gels and polyester membranes using adhesive layers would simplify the fabrication process which in combination with the low cost of fabrication would enable the rapid development of multiple iterations of the device which would be necessary for the development of a rapid measurement tool for protein C.

4. Summary

Sepsis is “a life-threatening organ dysfunction caused by a dysregulated host response to infection” that results from a escalating interaction between the inflammatory response to an infection and the coagulation cascade and is further exacerbated by other factors such as a cytokine storm and apoptotic cell death. It is currently diagnosed using a SOFA (Sequential Organ Failure Assessment) score which grades the functioning of various organ systems by monitoring routinely tested laboratory variables. However, a full SOFA test requires lab tests for platelet counts, bilirubin level and creatinine level which is time consuming. A rapid bedside test, qSOFA was recommended for screening using the Glasgow coma scale in combination with one of systolic blood pressure and respiratory rate.

Numerous biomarkers have been identified to improve the ability to diagnose and predict sepsis outcomes. This includes Procalcitonin, C-reactive protein, TNF-α, CD64, IL – 6 and PAI 1, cfDNA and protein C among many others. At present, most of these biomarkers are detected using immunoassays. Benchtop and microfluidic assays that have been used for detection of some of the popular biomarkers were summarized. In addition, numerous panels for rapid detection/prognosis of sepsis were studied. One of the panels that was recommended consisted of measuring cfDNA, protein C, platelet count, creatinine, Glasgow Coma Scale [GCS] score, and lactate offered better predictive power for prognosis than SOFA. Of these, protein C and cfDNA are the only two biomarkers that do

not have suitable assays for detection. Current assays for cfDNA were focused on the high-resolution measurement of cfDNA which was unnecessary for sepsis which induces massive increase of cfDNA concentration to a range of 1-5 µg/mL. A simplified portable, bedside assay with a minimal use of external apparatus and training is currently unavailable and needs to be developed. Protein C is currently measured using a multi-step functional/chromogenic assay or through the use of an immunoassay. While the immunoassay is a single stepped assay suitable for diagnostics, it is extremely expensive as it requires target antibodies. An assay that targets protein C using a generic fluorescent tag would greatly reduce cost and improve the usability of protein C as a biomarker. Furthermore, using a fluorescent tag for detection would simplify the integration of detection methods for cfDNA and protein C which would be of helpful in the eventual use of both biomarkers as part of a panel of biomarkers.

The choice of fabrication methods in the development of microfluidic devices for the detection of cfDNA and protein C was summarized. PDMS, which is the most used substrate in microfluidics was found to be unsuitable for cfDNA detection due to the hydrophobicity of PDMS. Similarly, it was found to be unsuitable for protein C measurement as the integration of gels with PDMS is challenging due to its low surface energy and mechanical flexibility. Paper microfluidic devices were considered as an alternative due to the low cost of fabrication but were found to be unsuitable due to the low volume trapped per area of paper, low wet strength and limited choice of material. Thread microfluidic devices were a better choice for the detection of cfDNA due to the larger volume storage capacity and larger choice of materials of threads compared to paper. Xurography was a better alternative for the measurement of protein C due to the wide variety of properties of plastics, ease of integration with gels and membranes, low cost of fabrication and rapid prototyping.

5. Objectives of the thesis

The objective of this doctoral thesis is the development of tools for the rapid detection and measurement of biomarkers for sepsis diagnosis or prognosis. The objective was met through the development of two formats of microfluidic devices designed for the measurement of cfDNA and protein C using a common detection method that would enable eventual integration. The format for the detection of cfDNA was built upon a larger framework that showed the use of threads for rapid aliquoting and detection of biomarkers that could be measured without prior separation. This was combined with a custom-built portable fluorescence camera for a rapid fluorescence assay. The measurement of protein C involved the development of a technique for separation of proteins based on their isoelectric point in addition to miniaturization of immobilized metal affinity chromatography. The resulting platforms were tested to show their capabilities to separate the respective biomarkers from plasma as an indication of their potential for diagnostics.

6. Thesis organization

The thesis contains of 6 main chapters in a "sandwich" thesis format. Chapter 1 provides introductory information on the reasons for development of low-cost devices to measure the concentration of biomarkers for sepsis and microfluidic fabrication technologies that can be used for fabrication. Chapters 2 and 3 are on the development of microfluidic isoelectric gating and miniaturized immobilized metal affinity chromatography using barium (Ba-IMAC) for low cost, single stepped measurement of protein C in plasma. Chapter 4 and 5 are on the development of fabrication, aliquoting and detection using thread microfluidic devices for detection of cfDNA in plasma without pre-concentration. Chapter 6 describes the relevant conclusions and future directions of research that could be developed from the developed technologies.

Chapter 1:

This chapter reviews the background and motivation behind the development of low-cost biomarker detection of sepsis. This includes an overview of the pathophysiology of sepsis and important cascades that play a role, resulting in changes of biomarker concentrations. Important biomarkers are described and some detection methods for principal biomarkers are explained. Utility of cfDNA and protein C for sepsis prognosis is elucidated and their detection methods described. The need for low-cost methods is explained and fabrication methods for such a goal are provided with their advantages and challenges described. The reasons for using the choice of fabrication methods used are detailed.

Chapter 2:

This chapter details the development of agarose based isoelectric gates for the separation of protein C. It describes the principle of operation, limitations of the technology and examples of its operation to show separation in simple matrices such as in egg white. This study showed that successful operation of isoelectric gates would be suitable for separating proteins based on their isoelectric point.

Chapter 3:

This chapter describes the development of miniaturized immobilized metal affinity chromatography using barium (Ba-IMAC) and its integration with isoelectric gates. The isoelectric gates were used as the first stage of separation followed by an agarose gel placed on a membrane acting as the column for microfluidic Ba-IMAC for a second stage of separation. The combined system was shown to be able to measure the concentration protein C spiked in plasma at concentrations necessary for prognosis of sepsis.

Chapter 4:

This chapter describes the development of a thread microfluidic format for reagent storage and handling. A composite PDMS – thread format was developed for the automated control of sample

volume for simplified detection using a colorimetric imaging setup. This was validated by measuring the concentration of nitrite and pH in environmental samples of water at concentrations required for environmental monitoring.

Chapter 5:

This chapter used a simplified passive version of the device developed in chapter 4 for the detection of cfDNA in plasma. The device consisted of a capillary driven thread microfluidic device that was capable of aliquoting sample volumes and enabled single stepped measurement of cfDNA with no preconcentration steps. A portable fluorescent detection system was developed using a simplified version of the colorimetric system previously developed and integrated to form a POC testing setup for cfDNA. The integrated system was validated for the detection of cfDNA in plasma in the range required for prognosis of sepsis.

Chapter 6:

This chapter includes the conclusion of the thesis and suggested future works for both xurographic and thread microfluidic technologies and the potential to blend the systems together for integrated measurement of both biomarkers.

7. Research contributions

The principal objective of this thesis is the development of devices for the rapid detection and measurement of biomarkers for sepsis diagnosis and prognosis. The devices are designed to be faster than currently available techniques, single stepped with no external inputs after the initial setup and use fluorescent detection. A common detection method was used to aid in the eventual integration of the devices which would further improve the development of a POC device. The contributions made

during the development of these technologies can be broadly divided into applied contribution and fundamental contributions.

The fundamental contributions made during the thesis are the development of techniques for the separation of proteins using their isoelectric point and chemical affinity and the development of fluorescent signal amplification and aliquoting using threads. Specifically, the separation of proteins using isoelectric point was established using agarose gels buffered with commonly used buffering compounds as isoelectric gates for the separation of proteins based on their isoelectric points. This enabled tuning of the gates to target specific proteins while using a nonspecific dye which reduced costs in comparison to comparable techniques. The separation of proteins using their chemical affinity was through the development of a miniaturized format for immobilized metal affinity chromatography (IMAC) using Barium for the measurement of protein C which has not been demonstrated before. The format was miniaturized using a xurographic device integrated with a polyester membrane. An agarose gel containing IMAC beads bound to Barium was deposited on this membrane. The gel was then used to trap proteins containing a γ-carboxyglutamic acid domain due to high affinity of this domain for Barium. The gravity driven process of conventional IMAC was replaced by electrophoretic transport to improve the speed of separation. This enabled the targeting of specific proteins by their chemical affinity at a much lower cost than immunoassays. Patterning methods were developed, and characterization was performed for the use of threads as a controllable medium for aliquoting fluid samples. Length and twists per cm were found to be parameters that needed to be controlled for adequate control of trapped fluid volume. This simplified fluidic operations for use in POC devices and is a necessary step for the development of passive thread microfluidics. The use of threads in amplifying reflective fluorescence measurement was characterized and compared with non-

thread devices to demonstrate an advantage for thread microfluidic devices that has not been previously described.

The applied contributions that resulted from the thesis are the development of an integrated microfluidic device for protein C quantification and the first passive cfDNA quantification device. The microfluidic device for measuring protein C used isoelectric gating as the first stage of separation and Ba-IMAC as the second stage of separation to measure the concentration of protein C in plasma using a nonspecific dye and with minimal sample preparation. This method was viable in the presence of interfering proteins at a concentration 1000-fold higher in the same solution and at a much lower cost than the currently used immunoassays. The use of xurography enabled the use of geometric variations in channel size to strategically concentrate the electric field and minimize run time while operating at a voltage of 15 – 100 V which is significantly lower than that used for traditional dIEF (digital isoelectric focusing) and cIEF (capillary isoelectric focusing) formats. Passive cfDNA quantification was developed through the fabrication of a thread-silicone composite that used threads to amplify the fluorescence response and capillary forces to aliquot sample volumes. The device used a generic dsDNA binding fluorescent dye and was paired with a custom-built portable fluorescence imaging setup for measuring cfDNA concentration in plasma at concentrations necessary for the prognosis of sepsis in a single step within 20 minutes. This is a lower cost and easier to use solution for POC prognosis of cfDNA than any other detection methods that are currently available.

References

[1] M. Singer, C.S. Deutschman, C.W. Seymour, M. Shankar-Hari, D. Annane, M. Bauer, R. Bellomo, G.R. Bernard, J.-D. Chiche, C.M. Coopersmith, R.S. Hotchkiss, M.M. Levy, J.C. Marshall, G.S. Martin, S.M. Opal, G.D. Rubenfeld, T. van der Poll, J. Vincent, D.C. Angus, The Third International Consensus Definitions for Sepsis and Septic Shock (Sepsis-3)., J. Am.

Med. Assoc. 315 (2016) 801–10. https://doi.org/10.1001/jama.2016.0287.

[2] Statistics Canada, Leading causes of death, total population, by age group [Data table], (2021). https://doi.org/https://doi.org/10.25318/1310039401-eng.

[3] C.M. Martin, F. Priestap, H. Fisher, R.A. Fowler, D.K. Heyland, S.P. Keenan, C.J. Longo, T. Morrison, D. Bentley, N. Antman, A prospective, observational registry of patients with severe sepsis: The Canadian Sepsis Treatment and Response Registry, Crit. Care Med. 37 (2009) 81–88. https://doi.org/10.1097/CCM.0b013e31819285f0.

[4] K. Farrah, L. McIntyre, C.J. Doig, R. Talarico, M. Taljaard, M. Krahn, D. Fergusson, A.J. Forster, D. Coyle, K. Thavorn, Sepsis-Associated Mortality, Resource Use, and Healthcare Costs: A Propensity-Matched Cohort Study*, Crit. Care Med. 49 (2021). https://journals.lww.com/ccmjournal/Fulltext/2021/02000/Sepsis_Associated_Mortality,_Resource_Use,_and.6.aspx.

[5] Y. Hattori, K. Hattori, T. Suzuki, N. Matsuda, Recent advances in the pathophysiology and molecular basis of sepsis-associated organ dysfunction: Novel therapeutic implications and challenges, Pharmacol. Ther. 177 (2017) 56–66. https://doi.org/10.1016/j.pharmthera.2017.02.040.

[6] B. Gyawali, K. Ramakrishna, A.S. Dhamoon, Sepsis: The evolution in definition, pathophysiology, and management, SAGE Open Med. 7 (2019) 205031211983504. https://doi.org/10.1177/2050312119835043.

[7] J.G. Dib, K. Zarikian, The role of activated protein C in sepsis, Hosp. Pharm. 39 (2004) 558–563. https://doi.org/10.1177/001857870403900610.

[8] P. Arina, M. Singer, Pathophysiology of sepsis, Jacobi, Judith. 34 (2002) 77–84.

https://doi.org/1079-2082/02/0202-00S3.

[9] Diapharma, Protein C, (2018). https://diapharma.com/protein-c/ (accessed December 14, 2018).

[10] N.L. Jackson Chornenki, R. Coke, A.C. Kwong, D.J. Dwivedi, M.K. Xu, E. McDonald, J.C. Marshall, A.E. Fox-Robichaud, E. Charbonney, P.C. Liaw, Comparison of the source and prognostic utility of cfDNA in trauma and sepsis, Intensive Care Med. Exp. 7 (2019). https://doi.org/10.1186/s40635-019-0251-4.

[11] M.L. Ekaney, G.P. Otto, M. Sossdorf, C. Sponholz, M. Boehringer, W. Loesche, D. Rittirsch, A. Wilharm, O. Kurzai, M. Bauer, R.A. Claus, Impact of plasma histones in human sepsis and their contribution to cellular injury and inflammation, Crit. Care. 18 (2014) 1–9. https://doi.org/10.1186/s13054-014-0543-8.

[12] Y. Zhang, Y. Zhou, Y. Yang, D. Pappas, Microfluidics for sepsis early diagnosis and prognosis: A review of recent methods, Analyst. 146 (2021) 2110–2125. https://doi.org/10.1039/d0an02374d.

[13] P.C. Liaw, A.E. Fox-Robichaud, K.-L. Liaw, E. McDonald, D.J. Dwivedi, N.M. Zamir, L. Pepler, T.J. Gould, M. Xu, N. Zytaruk, S.K. Medeiros, L. McIntyre, J. Tsang, P.M. Dodek, B.W. Winston, C. Martin, D.D. Fraser, J.I. Weitz, F. Lellouche, D.J. Cook, J. Marshall, Mortality Risk Profiles for Sepsis, Crit. Care Explor. 1 (2019) e0032. https://doi.org/10.1097/cce.0000000000000032.

[14] C. Pierrakos, D. Velissaris, M. Bisdorff, J.C. Marshall, J.L. Vincent, Biomarkers of sepsis: Time for a reappraisal, Crit. Care. 24 (2020) 1–15. https://doi.org/10.1186/s13054-020-02993-5.

[15] B.M. Biron, A. Ayala, J.L. Lomas-Neira, Biomarkers for sepsis: What is and what might be?, Biomark. Insights. 10 (2015) 7–17. https://doi.org/10.4137/BMI.S29519.

[16] F. Fruergaard, J.A. Petersen, European Journal of Internal Medicine Novel biomarkers for sepsis : A narrative review, Eur. J. Intern. Med. 45 (2017) 46–50. https://doi.org/10.1016/j.ejim.2017.09.030.

[17] A. Teggert, H. Datta, Z. Ali, Biomarkers for point-of-care diagnosis of sepsis, Micromachines. 11 (2020). https://doi.org/10.3390/mi11030286.

[18] P. Croft, D.G. Altman, J.J. Deeks, K.M. Dunn, A.D. Hay, H. Hemingway, L. LeResche, G. Peat, P. Perel, S.E. Petersen, R.D. Riley, I. Roberts, M. Sharpe, R.J. Stevens, D.A. Van Der Windt, M. Von Korff, A. Timmis, The science of clinical practice: Disease diagnosis or patient prognosis? Evidence about "what is likely to happen" should shape clinical practice, BMC Med. 13 (2015) 1–8. https://doi.org/10.1186/s12916-014-0265-4.

[19] Thermo Fisher Scientific, CRP Human ELISA Kit, (2021). https://www.thermofisher.com/elisa/product/CRP-Human-ELISA-Kit/KHA0031.

[20] Thermo Fisher Scientific, Procalcitonin Human ELISA Kit, (2021). https://www.thermofisher.com/elisa/product/Procalcitonin-Human-ELISA-Kit/EHPCT.

[21] Bosterbio, Human TNF-Alpha ELISA Kit, (2021). https://www.bosterbio.com/human-tnf-alpha-picokine-trade-elisa-kit-ek0525-boster.html.

[22] P. Buchegger, U. Sauer, H. Toth-Székély, C. Preininger, Miniaturized protein microarray with internal calibration as point-of-care device for diagnosis of neonatal sepsis, Sensors. 12 (2012) 1494–1508. https://doi.org/10.3390/s120201494.

[23] U. Sauer, P. Domnanich, C. Preininger, Protein chip for the parallel quantification of high and low abundant biomarkers for sepsis, Anal. Biochem. 419 (2011) 46–52. https://doi.org/10.1016/j.ab.2011.07.038.

[24] E.K. Sackmann, A.L. Fulton, D.J. Beebe, The present and future role of microfluidics in biomedical research., Nature. 507 (2014) 181–9. https://doi.org/10.1038/nature13118.

[25] C. Dixon, A.H.C. Ng, R. Fobel, M.B. Miltenburg, A.R. Wheeler, An inkjet printed, roll-coated digital microfluidic device for inexpensive, miniaturized diagnostic assays, Lab Chip. (2016). https://doi.org/10.1039/C6LC01064D.

[26] A. Tay, A. Pavesi, S.R. Yazdi, C.T. Lim, M.E. Warkiani, Advances in microfluidics in combating infectious diseases, Biotechnol. Adv. 34 (2016) 404–421. https://doi.org/10.1016/j.biotechadv.2016.02.002.

[27] A.L. Blomkalns, Lactate - A Marker for Sepsis and Trauma, EMCREG-International. (2007) 43–49.

[28] J. Levraut, C. Ichai, I. Petit, J.-P. Ciebiera, O. Perus, D. Grimaud, Low exogenous lactate clearance as an early predictor of mortality in normolactatemic critically ill septic patients., Crit. Care Med. 31 (2003) 705–710. https://doi.org/10.1097/01.CCM.0000045561.85810.45.

[29] Nova Biomedical, StatStrip Lactate, (2021). https://novabiomedical.com/statstrip-lactate/index.php.

[30] S.A. Glasmacher, P. Bonongwe, W. Stones, Point-of-care lactate and creatinine analysis for sick obstetric patients at Queen Elizabeth Central Hospital in Blantyre, Malawi: A feasibility study, Malawi Med. J. 28 (2016) 15–18. https://doi.org/10.4314/mmj.v28i1.4.

[31] L. Jacobs, H.R. Wong, Emerging infection and sepsis biomarkers: will they change current therapies?, Expert Rev. Anti. Infect. Ther. 14 (2016) 1–13. https://doi.org/10.1080/14787210.2016.1222272.

[32] M. Oberhoffer, H. Vogelsang, S. Rußwurm, T. Hartung, K. Reinhart, Outcome prediction by traditional and new markers of inflammation in patients with sepsis, Clin. Chem. Lab. Med. 37 (1999) 363–368. https://doi.org/10.1515/CCLM.1999.060.

[33] D. Rascher, A. Geerlof, E. Kremmer, P. Krämer, S. Michael, A. Hartmann, M. Rieger, Total internal reflection (TIRF)-based quantification of procalcitonin for sepsis diagnosis - A point-of-care testing application, Biosens. Bioelectron. 59 (2014) 251–258. https://doi.org/10.1016/j.bios.2014.03.052.

[34] P. Schuetz, M. Christ-Crain, A.R. Huber, B. Müller, Long-term stability of procalcitonin in frozen samples and comparison of Kryptor® and VIDAS® automated immunoassays, Clin. Biochem. 43 (2010) 341–344. https://doi.org/10.1016/j.clinbiochem.2009.08.029.

[35] H.-G. Bernstein, K.-H. Braunewell, Comparison of a New Procalcitonin Assay from Roche with the Established Method on the Brahms Kryptor, Clin. Chem. 55 (2009) 1041–1043. https://doi.org/10.1373/clinchem.2008.116970.

[36] Á. Molinero-Fernández, M.Á. López, A. Escarpa, An on-chip microfluidic-based electrochemical magneto-immunoassay for the determination of procalcitonin in plasma obtained from sepsis diagnosed preterm neonates, Analyst. 145 (2020) 5004–5010. https://doi.org/10.1039/d0an00624f.

[37] P. Póvoa, C-reactive protein: A valuable marker of sepsis, Intensive Care Med. 28 (2002) 235–243. https://doi.org/10.1007/s00134-002-1209-6.

[38] P. Póvoa, E. Almeida, P. Moreira, A. Fernandes, R. Mealha, A. Aragão, H. Sabino, C-reactive protein as an indicator of sepsis, Intensive Care Med. 24 (1998) 1052–1056. https://doi.org/10.1007/s001340050715.

[39] J. Park, J.K. Park, Pressed region integrated 3D paper-based microfluidic device that enables vertical flow multistep assays for the detection of C-reactive protein based on programmed reagent loading, Sensors Actuators, B Chem. 246 (2017) 1049–1055. https://doi.org/10.1016/j.snb.2017.02.150.

[40] W. Bin Lee, Y.H. Chen, H.I. Lin, S.C. Shiesh, G. Bin Lee, An integrated microfluidic system for fast, automatic detection of C-reactive protein, Sensors Actuators, B Chem. 157 (2011) 710–721. https://doi.org/10.1016/j.snb.2011.04.087.

[41] Y.N. Yang, H.I. Lin, J.H. Wang, S.C. Shiesh, G. Bin Lee, An integrated microfluidic system for C-reactive protein measurement, Biosens. Bioelectron. 24 (2009) 3091–3096. https://doi.org/10.1016/j.bios.2009.03.034.

[42] R.K. Gupta, A. Periyakaruppan, M. Meyyappan, J.E. Koehne, Label-free detection of C-reactive protein using a carbon nanofiber based biosensor, Biosens. Bioelectron. 59 (2014) 112–119. https://doi.org/10.1016/j.bios.2014.03.027.

[43] V. Castro-López, J. Elizalde, M. Pacek, E. Hijona, L. Bujanda, A simple and portable device for the quantification of TNF-α in human plasma by means of on-chip magnetic bead-based proximity ligation assay, Biosens. Bioelectron. 54 (2014) 499–505. https://doi.org/10.1016/j.bios.2013.10.039.

[44] M. Herrmann, T. Veres, M. Tabrizian, Quantification of low-picomolar concentrations of TNF-α in serum using the dual-network microfluidic ELISA platform, Anal. Chem. 80 (2008) 5160–

5167. https://doi.org/10.1021/ac800427z.

[45] K. Abe, Y. Hashimoto, S. Yatsushiro, S. Yamamura, M. Bando, Y. Hiroshima, J.I. Kido, M. Tanaka, Y. Shinohara, T. Ooie, Y. Baba, M. Kataoka, Simultaneous Immunoassay Analysis of Plasma IL-6 and TNF-α on a Microchip, PLoS One. 8 (2013) 6–13. https://doi.org/10.1371/journal.pone.0053620.

[46] S. Cesaro-Tadic, G. Dernick, D. Juncker, G. Buurman, H. Kropshofer, B. Michel, C. Fattinger, E. Delamarche, High-sensitivity miniaturized immunoassays for tumor necrosis factor α using microfluidic systems, Lab Chip. 4 (2004) 563–569. https://doi.org/10.1039/b408964b.

[47] A. Rhodes, M. Cecconi, Cell-free DNA and outcome in sepsis., Crit. Care. 16 (2012) 170. https://doi.org/10.1186/cc11508.

[48] J. Yang, P.R. Selvaganapathy, T.J. Gould, D.J. Dwivedi, D. Liu, A.E. Fox-Robichaud, P.C. Liaw, A microfluidic device for rapid quantification of cell-free DNA in patients with severe sepsis, Lab Chip. 15 (2015) 3925–3933. https://doi.org/10.1039/C5LC00681C.

[49] D.J. Dwivedi, L.J. Toltl, L.L. Swystun, J. Pogue, K.L. Liaw, J.I. Weitz, D.J. Cook, A.E. Fox-Robichaud, P.C. Liaw, Prognostic utility and characterization of cell-free DNA in patients with severe sepsis, Crit. Care. 16 (2012). https://doi.org/10.1186/cc11466.

[50] Z. Xu, Y. Qiao, J. Tu, Microfluidic technologies for cfDNA isolation and analysis, Micromachines. 10 (2019). https://doi.org/10.3390/mi10100672.

[51] S.J. Reinholt, A.J. Baeumner, Microfluidic isolation of nucleic acids, Angew. Chemie - Int. Ed. 53 (2014) 13988–14001. https://doi.org/10.1002/anie.201309580.

[52] T. Nakagawa, T. Tanaka, D. Niwa, T. Osaka, H. Takeyama, T. Matsunaga, Fabrication of

amino silane-coated microchip for DNA extraction from whole blood, J. Biotechnol. 116 (2005) 105–111. https://doi.org/10.1016/j.jbiotec.2004.08.018.

[53] C.E. Jin, B. Koo, T.Y. Lee, K. Han, S.B. Lim, I.J. Park, Y. Shin, Simple and Low-Cost Sampling of Cell-Free Nucleic Acids from Blood Plasma for Rapid and Sensitive Detection of Circulating Tumor DNA, Adv. Sci. 5 (2018) 1800614. https://doi.org/10.1002/advs.201800614.

[54] M.C. Morales, J.D. Zahn, Droplet enhanced microfluidic-based DNA purification from bacterial lysates via phenol extraction, Microfluid. Nanofluidics. 9 (2010) 1041–1049. https://doi.org/10.1007/s10404-010-0623-2.

[55] A.E. Fox-Robichaud, L.A. McIntyre, A. Turgeon, R. Green, R. Zarychanski, S. Bagshaw, I. Stiell, A. Worster, B. Rowe, M. Emond, D. Dwivedi, P.C. Liaw, The precise pilot trial: Temporal changes in thrombin generation, protein C levels and activated protein C generation in early septic shock, Am. J. Respir. Crit. Care Med. 181 (2010) 6146. http://ajrccm.atsjournals.org/cgi/reprint/181/1_MeetingAbstracts/A6146?sid=8cb89aaf-c3c2-47cb-8276-ae5c8d143d17%5Cnhttp://ovidsp.ovid.com/ovidweb.cgi?T=JS&CSC=Y&NEWS=N&PAGE=fulltext&D=emed10&AN=70844387%5Cnhttp://sfx.scholarsportal.info/uhn?sid=OVID:embas.

[56] S. Emani, R. Sista, H. Loyola, C.C. Trenor, V.K. Pamula, S.M. Emani, Novel microfluidic platform for automated lab-on-chip testing of hypercoagulability panel, Blood Coagul. Fibrinolysis. 23 (2012) 760–768. https://doi.org/10.1097/MBC.0b013e328358e982.

[57] D. Josic, L. Hoffer, A. Buchacher, Preparation of vitamin K-dependent proteins, such as

clotting factors II, VII, IX and X and clotting inhibitor Protein C, J. Chromatogr. B Anal. Technol. Biomed. Life Sci. 790 (2003) 183–197. https://doi.org/10.1016/S1570-0232(03)00082-5.

[58] R.G. Discipio, E.W. Davie, Characterization of Protein S , a 7-Carboxyglutamic Acid Containing Protein from Bovine and Human Plasma "', 18 (1979).

[59] A. Ichinose, H. Takeya, E. Espling, S. Iwanaga, W. Kisiel, E.W. Davie, Amino acid sequence of human protein Z, A vitamin K-dependent plasma glycoprotein, Biochem. Biophys. Res. Commun. 172 (1990) 1139–1144. https://doi.org/10.1016/0006-291X(90)91566-B.

[60] W. Kisiel, Human Plasma Protein C- ISOLATION, CHARACTERIZATION, AND MECHANISM OF ACTIVATION BY alpha-THROMBIN, J. Clin. Invest. 64 (1979) 761–769.

[61] A. Jean, C. Boyer, C. Rothschild, M. Wolf, DETERMINATION OF PROTEIN C BY AN IMMUNOENZYMATIC ASSAY, Protein C Biochem. Med. Asp. Proc. Int. Work. C Biochem. Med. Asp. Proc. Int. Work. (1985).

[62] P. Comp, R. Nixon, C. Esmon, Determination of functional levels of protein C, an antithrombotic protein, using thrombin-thrombomodulin complex, Blood. 63 (1984) 15–21. https://doi.org/10.1182/blood.V63.1.15.15.

[63] H. Wu, D.F. Bruley, Homologous human blood protein separation using immobilized metal affinity chromatography: Protein C separation from prothrombin with application to the separation of factor IX and prothrombin, Biotechnol. Prog. 15 (1999) 928–931. https://doi.org/10.1021/bp9901015.

[64] H. Wu, D.F. Bruley, Chelator, metal ion and buffer studies for protein C separation, Comp.

Biochem. Physiol. - A Mol. Integr. Physiol. 132 (2002) 213–220. https://doi.org/10.1016/S1095-6433(01)00550-5.

[65] J.. Dalton, D.. Bruley, K.. Kang, W.. Drohan, SEPARATION OF RECOMBINANT HUMAN PROTEIN C FROM TRANSGENIC ANIMAL MILK USING IMMOBILIZED METAL AFFINITY CHROMATOGRAPHY, 1997.

[66] R.A. Marlar, D.M. Adcock, Clinical evaluation of protein C: A comparative review of antigenic and functional assays, Hum. Pathol. 20 (1989) 1040–1047. https://doi.org/10.1016/0046-8177(89)90221-9.

[67] G. Owen, D.I. P-thrombin-sepharose, A functional assay of protein C in human plasma, Blood. 63 (1984) 671–675.

[68] R.A. Marlar, J.N. Gausman, Laboratory testing issues for protein C, protein S, and antithrombin, Int. J. Lab. Hematol. 36 (2014) 289–295. https://doi.org/10.1111/ijlh.12219.

[69] G. Laborada, M. Rego, A. Jain, M. Guliano, J. Stavola, P. Ballabh, A.N. Krauss, P.A.M. Auld, M. Nesin, Diagnostic Value of Cytokines and C-reactive Protein in the First 24 Hours of Neonatal Sepsis, Am. J. Perinatol. 20 (2003) 491–501. https://doi.org/10.1055/s-2003-45382.

[70] M. a Eddings, M. a Johnson, B.K. Gale, Determining the optimal PDMS–PDMS bonding technique for microfluidic devices, J. Micromechanics Microengineering. 18 (2008) 067001. https://doi.org/10.1088/0960-1317/18/6/067001.

[71] A. Mata, A.J. Fleischman, S. Roy, Characterization of polydimethylsiloxane (PDMS) properties for biomedical micro/nanosystems., Biomed. Microdevices. 7 (2005) 281–93. https://doi.org/10.1007/s10544-005-6070-2.

[72] K. Raj M, S. Chakraborty, PDMS microfluidics: A mini review, J. Appl. Polym. Sci. 137 (2020) 1–14. https://doi.org/10.1002/app.48958.

[73] A.W. Martinez, S.T. Phillips, M.J. Butte, G.M. Whitesides, Patterned paper as a platform for inexpensive, low-volume, portable bioassays, Angew. Chemie - Int. Ed. 46 (2007) 1318–1320. https://doi.org/10.1002/anie.200603817.

[74] X. Li, J. Tian, G. Garnier, W. Shen, Fabrication of paper-based microfluidic sensors by printing, Colloids Surfaces B Biointerfaces. 76 (2010) 564–570. https://doi.org/10.1016/j.colsurfb.2009.12.023.

[75] L. Cai, Y. Wang, Y. Wu, C. Xu, M. Zhong, H. Lai, J. Huang, Fabrication of a microfluidic paper-based analytical device by silanization of filter cellulose using a paper mask for glucose assay, Analyst. 139 (2014) 4593–4598. https://doi.org/10.1039/C4AN00988F.

[76] H. Yagoda, Applications of Confined Spot Tests in Analytical Chemistry: Preliminary Paper, Ind. Eng. Chem. Anal. Ed. 9 (1937) 79–82. https://doi.org/10.1021/ac50106a012.

[77] P. de Tarso Garcia, T.M. Garcia Cardoso, C.D. Garcia, E. Carrilho, W.K. Tomazelli Coltro, A handheld stamping process to fabricate microfluidic paper-based analytical devices with chemically modified surface for clinical assays, RSC Adv. 4 (2014) 37637–37644. https://doi.org/10.1039/C4RA07112C.

[78] W. Dungchai, O. Chailapakul, C.S. Henry, A low-cost, simple, and rapid fabrication method for paper-based microfluidics using wax screen-printing, Analyst. 136 (2011) 77–82. https://doi.org/10.1039/C0AN00406E.

[79] S. Ma, Y. Tang, J. Liu, J. Wu, Visible paper chip immunoassay for rapid determination of bacteria in water distribution system, Talanta. 120 (2014) 135–140.

https://doi.org/10.1016/j.talanta.2013.12.007.

[80] E. Carrilho, A.W. Martinez, G.M. Whitesides, Understanding Wax Printing: A Simple Micropatterning Process for Paper-Based Microfluidics, Anal. Chem. 81 (2009) 7091–7095. https://doi.org/10.1021/ac901071p.

[81] C.L. Cassano, Z.H. Fan, Laminated paper-based analytical devices (LPAD): fabrication, characterization, and assays, Microfluid. Nanofluidics. 15 (2013) 173–181. https://doi.org/10.1007/s10404-013-1140-x.

[82] E.M. Fenton, M.R. Mascarenas, G.P. López, S.S. Sibbett, Multiplex Lateral-Flow Test Strips Fabricated by Two-Dimensional Shaping, ACS Appl. Mater. Interfaces. 1 (2009) 124–129. https://doi.org/10.1021/am800043z.

[83] D.M. Cate, J.A. Adkins, J. Mettakoonpitak, C.S. Henry, Recent Developments in Paper-Based Microfluidic Devices, Anal. Chem. 87 (2015) 19–41. https://doi.org/10.1021/ac503968p.

[84] J. Nie, Y. Liang, Y. Zhang, S. Le, D. Li, S. Zhang, One-step patterning of hollow microstructures in paper by laser cutting to create microfluidic analytical devices, Analyst. 138 (2013) 671–676. https://doi.org/10.1039/C2AN36219H.

[85] D.M. Cate, J.A. Adkins, J. Mettakoonpitak, C.S. Henry, Recent Developments in Paper-Based Microfluidic Devices, Anal. Chem. 87 (2015) 19–41. https://doi.org/10.1021/ac503968p.

[86] M. Reches, K.A. Mirica, R. Dasgupta, M.D. Dickey, M.J. Butte, G.M. Whitesides, Thread as a Matrix for Biomedical Assays, ACS Appl. Mater. Interfaces. 2 (2010) 1722–1728. https://doi.org/10.1021/am1002266.

[87] X. Li, J. Tian, W. Shen, Thread as a versatile material for low-cost microfluidic diagnostics,

ACS Appl. Mater. Interfaces. 2 (2010) 1–6. https://doi.org/10.1021/am9006148.

[88] R. Safavieh, G.Z. Zhou, D. Juncker, Microfluidics made of yarns and knots: From fundamental properties to simple networks and operations, Lab Chip. 11 (2011) 2618–2624. https://doi.org/10.1039/c1lc20336c.

[89] S. Xing, J. Jiang, T. Pan, Interfacial microfluidic transport on micropatterned superhydrophobic textile, Lab Chip. 13 (2013) 1937–1947. https://doi.org/10.1039/c3lc41255e.

[90] B. Das, A. Das, V.K. Kothari, R. Fangueiro, Development of mathematical model to predict vertical wicking behaviour.part I: flow through yarn, J. Text. Inst. 102 (2011) 957–970. https://doi.org/10.1080/00405000.2010.529281.

[91] J. Berthier, K.A. Brakke, D. Gosselin, E. Berthier, F. Navarro, Thread-based microfluidics: Flow patterns in homogeneous and heterogeneous microfiber bundles, Med. Eng. Phys. 48 (2017) 55–61. https://doi.org/10.1016/j.medengphy.2017.08.004.

[92] J.M. Cabot, N.P. Macdonald, S.C. Phung, M.C. Breadmore, B. Paull, Fibre-based electrofluidics on low cost versatile 3D printed platforms for solute delivery, separations and diagnostics; from small molecules to intact cells, Analyst. 141 (2016) 6422–6431. https://doi.org/10.1039/c6an01515h.

[93] T. Wu, T. Xu, L.P. Xu, Y. Huang, W. Shi, Y. Wen, X. Zhang, Superhydrophilic cotton thread with temperature-dependent pattern for sensitive nucleic acid detection, Biosens. Bioelectron. 86 (2016) 951–957. https://doi.org/10.1016/j.bios.2016.07.041.

[94] H. Li, C. Liu, D. Wang, C. Zhang, Programmable fluid transport on photolithographically micropatterned cloth devices: Towards the development of facile, multifunctional colorimetric

diagnostic platforms, Sensors Actuators, B Chem. 255 (2018) 2416–2430. https://doi.org/10.1016/j.snb.2017.08.215.

[95] D.R. Ballerini, X. Li, W. Shen, Flow control concepts for thread-based microfluidic devices, Biomicrofluidics. 5 (2011). https://doi.org/10.1063/1.3567094.

[96] P. Wu, C. Zhang, Low-cost, high-throughput fabrication of cloth-based microfluidic devices using a photolithographical patterning technique, Lab Chip. 15 (2015) 1598–1608. https://doi.org/10.1039/c4lc01135j.

[97] M. Liu, C. Zhang, F. Liu, Understanding wax screen-printing: A novel patterning process for microfluidic cloth-based analytical devices, Anal. Chim. Acta. 891 (2015) 234–246. https://doi.org/10.1016/j.aca.2015.06.034.

[98] P. Bhandari, T. Narahari, D. Dendukuri, Fab-Chips: A versatile, fabric-based platform for low-cost, rapid and multiplexed diagnostics, Lab Chip. 11 (2011) 2493–2499. https://doi.org/10.1039/c1lc20373h.

[99] T.L. Owens, J. Leisen, H.W. Beckham, V. Breedveld, Control of microfluidic flow in amphiphilic fabrics, ACS Appl. Mater. Interfaces. 3 (2011) 3796–3803. https://doi.org/10.1021/am201003b.

[100] S.H. Jeon, K.H. Hwang, J.S. Lee, J.H. Boo, S.H. Yun, Plasma treatments of wool fiber surface for microfluidic applications, Mater. Res. Bull. 69 (2015) 65–70. https://doi.org/10.1016/j.materresbull.2015.02.025.

[101] S. Farajikhah, J. Choi, D. Esrafilzadeh, J. Underwood, P.C. Innis, B. Paull, G.G. Wallace, 3D textile structures with integrated electroactive electrodes for wearable electrochemical sensors, J. Text. Inst. 111 (2020) 1587–1595. https://doi.org/10.1080/00405000.2020.1720968.

[102] S. Khaliliazar, I. Öberg Månsson, A. Piper, L. Ouyang, P. Réu, M.M. Hamedi, Woven Electroanalytical Biosensor for Nucleic Acid Amplification Tests, Adv. Healthc. Mater. 10 (2021) 1–10. https://doi.org/10.1002/adhm.202100034.

[103] J.M. Cabot, L.Y. Daikuara, Z. Yue, P. Hayes, X. Liu, G.G. Wallace, B. Paull, Electrofluidic control of bioactive molecule delivery into soft tissue models based on gelatin methacryloyl hydrogels using threads and surgical sutures, Sci. Rep. 10 (2020) 1–10. https://doi.org/10.1038/s41598-020-63785-z.

[104] C. Carrell, A. Kava, M. Nguyen, R. Menger, Z. Munshi, Z. Call, M. Nussbaum, C. Henry, Beyond the lateral flow assay: A review of paper-based microfluidics, Microelectron. Eng. 206 (2019) 45–54. https://doi.org/10.1016/j.mee.2018.12.002.

[105] A. Nilghaz, L. Zhang, M. Li, D.R. Ballerini, W. Shen, Understanding thread properties for red blood cell antigen assays: Weak ABO blood typing, ACS Appl. Mater. Interfaces. 6 (2014) 22209–22215. https://doi.org/10.1021/am505849e.

[106] A. Prabhu, G. Nandagopal M. S., P. Peralam Yegneswaran, V. Prabhu, U. Verma, N.K. Mani, Thread integrated smart-phone imaging facilitates early turning point colorimetric assay for microbes, RSC Adv. 10 (2020) 26853–26861. https://doi.org/10.1039/d0ra05190j.

[107] D. Bartholomeusz, J.D. Andrade, D.A. Bartholomeusz, R.W. Boutté, J.D. Andrade, Xurography – Rapid Prototyping of Microstructures Using a Cutting Plotter Xurography : Rapid Prototyping of Microstructures Using a Cutting Plotter, (2006). https://doi.org/10.1109/JMEMS.2005.859087.

[108] A. Mohammadzadeh, A.E. Fox-Robichaud, P.R. Selvaganapathy, Rapid and inexpensive method for fabrication of multi-material multi-layer microfluidic devices, J. Micromechanics

Microengineering. 29 (2019) 015013. https://doi.org/10.1088/1361-6439/aaf25a.

[109] A. Mohammadzadeh, A.E.F. Robichaud, P.R. Selvaganapathy, Rapid and Inexpensive Method for Fabrication and Integration of Electrodes in Microfluidic Devices, J. Microelectromechanical Syst. (2019) 1–9. https://doi.org/10.1109/jmems.2019.2914110.

[110] M. Islam, R. Natu, R. Martinez-Duarte, A study on the limits and advantages of using a desktop cutter plotter to fabricate microfluidic networks, Microfluid. Nanofluidics. 19 (2015) 973–985. https://doi.org/10.1007/s10404-015-1626-9.

[111] D.I. Walsh, D.S. Kong, S.K. Murthy, P.A. Carr, Enabling Microfluidics: from Clean Rooms to Makerspaces, Trends Biotechnol. 35 (2017) 383–392. https://doi.org/10.1016/j.tibtech.2017.01.001.

Chapter 2: Isoelectric Gating Using Agarose

Full Citation: S. Damodara, D.J. Dwivedi, P.C. Liaw, A.E. Fox-Robichaud, P.R. Selvaganapathy, Single step separation and concentration of biomarker proteins using agarose based miniaturized isoelectric gates for point of care diagnostics, Sensors Actuators, B Chem. 330 (2021).

Single step separation and concentration of biomarker proteins using agarose based miniaturized isoelectric gates for point of care diagnostics

Sreekant Damodara[1], Dhruva J. Dwivedi[2] and Patricia C. Liaw[2], Alison E. Fox-Robichaud[2], P. Ravi Selvaganapathy[1]* on behalf of the Canadian Critical Care Translational Biology Group
[1]Department of Mechanical Engineering, McMaster University, Hamilton, CANADA
[2]Department of Medicine, McMaster University, Hamilton, CANADA

Abstract: Bedside diagnostics using protein biomarkers requires rapid concentration, isolation and measurement of these specific biomarkers from a complex matrix in a low cost and portable manner. Traditional separation using gel electrophoresis separates the sample into all its constituent elements and requires high voltages and/or long runtime which is often unnecessary for diagnostics where only a specific biomarker needs to be quantified. Digital isoelectric trapping can be used to isolate and concentrate proteins but requires UV cured immobline gels that have defined pH values and are not tunable to target specific proteins. Here, we have developed miniaturized isoelectric gates to separate, concentrate and quantify a targeted biomarker based on its isoelectric point, from a complex matrix in under 20 minutes. We designed specific isoelectric gates to concentrate and quantify bovine serum albumin (BSA) at a concentration of 1-5 mg/mL with a peak concentration of over 300 mg/mL, while maintaining solubility. Next, we demonstrated isolation of human protein C from a mixture with 1000-fold higher concentration of BSA with no additional processing. Finally, we demonstrated rapid (< 20 min) separation, concentration and quantification of ovomucoid in a fresh hen egg using dual isoelectric gates at pH 3.9 and 4.3 to trap ovomucoid with an isoelectric point of 4.1 using a low applied voltage of only 13 V. By using low cost agarose gels instead of expensive immobilines, this device reduced the cost and complexity of separation. The combination of low-cost, tunability, fast-runtime, low-operating voltage makes this technique attractive for use in point-of-care biomarker detection without specific antibodies.

1. Introduction

Proteins perform a wide array of functions within the body including catalysing specific reactions, transporting signals throughout the body, coordinating cellular processes and storing vital molecules. Circulating protein levels are altered in a variety of diseased states including diabetes [1], sepsis [2], and cancer [3]. Identifying, isolating and quantifying proteins in blood is essential to improving our understanding of diseases, aid the discovery of biomarkers and improve diagnostics [4]. However, blood is a complex matrix consisting of over 500 proteins, glucose, mineral ions, dissolved gases and blood cells. Due to the complexity and number of proteins present in blood, various techniques have been developed to separate and quantify proteins.

Immunoassays are the most commonly employed techniques for isolating and measuring the concentration of a protein of interest, however, they require use of specific fluorescent or electrochemical tags [3] which increases the cost of the assay. They also require sample cleaning to reduce nonspecific interactions and are not easily amenable to concentrate proteins. Other common techniques for protein separation use electrophoretic forces in a slab gel based environment [4–7]. These techniques separate proteins based on the size[8], isoelectric point [9] or a combination of both [6]. Miniaturizing separation presents numerous advantages including reduced sample volume, high efficiency separation, efficient heat dissipation and ease of multiplexing [10]. Capillary gel electrophoresis (CGE) has been demonstrated with preconcentration and has been reported showing separation times of under 4 minutes with an applied voltage of 1200 V [11]. A multiplexed fsPAGE running 96-plex PAGE separation in a format similar to slab gels has also been demonstrated showing separation of ovalbumin, BSA and TI in 6 minutes with an applied voltage of 100 V/cm[10]. While CGE presents numerous advantages over macroscale gel electrophoresis, it requires high voltages for rapid separation [12]. Solution based free flow electrophoretic methods were developed to increase

the speed of separation and ease direct sample collection [13]. This includes techniques such as zone electrophoresis, field step electrophoresis and isotachophoresis which separate by electrophoretic mobility and capillary isoelectric focusing (cIEF) which separates by pI have been extensively studied [13]. However, these methods require constant and precise sample flow using an external pump which reduces portability and still requires voltage of over 100 V/cm. In addition to these methods, cIEF in the direction of flow [14,15] has been reported with runtimes as low as 150s with an applied voltages of up to 4000 V [16] which limits its use as a point of care diagnostic method. Combinations of the above methods have been reported to improve separation efficiency such as 2D separation using a combination of IEF and CE on a chip that shows separation in under 5 minutes but requires a voltage of 500 V/cm [17]. These separation methods use high voltages unfeasible for portable applications and are designed to separate the sample into all its constituent elements which is not necessary for diagnostic applications that require the quantification of a single specific biomarker. The separation and quantification of all proteins in a mixture using a continuous separation method such as IEF is dependent on the length of the channel, concentration of the components, electric field and pH gradient used as shown below [17].

$$n = L/4\sigma$$

$$\sigma^2 = \frac{C}{EdpH/dx}$$

Where n is the peak capacity, L is the separation length, σ is the variance of the focused concentration distribution, C is a grouped term representing the properties of the sample species, E is the applied electric field. This relationship results in a limitation in the protein load that can be separated in continuous separations. A high concentration protein would necessitate the use of a high voltage or high pH gradient to ensure separation at the cost of longer runtime, higher temperature, or reduced pH range. Furthermore, proteins precipitate out of solution when they stabilise at their isoelectric

point[18] which further limits the peak concentration that can be separated using continuous pH gradients.

Use of discrete pH barriers (gate) to sort proteins into wells by isoelectric point in place of continuous separation allows for targeted separation and decouples the size of the device (length of the channel) from its resolution. Furthermore, it also maintains the solubility of proteins in solution as the protein is trapped between gates that are at a different pH. This is called isoelectric trapping (IET) and was demonstrated in wells using 120-480 µl of solution per well [19] with various separating membrane such as PVA hydrogels and copolymerizing acrylamide [20]. However, the devices used voltages of up to 1000 V for separation in 20-60 minutes [19]. Commercial IET devices operate at high voltages and require 3-24 hours for operation [19]. Finally, these methods have only been used to sort proteins into large (1pH unit wide) fractions as a sample clean-up or prefractionation step prior to subsequent unit operations [19,21].

Miniaturization and integrating detection with isoelectric traps has been shown using Digital Isoelectric focusing (dIEF) in which proteins tagged with fluorescent markers similar to difference gel electrophoresis (DIGE) gels [3] were separated in an immobiline based IET system [22,23]. However, the fabrication of dIEF devices required photopolymerization of the acrylamide gels in the capillary which increases the cost and complexity of the device, in addition to a high voltage of 50-200 V/cm. The fabrication process in a glass microfluidic device required the formation of a continuous pH gradient before polymerizing sections of it to form gates. As a result, the process retains some of the drawbacks of continuous separation.

The existing methods are not well suited for separating and identifying an individual biomarker typically present at a low concentration (on the order of a few µg/mL) from proteins with close isoelectric points and present at much higher concentrations (on the order of mg/mL) in the same

sample matrix without significantly high voltages or a long runtime (over 30 minutes). Techniques such as IPG cannot be used directly as commercially available IPG strips have a peak loading capacity of 100 µg for a 7 cm strip[24]. As a result, if a sample consists of low biomarker concentration (say ~1-5 µg/ml) with a high concentration of another interfering protein (say ~5 mg/mL), only a fraction (~0.02-0.1 µg) of the biomarker will be trapped in the gel which makes it significantly harder to measure accurate changes in concentration. In such a scenario, immunoassays which can extract low concentration proteins using a specific antibody binding are used. Alternatively, a preparative step to remove high concentration proteins like albumin prior to running slab gel or 2D separation processes or a post separation step with specific binding is used for measurement. In addition to extra complexity, such additional steps alter the composition of sample matrix (such as blood) in unpredictable ways which could reduce the effectiveness of using the assay for diagnostics. At present, to the best of our knowledge, there is no available method that can separate, concentrate and measure the concentration of an individual targeted protein in a single step without using a protein-specific tag while operating at a low voltage and with a rapid runtime. The demonstration of a technique that can accomplish this would be the first step towards the development of a diagnostic device that can be used for bedside detection of a targeted biomarker without specific antibodies or dyes.

Simultaneous concentration, isolation and measurement of a low concentration biomarker [2] from a complex matrix consisting of other proteins at higher concentration in a low-cost and portable device is necessary for point of care diagnostics. For instance, human protein C (hPC) has been identified as a biomarker for sepsis prognostics [25,26]. The current method to isolate hPC from serum requires a multistep process to first remove high concentration proteins such as albumin (50 mg/mL compared to the 5µg/mL of hPC in healthy volunteers). Similarly, ovomucoid is the most prominent allergy causing protein in eggs and has a concentration of 13.2 mg/mL compared to about 65mg/mL of ovalbumin in raw egg white which has a total of 120 mg/mL of proteins. In this paper, we demonstrate

a technique for the simultaneous isolation, concentration and measurement of a targeted protein from a complex mixture using isoelectric gates. The gates were made using low cost, high porosity agarose membranes and cast in a device made of inexpensive xurographically patterned polyethylene terephthalate (PET) [27–29]. The gates are tunable to the protein of interest and enable a versatile platform to isolate proteins in specific range of isoelectric points. Quantitative fluorescence measurement was performed using a non-specific protein tag in combination with a microscope, using both the inbuilt camera and a mounted cell phone, the LG G5. We show that the fabricated device can be used to separate proteins with different isoelectric points even at high concentration differentials while reducing the time needed for separation to 10-20 minutes using an applied voltage of 15 V. hPC was separated and measured from a mixture with BSA present at a concentration 1000 times higher. Separation of a single protein from a more complex matrix was demonstrated by separating, concentrating and measuring ovomucoid concentration from egg white in a single step.

2. Device design and working principle

Selective isolation and trapping of the protein was accomplished by trapping the protein of interest between two pH gates with values targeted to the protein of interest. The pH gates above and below the isoelectric point (pI) of the protein of interest were prepared using buffered agarose gels, and an electric field was applied to trap the protein of interest between the two gates while the rest of the proteins were either blocked from entering the region or allowed to transit through. A device to integrate specific pH gels to function as gates was developed using polyethylene terephthalate (PET) which is a transparent, inert, non-fluorescent material. The fabricated device was mounted onto a fluorescent microscope for real time monitoring of protein concentrations. The microscope itself can be easily miniaturized in the later stages of the development of a true diagnostic device, as a very low magnification was used. Two versions of the device were fabricated, a mono-gated device to

demonstrate the motion of proteins through agarose gels and the concentration and measurement of proteins at the pH gate (Fig. 1(a) and a di-gated device to demonstrate the separation of a low concentration protein from mixtures (Fig. 1(b)).

The device consists of 40 μL reservoirs in the top layer, placed 2.5 mm apart from each other with indents made at the ends to reliably position electrodes as shown in fig. 1(a)(b). The reservoirs were connected through connecting channels in the bottom layer which act as isoelectric gates and were filled with agarose. The gates have dimensions of 4.5x1 mm and were chosen to increase the local electric field intensity while providing adequate buffering capacity. The mono-gated device contains a secondary electrode chamber of radius 1.5 mm, 1mm from the cathode reservoir and connected via a 4 mm wide connector in the bottom layer. This was done to minimize imaging artifacts caused by bubble formation at the cathode, adjacent to the measuring area. This was unnecessary in the di-gated device as the measurements were made in the central reservoir unaffected by bubble formation at the electrodes in the side chambers. Graphite electrodes were used to maintain an inert boundary at the electrode interface and were immersed into the solution at the ends of the device to apply an electric field across the device.

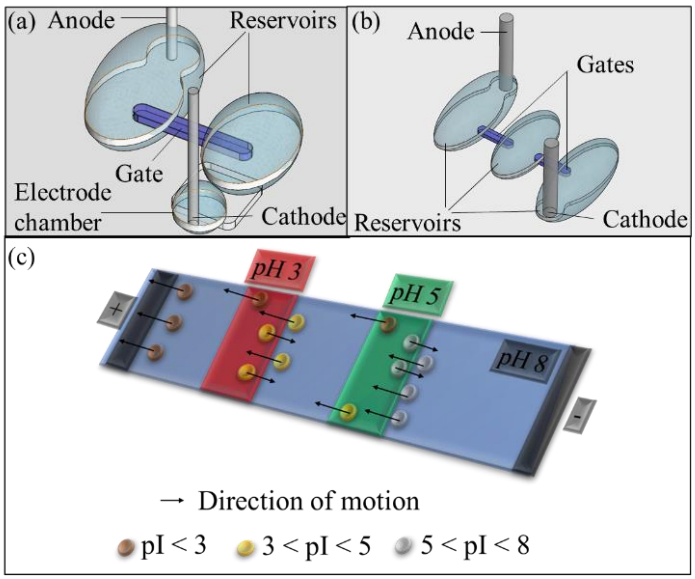

Figure 6: Isometric views of (a) mono-gated device and (b) di-gated device showing the layout of the reservoirs, gates and the position of the secondary electrode chamber in mono-gated devices. (c) Schematic of isoelectric trapping principle.

Agarose gels were used in place of the traditionally used polyacrylamide gels to form the pH gates. Agarose gels are reported to have a pore size of 200–500 nm compared to the 5-100 nm pore size of polyacrylamide gels [30] with some reports for 1% agarose showing a pore size of ~160nm [31]. The higher porosity reduces the drag force experienced by the proteins in motion reducing the required operating voltage and runtime. Microfabrication of the gates using xurography results in a focusing of the applied electric field in the gates enhancing the rate of migration of proteins through them. Numerical simulations using COMSOL multiphysics software (Supplementary material 1 – Figure S1) were used to model the electric field distribution in the device and determine the local electric field at the pH gates. Simulations were run using an applied potential of 15 V to design two versions of the device. The results showed that the electric field was concentrated in the connecting channel regions. The connecting channel in the mono-gated device had a peak field strength of 44.35 V/cm and the di-gated device had a peak electric field of 20.36 V/cm while the reservoirs had an electric field of around 5 V/cm. The much higher electric field in the gel filled connecting channels where the mobility of target proteins while maintaining a low electric field in the higher mobility aqueous phase improves the overall separation time of proteins in the mixture. The electric field obtained in the connecting channels of the device while operating at 15 V is higher than the 10 V/cm obtained in traditional gels operating with 200 V power supplies [9] but lower than high voltage gels.

On application of a potential across the electrodes in the device, proteins buffered in 2x TAE (Tris-acetate-EDTA buffer) (pH 8.2) with pI of less than 8.2 migrate electrophoretically away from the cathode and towards the pH gates. In a mono-gated device used for concentration, the pH of the gate

is set to be slightly lower than the pI of the target protein of interest. When the protein reaches the gate, the protein is trapped at the interface in a constant back and forth motion, concentrating it while maintaining its solubility as the pH of the medium is always slightly above or below the pI of the protein as shown in Fig. 1(c). In a di-gated device used for separation and concentration, a second gel with a pH higher than the pI of the protein is used to screen other proteins with higher pI's. As the pH of gel is higher than the pI of the targeted protein, but less than 8.2, it migrates through the gel at a reduced rate as the direction of the electrophoretic force remains the same. As illustrated in fig. 1(c), proteins with a pI between 3 and 5, can be separated from proteins with a pI <3 or > 5 using gates of pH 3 and 5.

3. Materials and methods

3.1 Materials

Powdered Agarose, 50x TAE buffer concentrate, citric acid, sodium phosphate dibasic, sodium chloride, bovine serum albumin (BSA), gamma globulins from bovine serum and ovomucoid from hen egg were obtained from Sigma Aldrich. Purified protein C concentrate (100µg/mL) was obtained from Thrombosis & Atherosclerosis Research Institute(TaARI). Qubit protein assay kit was obtained from Thermo Fisher Scientific.0.005" thick polyethylene tetraphalate (PET) and 0.002" 7952MP transfer tape were obtained from 3M. Polydimethyl siloxane (PDMS) was obtained from Dow Corning. Graphite rods with a diameter of 0.1" were obtained for use as electrodes from Graphitestore.

Buffers used in the agarose gel gates were prepared by mixing 0.2 - 0.4 M of citric acid and 0.2 - 0.6 M of sodium phosphate dibasic to obtain a pH of 3 - 7. Buffers of pH 7.5 - 8.2 for the reservoirs and sample preparation were obtained by diluting a 50x TAE concentrate to 2x TAE. 2x TAE consisted of 80 mM tris, 40 mM acetic acid and 2 mM EDTA.

Protein samples were prepared by diluting BSA and ovomucoid powders in 2x TAE. Human protein C samples were prepared by diluting a concentrated stock solution of 20 µg/mL obtained from TaARI using 2x TAE . Egg white was obtained from a fresh hen egg and diluted to the required range using 2x TAE. The sample for experiments were prepared by following the protocol for Qubit Protein Assay. Briefly, 1 µl of fluorescent dye was diluted with 199 µl of provided sample buffer on the day of the experiment; 190 µl of this dilution was mixed with 10 µl of protein samples of differing concentrations. These samples were then allowed to mix for 15 minutes before pipetting 40 µl into the device. This dye tags all proteins in the sample up to a maximum of 5 mg/mL, as stated in the data sheet. The dye binds by simple charge interaction and does not bind by hydrogen or covalent binding, so it is expected to have minimal effect on the pI of the protein. This was found to be true in experiments with pH windows of 0.4 units, which is the highest resolution tested during this set of experiments. More thorough characterization will be done at a future date. BSA was used to show separation from a protein at high concentration, due to a similar isoelectric point and weight to human serum albumin (HSA) while being more accessible. It has a molecular weight of 66.4 kDa and an isoelectric point of 5.2 [32] compared to HSA with a weight of 66.4 kDa and isoelectric point of 5.6-5.8 [33]. Protein C is a biomarker for sepsis prognostication and has been shown to decrease from a concentration of 5.3±0.2 µg/ml in healthy individuals and sepsis survivors to 2.05±1 µg/ml in non survivors of sepsis [25]. It has an isoelectric point of 4.4 - 4.8. Ovomucoid is the most allergic component of egg white and has been used to test for egg allergies. It is a trypsin inhibitor with antimicrobial properties that is currently being investigated [34]. It has an isoelectric point of 4.1 and a molecular weight of 28 kDa[35]. A summary of the proteins used, and their isoelectric points are shown in Table 1.

Table 2: Proteins used and their isoelectric points

Protein	Isoelectric point (pI)
Bovine serum albumin (BSA)	5.2 – 5.8
Protein C	4.4 - 4.8
Ovomucoid	4.1
Ovalbumin	4.54

3.2 Fabrication

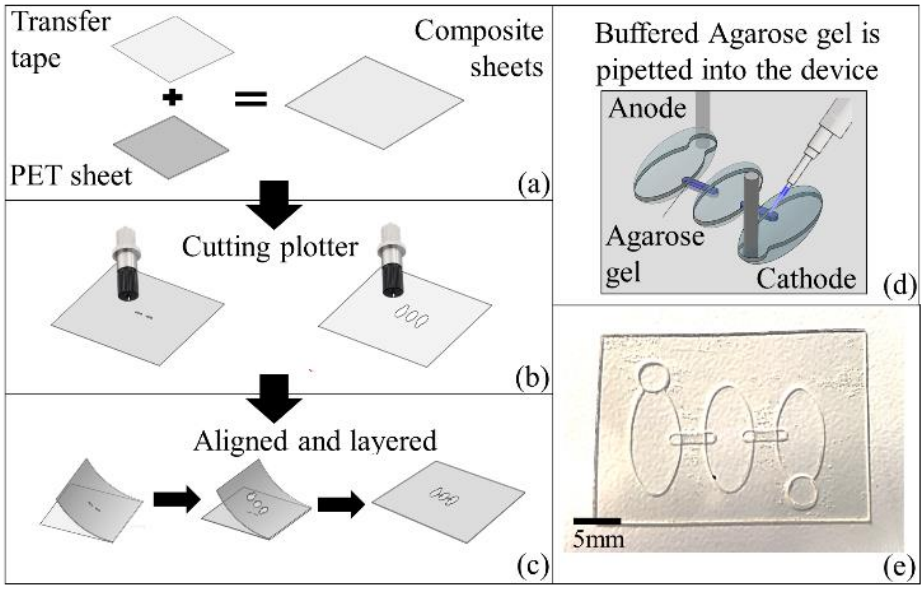

Figure 7: Schematic of the fabrication process showing (a) Combining transfer tape with PET sheet to form composite sheets (b) Shaping of the composite sheets using a cutting plotter (c) Cut sheets were aligned, layered and laminated together to form complete device (d) Pipetting agarose gels into the device and adding buffers prior to use (e) Fabricated device

The device was fabricated using a variation on xurography [27,36]. The fabrication method for a di-gated device is shown in Fig. 2. Polyethylene Tetraphalate (PET) with a thickness of 127 μm was adhered to a double-sided transfer tape[37] and laminated to make composite sheets as shown in Fig 2(a). A cutting plotter (Graphtec FC8600) was used to cut the composite sheets based on channel and reservoir designs as shown in Fig. 2(b). The cut sheets were integrated into a complete device by manually aligning and layering them with the adhesive side of the top layer facing the PET face of the bottom layer and subsequently laminating it as shown in Fig. 2(c). Prior to use, hot agarose at a temperature of 80-90º was pipetted into the channels between the reservoirs which were designed to contain the agarose and maintain a consistent area of contact with the samples in the reservoirs as shown in Fig. 2(d). The device was made to be a low cost, disposable device to prevent cross contamination between samples with an expected cost per assay of less than $1 per run. A cost analysis for a single device is provided in supplementary material 3. High aspect ratio reservoirs for the measurement of the fluorescent intensity of the complete sample was prepared by punching through 1cm tall PDMS and adhering it to 3M tape.

4. Experimental setup

The experimental setup consists of the device placed on a fluorescence microscope (Nikon Eclipse TE2000-S) and connected to a power supply (Trek 677B) which was operated in current limiting mode set at 0.5 mA which resulted in an operational voltage of 10-15 V during the start of the experiments and increase to 21 V over 15 minutes. An excitation window of 455±25 nm and an emission window of 600±30 nm were used for fluorescence imaging. A cell phone, the LG G5 was mounted on the eyepiece of the microscope using a 3D printed holder to increase the field of view compared to the inbuilt camera. The schematic is shown in Fig. 3.

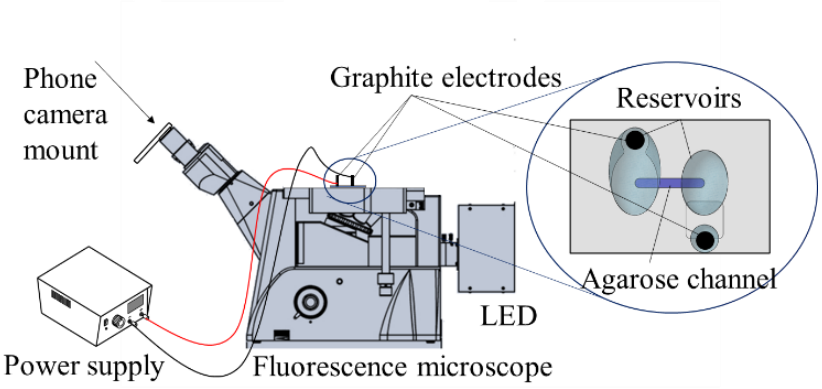

Figure 8: Schematic of experimental setup

Experiments were conducted by pipetting gels with the required pH into the connecting channels, depositing the sample in the anode reservoir and 2x TAE buffer in the other reservoirs. Every run was conducted in a new device, which was discarded appropriately after the run. A 20 µL volume of each solution was used in the mono-gated devices and 40 µL in the di-gated devices. The prepared device was then placed on a fluorescent microscope for observation and graphite electrodes were placed at the far end of the reservoirs and connected to the power supply. Images were captured using the camera on the LG G5 mounted on the microscope eyepiece using OpenCamera or the inbuilt point grey camera FL3-U3-32S2C-CS. The LG G5 images were taken with a shutter speed of 1.5 s. The point grey camera images were taken with a shutter speed of 400 ms. Images were taken every 30 seconds to capture time variation of fluorescence intensity during concentration.

Image processing

The RAW images obtained from the cameras were analysed using ImageJ. The images from the point grey camera were used for mono-gated devices. The images were centred at the entrance to the gel which was then analysed using ImageJ. A macro code (Supplementary material 2) was used to calculate the change in integrated density of the image, termed as Relative Integrated Density (RID) to separate the low intensity artifacts produced by bubble generation from the higher intensity change

in fluorescence intensity due to concentration. The phone camera (LG G5) was used for di-gated devices and the average greyscale intensity of the full image centred at the entrance to the second gel was plotted against the concentration of protein C. RID was not required for di-gated devices due to the separation of the measurement region from the electrodes by the gel filled channel. Intensities were measured for three samples at each concentration and their means and standard deviations were calculated.

pH stability analysis

The pH of the gels was tested for stability using a colorimetric universal pH sensing dye. Images were taken every minute using a microscope. The images had their contrast enhanced to improve visibility of the dye and converted to the HSB (Hue-saturation-brightness) color space. The Hue in a region of interest (ROI) spanning the width of the gel and a length of 0.5mm were calculated using ImageJ. The relative change in hue was plotted to observe the changes in pH.

5. Results and discussion

5.1 Agarose based isoelectric gates

Isoelectric gates were fabricated using agarose gels to control the motion of proteins by altering the local pH environment around the proteins. They were fabricated by using high concentration solutions of citrate-phosphate buffer and adding 1% agarose. The solution was then heated in a microwave and allowed to dissolve completely before pipetting into the connecting channels. Using agarose in place of the traditional immobilized pH gradient gels (IPG) enables tuning pH of the gel to target a specific protein. However, transport by diffusion and electrokinetics can affect the stability of the pH in the gel region. In particular, the stability of pH in a hydrogel when exposed to electric fields has not been previously tested. To determine the stability of agarose pH gates and the mechanisms associated with the change in pH, several experiments were conducted. First, mono-gated and di-gated devices with

gates of pH of 4.3 and 6.2 were used. A solution of 2x TAE with a pH 8.2 was filled in the reservoirs. The colorimetric change in pH over time in the middle section of the gates was measured as described in methods section.

The images obtained over 30 mins are shown in Fig. 4(a) and its quantification is shown in Fig 4(b). When no potential was applied, there was virtually no visible change in the hue of the gel indicating that pure diffusional transport of buffering ions out of the gel and into the reservoirs is not significant over the durations of a typical assay. This is expected as the gel prevents convective mixing between the reservoir and channel while the higher buffering capacity of the gel buffer compared to the reservoirs mitigates change in pH.

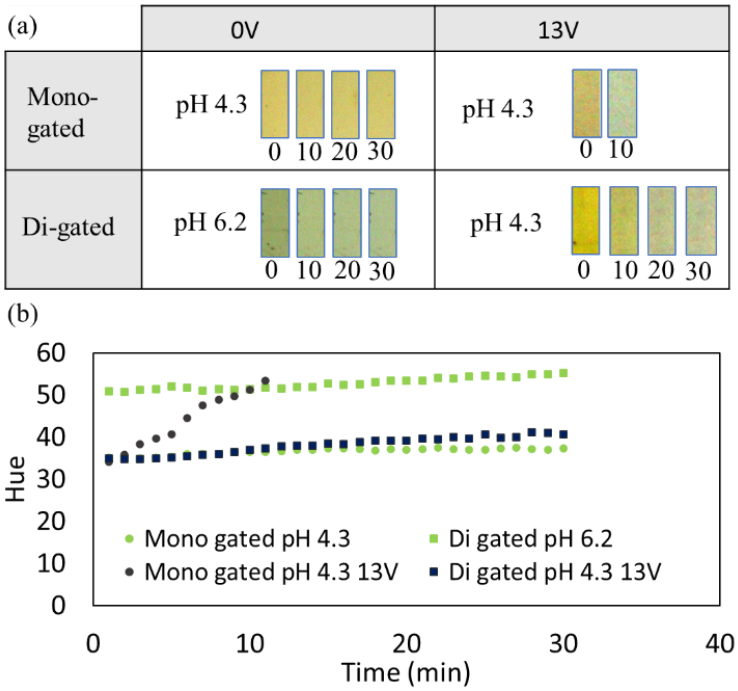

Figure 9: Colorimetric testing of pH stability in (a) mono and di-gated devices with no current applied(b) Stability graphs with no current (in green) and at 13V (in blue) in mono-gated (circle) and di-gated devices (square).

Next, experiments were repeated with the application of a potential of 13 V across the ends of the device which corresponds to an electric field of 38.44 V/cm and 19.22 V/cm in pH gates of the mono-gated and di-gated device, respectively. This low voltage is typical of operation of our device and ensures portability. Images obtained over a period of 30 minutes are shown in Fig 4(a) and quantified in Fig 4(b). The application of electric field has a significant effect on pH. The resulting electric field reduces pH stability of the device potentially due to a combination of electroosmotic flow through the gel and the formation of acidic and basic ions at the anode and cathode respectively which alter the local pH at the electrode. This overcomes the buffering capacity of the solution in the reservoirs and reduces the buffering capacity of the gels much more rapidly than just diffusive interaction between the buffering solution and the gel. The mono-gated device showed slow gradual deterioration of the pH gate till ~7 minutes followed by a dramatic change in pH after as evidenced by the change in slope as shown in Fig. 4(b). This change in pH can result in the movement of the trapped protein into the gel after a fixed time. The di-gated device showed only a gradual degradation of the gate over the 30 minutes due to the lower effective electric field applied at the gates and due to each gate being affected by only acidic or basic ions. As a result, the mono-gated device can be used for rapid concentration and quantification in under 7 minutes with a large gap between the pH of the gate and the pI of the trapped protein to account for the degradation of the gate in the 7 minute window. Due to the need for this, the mono gated device cannot be used for separations but can be used for concentration. Di-gated devices, due to the higher stability can be used simultaneous separation, concentration and quantification.

5.2 Transport/accumulation at isoelectric gates

The use of isoelectric gates to control the transport or accumulation of proteins based on the pH of the gels was demonstrated using samples containing 1-5 mg/mL of bovine serum albumin (BSA) in a

mono-gated device. Two devices with pH gates of pH 4.3 and 6.2 respectively were used to demonstrate the behaviour of BSA (pI 5.2) at gates above and below its pI. A 20 μL sample of 5mg/mL BSA buffered with 2x TAE at pH 8.2 was loaded into the sample reservoir and 2x TAE was loaded in the second reservoir. An electric field of 15 V, corresponding to an electric field of 44.35 V/cm was applied across the device for 15 minutes. An illumination of 15% of the LED was used to obtain images every 30 seconds. On application of the field, the BSA buffered in 2x TAE is negatively charged and migrates away from the cathode and is trapped at the interface between the pH 4.3 gate (pH less the isoelectric point of BSA) and the sample reservoir as shown in Fig. 5(a) resulting in its accumulation at that interface. After ~10 minutes, when the pH of the gel begins to change, the BSA breaks through the gel along with the interface at which the gel pH is lower than the isoelectric point of BSA as shown in Fig. 5(a). When the pH 6.2 gel gate device is used instead, BSA maintains its negative charge on entering the gel and is transported through the pH 6.2 gel with no accumulation as shown in Fig. 5(b). This demonstrates that the agarose gel can be used as a gate to control the transport of proteins and by tuning its pH, the gel gate can be designed to trap and concentrate a protein of known pI.

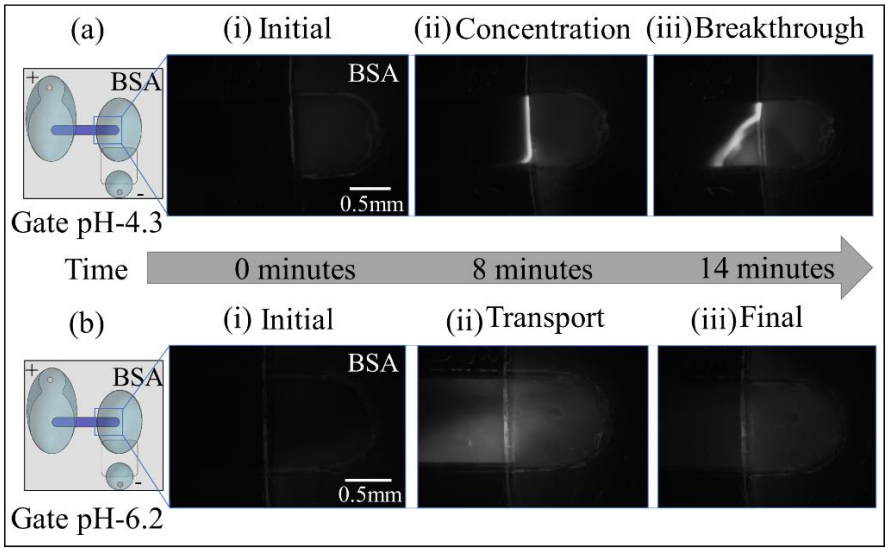

Figure 10: (a-i,ii) Concentration of BSA with isoelectric point of 5.2 - 5.8 trapped at a pH barrier of pH 4.3 (iii) Breakthrough of BSA due to change in pH of gate (b) Transport of BSA through a pH barrier of pH 6.2.

5.3 Simultaneous concentration and quantification of BSA in mono-gated devices

While the previous experiment shows the qualitative concentration of a protein at the interface, the next objective was to show that the device can be used simultaneously accumulate and measure the concentration of the protein in the sample. To demonstrate this application, BSA was used as a model protein and samples of buffered BSA were dispensed into a mono-gated device with a gate at a pH 3. Even though BSA's isoelectric point was between 5.2 - 5.8, a significantly lower pH gate was used to prevent breakthrough of protein through the gate during these experiments. Three samples each of 2x TAE containing BSA at concentrations of 0.25, 0.5, 1.0, 2.0, 5.0 mg/mL were prepared using the procedure described in the methods section and an electric field of 44.35 V/cm (13 V) was applied to concentrate the protein in the sample at the gate for about 10 minutes. This timeframe ensured that the entire protein in the sample well was concentrated, and the intensity reached a steady value. Fluorescent images were obtained every 30 seconds and RID calculated from the measured intensity

at the reservoir-gel channel interface of the pH 3 gate. The change of RID with time using a sample with 0.5 mg/mL BSA is plotted in Fig. 6(a) and shows an increase with time indicating an increase in protein concentration at the interface. There is a slow increase in protein concentration for the first ~80 s before the growth rate increases rapidly due to the ovoid droplet shape of the reservoir. The distribution of protein in the reservoir results in a time delay before the bulk of the protein from the central, high volume region of the reservoir flows towards the gate. The RID then plateaus after 200 seconds of concentration when all the protein in the reservoir is accumulated at the gate. This behaviour was observed at all protein concentrations with varying plateauing times. The steady state RID's at each concentration are plotted against the initial concentration of the samples in Fig. 6(b) and show the increase in saturation intensities with initial concentration. The graph shows a reduction in slope as sample concentrations are increased above 1 mg/mL. This behaviour at higher concentration is expected due to the protein concentration reaching the saturation limit of the Qubit fluorescent dye (5 mg/mL) as mentioned in the data sheet. The correlation between the final intensity and the initial protein concentration of the sample shows that the device can be used for measurement of protein concentration in a sample using a gel at pH lower than the pI of the protein of interest. Of note is that no BSA was precipitated out of solution despite local concentration at the interface exceeding 300 mg/mL in an environment with a high salt concentration.

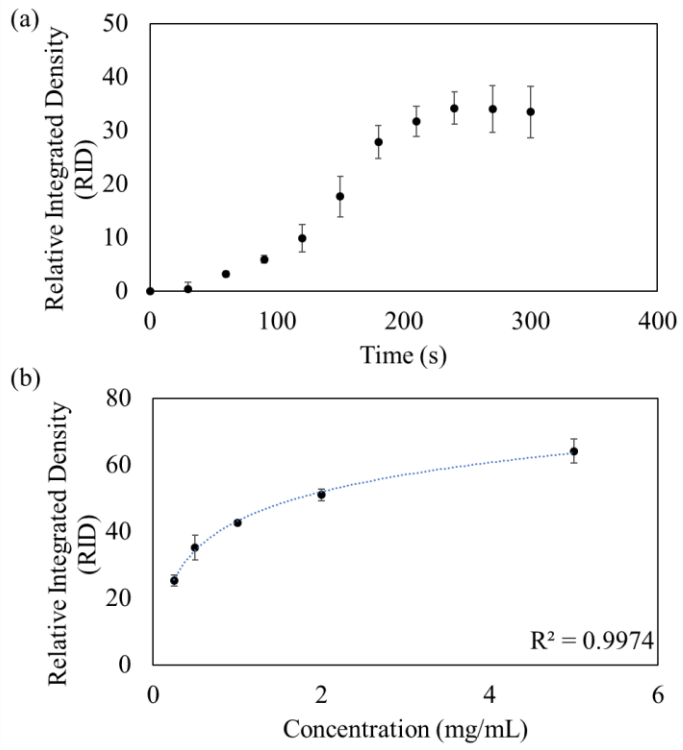

Figure 11: (a) Saturation of RID after electrophoresis for 5 using samples with a concentration of 0.5 mg/mL BSA (n=3) (b) Graph showing increase in RID at saturation at different concentrations of BSA (n=3)

5.4 Simultaneous separation, concentration and quantification of Protein C in di-gated devices

The next step was to show the utility of using pH gates to simultaneously separate the protein of interest from other high proteins in the mixture while concentration and measuring its intensity. A fundamental advantage possessed by the device over continuous separations, where the concentration of the other proteins is unimportant is also demonstrated. This is necessary for a bedside diagnostic device as biomarkers are normally present in a sample with other proteins at higher concentrations. Protein C is a natural anticoagulant that inhibits the blood coagulation cascade. Low plasma levels of protein C have been shown to predict poor outcome in sepsis, a condition characterized by a

systemic hypercoagulable state[24] in sepsis. A reduction in concentration from 5 µg/mL to about 1 µg/mL was found in non survivors of sepsis [25]. However, it is normally found in plasma mixed with albumin (concentration of about 50 mg/mL) and requires multiple steps for separation and measurement.

We show the use of a di-gated device for simultaneous separation, concentration and measurement of 1 - 5 µg/mL of human Protein C (hPC) from a mixture with 5 mg/mL BSA using gates of pH 3 and 5. A concentration of 5 mg/mL for BSA was used as that was the saturation limit of the dye when following the established protocol. Human protein C has a molecular weight (56 kDa) similar to BSA and an isoelectric point of 4.4 - 4.8. As the properties of BSA are similar to HSA, this was used as a test case to show the efficacy of this device in separating proteins of widely different concentrations. First, experiments were conducted using three samples each of different concentration of hPC (0.0, 1.0, 2.0, 5.0 µg/mL) in 2x TAE buffer to form a baseline measurement of the fluorescent intensity. The hPC migrates through the pH 5 gate and collects at the pH 3 gate as it has an isoelectric point below 5 and above 3. The average intensity at the pH 3 gate shown in Fig. 7 (light blue) for samples with various concentrations of hPC. To measure the fraction of protein C trapped at the interface, three reservoirs made with high aspect ratio PDMS was filled with 40 µL of a 5 µg/mL buffered hPC and the fluorescence intensity was measured. Next, three samples each were prepared with a mixtures of 0.0, 1.0, 2.0, 5.0 µg/mL of hPC and 5mg/mL of BSA which were then assayed on the di-gated device. The pH 5 gate is expected to block the BSA from moving into the field of view of the microscope due to its higher isoelectric point while allowing the hPC to pass through it. The hPC is accumulated at the pH 3 gate as before. As the transport of the hPC is identical in both cases, the obtained intensities should match up with the earlier obtained values using pure hPC. The intensities obtained at the pH 3 gate with the mixture samples is as shown in Fig. 7 (dark blue). Following this, an additional three samples consisting of 5 µg/mL hPC, 5 mg/mL BSA in the same buffer with the

addition of 90 mM of sodium chloride were prepared. These samples were prepared with a salt concentration of~300 mmol/L compared to the ~120 mmol/L of 2x TAE used before and were used to verify that the device could be used at physiological salt concentration (289±3 mmol/L[38]) without desalting. The samples were run following the same protocol, and the fluorescent intensity measured.

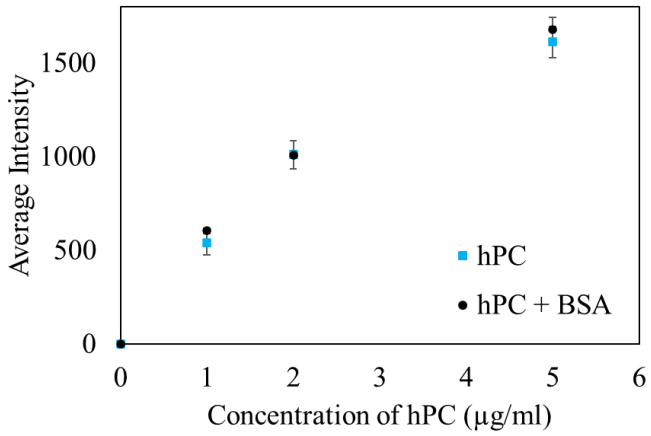

Figure 12: Fluorescent intensity of different concentrations of human protein C in buffered sample (light blue) and after separation from BSA (dark blue) using 2 barriers of pH 3 and 5 (n=3)

The intensity of 5 µg/mL of hPC that was measured was 1614 ± 82. When compared to the complete fluorescence intensity obtained using the 40µL sample, which had an intensity of 1843±108, the device had a capture efficiency of 87.5±6.8%. This is similar to the efficiency reported previously using PEG coated PDMS. Following the separation from BSA, the intensity of hPC accumulated at pH 3 were slightly higher than that obtained from hPC alone by about 15%, 1.4% and 5.3% respectively at 1.0, 2.0 and 5.0 µg/mL of hPC. The increase in intensity can be due to the dispersed light from the concentration of BSA at the pH 5 gate which is also tagged by the fluorescent dye adding to the visible intensity. The non-linearity of the measured intensities is inherent to the fluorescent response of the dye [39]. The fluorescent intensity obtained using the sample with a physiological salt concentration containing 5 µg/mL hPC and 5 mg/mL BSA was 1561±156, which was 6.95% less than that obtained using the 2x TAE samples (1678±66) showing that the test can be

conducted without a previous desalting step, simplifying the workflow and enabling single step protein testing. In addition, as the intensities of 1.0, 2.0 and 5.0 μg/mL of hPC were clearly distinguishable from each other, we verify that the di-gated device can be used for simultaneous separation, concentration and measurement of a low concentration biomarker protein from higher concentration proteins in the mixture even with a three-order difference in concentration, and at physiological salt concentrations.

5.5 Isolation of Ovomucoid from egg white in di-gated devices

A di-gated device with a narrower pH window tuned to a target protein was then used to demonstrate separation and measurement of that protein from a complex matrix which is necessary to extract information on biomarker concentration in real world applications. For this purpose, we show the separation of ovomucoid from egg white. Ovomucoid is a prominent allergen causing protein in egg white and is used for allergy testing which requires its separation from egg white. Measurement of IgE response to ovomucoid concentrations helps predict symptomatic allergic reactions [40]. However, current methods for separation require multiple steps for separating and quantifying the concentration of ovomucoid in egg white due to the presence of a complex surrounding matrix with a wide variety of proteins at different concentrations [34].

Ovomucoid has an isoelectric point of 4.1 and has a concentration of 13.2 mg/mL. It is present in a mixture with numerous other proteins, fats, vitamins, and glucose. The major protein components in egg white with a similar pH range are ovalbumin with a concentration of about 65 mg/mL, pI of 4.54 and ovomucin with a concentration of 4.2 mg/mL, pI of 4.5 - 5. The numerous other proteins alongside the above mentioned add up to a total concentration of 120 mg/mL of protein. To separate the target protein with a pI of 4.1, an upper pH gate of 4.3 was chosen to maintain adequate charge on ovomucoid during motion through the gate while separating it from ovalbumin and ovomucoid. A

lower gate 0.2 pH units below the pI of ovomucoid was chosen to ensure that no other major proteins were trapped in the central reservoir. As a result, a lower pH gate of 3.9 was used.

As the concentration of proteins in egg white was much higher than measurement range of the optical detection unit, the egg white samples were diluted 4000 times so that the concentration of ovomucoid was diluted to ~ 3.3 µg/mL [34] based on literature values, which brought it to the same range as previously used in the measurement of hPC (1 - 5 µg/mL).

The di-gated device with gates of pH 4.3 and 3.9 was setup following the same protocol as used for hPC measurement previously. Calibration was performed ovomucoid buffered in TAE with three samples each at concentrations of 0.0, 1.0, 3.0 and 5.0 µg/mL. The samples were analysed on the di-gated device where the ovomucoid passed through the pH 4.3 gate and was collected at the pH 3.9 gate to obtain fluorescent intensities as shown in Fig. 8.

Following the calibration of the device, 3 samples of diluted egg white were analysed on the device. The other proteins in egg white either pass through both the pH 3.9 and 4.3 gate if their isoelectric point is under 3.9 or collect at the pH 4.3 gate if their isoelectric point is more than 4.3 while only ovomucoid collects at the pH 3.9 gate. The measured intensity at the pH 3.9 gate was then compared to the previously obtained calibration curve to measure the ovomucoid concentration in the egg white sample, which was found to be 3.22±0.28 µg/mL. This matches well with the value of about 3.3 µg/mL[34] expected after the 4000 fold dilution. As the fluorescent dye used binds to all proteins in egg white, measuring a concentration within the expected concentration range implies that none of the other egg white proteins such as ovalbumin (pI 4.5, expected concentration of 16.2 µg/mL [35]) or ovomucin (pI 4.5 - 5, expected concentration of 1 µg/mL [35]) entered the detection window. The measured intensity at different concentrations is very similar to those obtained with hPC after separation from BSA with slightly higher variation due to the different rates of motion as the proteins

pass through the pH gate. These results indicate the possibility of using the device to measure protein concentration without prior calibration for the protein as the fluorescent intensity obtained is protein agnostic. They demonstrate the use of the device as a method for targeted, rapid separation of a protein of choice from a matrix consisting of numerous other proteins using a tunable pH window. While the current size of the window is 0.4 pH units, additional work can be done to further stabilize the pH in the gels and increase the resolution of the device for more complex matrices such as blood.

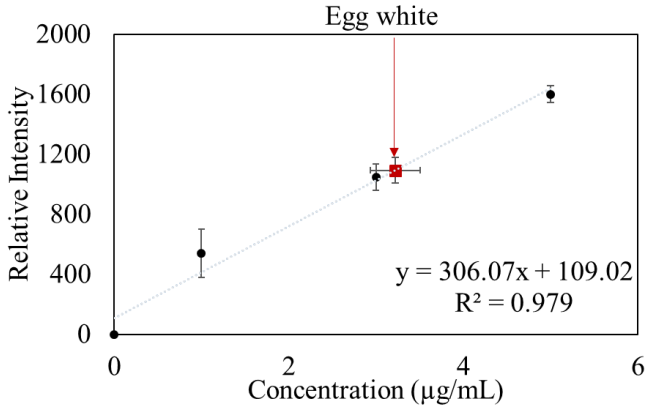

Figure 13: Graph comparing concentration of ovomucoid and intensity and measured intensity of ovomucoid in egg white (In red)

6. Conclusion

A rapid, low cost, highly miniaturized technique to separate a protein based on its isoelectric points using discrete, tuneable pH barriers made with agarose gels was demonstrated. pH-selective movement of BSA was demonstrated using pH barriers of pH 4.3 and 6.2 and a runtime of 15 minutes. BSA samples of different concentrations were run, and the correlation between Relative Integrated Density of fluorescence with the concentration of the protein was shown to demonstrate the ability to use the device for simultaneous concentration and quantitative protein measurement while maintaining solubility of proteins at extremely high concentrations. Simultaneous separation, concentration and measurement of a low concentration protein in the presence of a high

concentration protein was demonstrated by measurement of 1 – 5 µg/mL of human protein C in the presence of 5 mg/mL of BSA using barriers of pH 3 and 5. Selective concentration of a protein from a complex mixture was demonstrated by isolating, concentrating and measuring ovomucoid from egg white using gated of pH 3.9 and 4.3 that are tuned to the pI of ovomucoid (4.1). The obtained concentration was compared to literature-based values to show that no other major proteins were present in the same reservoir. This is also the highest resolution separation that has been obtained currently, with a pH difference of 0.3 pH units. While application of the device for diagnostics faces numerous challenges such as improving the resolution to within 0.1 pH units which is the theoretical limit of resolution with our current device as shown in supplementary information 4. This will be done increasing stability of pH gels and reducing electroosmotic flow. In addition, demonstration of the device with a complex matrix containing proteins with overlapping isoelectric points such as human protein C in plasma poses additional challenges. The results show that the developed device is a first step towards the development of a low-cost diagnostic device for isolating, concentrating, and quantifying a specific biomarker from a complex matrix such as egg white rapidly and without any pre-treatment. By judiciously choosing the pH of the gates, single or multiple proteins can be targeted that could be important in rapid screening and triaging for specific disease conditions. Finally, these gates can also be parallelized to identify multiple biomarkers in parallel.

7. Associated content

Supporting Information

COMSOL simulation used to measure field strength in connecting channels (file type, PDF)

Macro code used for measuring RID (file type, PDF)

Cost analysis of device (file type, PDF)

8. Author information

Corresponding Author

* selvaga@mcmaster.ca

Author Contributions

SD and PRS formulated the concept and experimental protocols with inputs from AEF. DJD and PCL provided protein C samples and provided inputs on biomarkers and protein behavior. SD wrote the paper with revisions and inputs from PRS, AEF, PCL and CCCTBG.

9. Acknowledgment

This work was supported by the Natural Sciences and Engineering Research Council of Canada (NSERC) and Canadian Institutes for Health Research (CIHR) through the Collaborative Health Research Program. PRS also acknowledges support from the Canada Research Chairs Program as well as the Discovery Accelerator Supplement grant.

10. References

[1] T. Huang, K. Glass, O.A. Zeleznik, J.H. Kang, K.L. Ivey, A.R. Sonawane, B.M. Birmann, C.P. Hersh, F.B. Hu, S.S. Tworoger, A network analysis of biomarkers for type 2 diabetes, Diabetes. 68 (2019) 281–290. https://doi.org/10.2337/db18-0892.

[2] B.M. Biron, A. Ayala, J.L. Lomas-Neira, Biomarkers for sepsis: What is and what might be?, Biomark. Insights. 10 (2015) 7–17. https://doi.org/10.4137/BMI.S29519.

[3] N. Kočevar, P. Hudler, R. Komel, The progress of proteomic approaches in searching for cancer biomarkers, N. Biotechnol. 30 (2013) 319–326. https://doi.org/10.1016/j.nbt.2012.11.011.

[4] A. Khalilpour, T. Kilic, S. Khalilpour, M.M. Álvarez, I.K. Yazdi, Proteomic-based biomarker discovery for development of next generation diagnostics, Appl. Microbiol. Biotechnol. (2016). https://doi.org/10.1007/s00253-016-8029-z.

[5] K.K.R. Tetala, M.A. Vijayalakshmi, A review on recent developments for biomolecule separation at analytical scale using microfluidic devices, Anal. Chim. Acta. 906 (2016) 7–21. https://doi.org/10.1016/j.aca.2015.11.037.

[6] M. Pergande, S. Cologna, Isoelectric Point Separations of Peptides and Proteins, Proteomes. 5 (2017) 4. https://doi.org/10.3390/proteomes5010004.

[7] P. Smejkal, D. Bottenus, M.C. Breadmore, R.M. Guijt, C.F. Ivory, F. Foret, M. Macka, Microfluidic isotachophoresis: A review, Electrophoresis. 34 (2013) 1493–1509. https://doi.org/10.1002/elps.201300021.

[8] R. Westermeier, Gel Electrophoresis, in: ELS, Wiley, 2013: pp. 1–13. https://doi.org/10.1002/9780470015902.a0005335.pub2.

[9] R. Westermeier, Electrophoresis in Practice, Fifth Edition, Wiley-VCH, 2016.

[10] T. a Duncombe, A.E. Herr, Photopatterned free-standing polyacrylamide gels for microfluidic protein electrophoresis., Lab Chip. 13 (2013) 2115–23. https://doi.org/10.1039/c3lc50269d.

[11] A. V Hatch, A.E. Herr, D.J. Throckmorton, J.S. Brennan, A.K. Singh, Ac0600454.Pdf, (2006) 4976–4984.

[12] M. Dawod, N.E. Arvin, R.T. Kennedy, Recent advances in protein analysis by capillary and microchip electrophoresis, 2017. https://doi.org/10.1039/c7an00198c.

[13] P. Novo, D. Janasek, Current advances and challenges in microfluidic free-flow

electrophoresis—A critical review, Anal. Chim. Acta. 991 (2017) 9–29. https://doi.org/10.1016/j.aca.2017.08.017.

[14] N.T. Tran, I. Ayed, A. Pallandre, M. Taverna, Recent innovations in protein separation on microchips by electrophoretic methods: An update, Electrophoresis. 31 (2010) 147–173. https://doi.org/10.1002/elps.200900465.

[15] G.J. Sommer, A. V Hatch, Review IEF in microfluidic devices, Electrophoresis. (2009) 742–757. https://doi.org/10.1002/elps.200800598.

[16] W. Tan, Z.H. Fan, C.X. Qiu, A.J. Ricco, I. Gibbons, Miniaturized capillary isoelectric focusing in plastic microfluidic devices, Electrophoresis. 23 (2002) 3638–3645. https://doi.org/10.1002/1522-2683(200210)23:20<3638::AID-ELPS3638>3.0.CO;2-Y.

[17] A.E. Herr, J.I. Molho, K.A. Drouvalakis, J.C. Mikkelsen, P.J. Utz, J.G. Santiago, T.W. Kenny, On-chip coupling of isoelectric focusing and free solution electrophoresis for multidimensional separations, Anal. Chem. 75 (2003) 1180–1187. https://doi.org/10.1021/ac026239a.

[18] J.S. Esteve-Romero, A. Bossi, P.G. Righetti, Purification of thermamylase in multicompartment electrolyzers with isoelectric membranes: The problem of protein solubility, Electrophoresis. 17 (1996) 1242–1247. https://doi.org/10.1002/elps.1150170712.

[19] P. Lim, R. North, G. Vigh, Rapid isoelectric trapping in a micropreparative-scale multicompartment electrolyzer, Electrophoresis. 28 (2007) 1851–1859. https://doi.org/10.1002/elps.200600846.

[20] H.C. Fleisher, G. Vigh, Hydrolytically stable, diaminocarboxylic acid-based membranes buffering in the pH range from 6 to 8.5 for isoelectric trapping separations, Electrophoresis. 26 (2005) 2511–2519. https://doi.org/10.1002/elps.200500198.

[21] S.M. Cologna, W.K. Russell, P.J. Lim, G. Vigh, D.H. Russell, Combining isoelectric point-based fractionation, liquid chromatography and mass spectrometry to improve peptide detection and protein identification, J. Am. Soc. Mass Spectrom. 21 (2010) 1612–1619. https://doi.org/10.1016/j.jasms.2010.04.010.

[22] J. Mai, G.J. Sommer, A. V. Hatch, Microfluidic digital isoelectric fractionation for rapid multidimensional glycoprotein analysis, Anal. Chem. 84 (2012) 3538–3545. https://doi.org/10.1021/ac203076p.

[23] G.J. Sommer, J. Mai, A.K. Singh, A. V. Hatch, Microscale isoelectric fractionation using photopolymerized membranes, Anal. Chem. 83 (2011) 3120–3125. https://doi.org/10.1021/ac200073p.

[24] Bio-Rad, ReadyStrip ™ IPG Strip Instruction Manual, Bio-Rad. (n.d.) 1–38. http://www.bio-rad.com/webroot/web/pdf/lsr/literature/4006166G.pdf.

[25] A.E. Fox-Robichaud, L.A. McIntyre, A. Turgeon, R. Green, R. Zarychanski, S. Bagshaw, I. Stiell, A. Worster, B. Rowe, M. Emond, D. Dwivedi, P.C. Liaw, The precise pilot trial: Temporal changes in thrombin generation, protein C levels and activated protein C generation in early septic shock, Am. J. Respir. Crit. Care Med. 181 (2010) 6146. http://ajrccm.atsjournals.org/cgi/reprint/181/1_MeetingAbstracts/A6146?sid=8cb89aaf-c3c2-47cb-8276-ae5c8d143d17%5Cnhttp://ovidsp.ovid.com/ovidweb.cgi?T=JS&CSC=Y&NEWS=N&PAGE=fulltext&D=emed10&AN=70844387%5Cnhttp://sfx.scholarsportal.info/uhn?sid=OVID:embas.

[26] P.C. Liaw, A.E. Fox-Robichaud, K.-L. Liaw, E. McDonald, D.J. Dwivedi, N.M. Zamir, L.

Pepler, T.J. Gould, M. Xu, N. Zytaruk, S.K. Medeiros, L. McIntyre, J. Tsang, P.M. Dodek, B.W. Winston, C. Martin, D.D. Fraser, J.I. Weitz, F. Lellouche, D.J. Cook, J. Marshall, Mortality Risk Profiles for Sepsis, Crit. Care Explor. 1 (2019) e0032. https://doi.org/10.1097/cce.0000000000000032.

[27] D. Bartholomeusz, J.D. Andrade, D.A. Bartholomeusz, R.W. Boutté, J.D. Andrade, Xurography – Rapid Prototyping of Microstructures Using a Cutting Plotter Xurography : Rapid Prototyping of Microstructures Using a Cutting Plotter, (2006). https://doi.org/10.1109/JMEMS.2005.859087.

[28] V. Faustino, S.O. Catarino, R. Lima, G. Minas, Biomedical microfluidic devices by using low-cost fabrication techniques: A review, J. Biomech. 49 (2016) 2280–2292. https://doi.org/10.1016/j.jbiomech.2015.11.031.

[29] M. Islam, R. Natu, R. Martinez-Duarte, A study on the limits and advantages of using a desktop cutter plotter to fabricate microfluidic networks, Microfluid. Nanofluidics. 19 (2015) 973–985. https://doi.org/10.1007/s10404-015-1626-9.

[30] J.L. Viovy, Electrophoresis of DNA and other polyelectrolytes: Physical mechanisms, Rev. Mod. Phys. 72 (2000) 813–872. https://doi.org/10.1103/RevModPhys.72.813.

[31] J.Y. Xiong, J. Narayanan, X.Y. Liu, T.K. Chong, S.B. Chen, T.S. Chung, Topology evolution and gelation mechanism of agarose gel, J. Phys. Chem. B. 109 (2005) 5638–5643. https://doi.org/10.1021/jp044473u.

[32] C.S. Patrickios, E.N. Yamasaki, Polypeptide amino acid composition and isoelectric point. II. Comparison between experiment and theory., Anal. Biochem. 231 (1995) 82–91. https://doi.org/10.1006/abio.1995.1506.

[33] C. Hoogland, K. Mostaguir, J.C. Sanchez, D.F. Hochstrasser, R.D. Appel, SWISS-2DPAGE, ten years later, Proteomics. 4 (2004) 2352–2356. https://doi.org/10.1002/pmic.200300830.

[34] E.D.N.S. Abeyrathne, H.Y. Lee, D.U. Ahn, Egg white proteins and their potential use in food processing or as nutraceutical and pharmaceutical agents-A review, Poult. Sci. 92 (2013) 3292–3299. https://doi.org/10.3382/ps.2013-03391.

[35] Y. Mine, Recent advances in the understanding of egg white protein functionality, Trends Food Sci. Technol. 6 (1995) 225–232. https://doi.org/10.1016/S0924-2244(00)89083-4.

[36] A. Mohammadzadeh, A.E.F. Robichaud, P.R. Selvaganapathy, Rapid and Inexpensive Method for Fabrication and Integration of Electrodes in Microfluidic Devices, J. Microelectromechanical Syst. (2019) 1–9. https://doi.org/10.1109/jmems.2019.2914110.

[37] 3M, 3M(TM) High Performance Adhesive Transfer Tape 7952MP Article, 2016.

[38] S.N. Cheuvront, R.W. Kenefick, K.R. Heavens, M.G. Spitz, A Comparison of Whole Blood and Plasma Osmolality and Osmolarity, J. Clin. Lab. Anal. 28 (2014) 368–373. https://doi.org/10.1002/jcla.21695.

[39] Thermo Fisher Scientific, Qubit ® Protein Assay Kits, (n.d.) 1–10.

[40] H. Ando, R. Movérare, Y. Kondo, I. Tsuge, A. Tanaka, M.P. Borres, A. Urisu, Utility of ovomucoid-specific IgE concentrations in predicting symptomatic egg allergy, J. Allergy Clin. Immunol. 122 (2008) 583–588. https://doi.org/10.1016/j.jaci.2008.06.016.

Chapter 3: Integration of Ba-IMAC with isoelectric gates for protein C measurement in plasma

Microfluidic device for single step measurement of protein C in plasma samples for sepsis prognosis

Sreekant Damodara[1], Dhruva J. Dwivedi[2] and Patricia C. Liaw[2], Alison E. Fox-Robichaud[2], P. Ravi Selvaganapathy[1]* on behalf of the Canadian Critical Care Translational Biology Group
[1]Department of Mechanical Engineering, McMaster University, Hamilton, CANADA
[2]Department of Medicine, McMaster University, Hamilton, CANADA

Abstract

Protein C is a vitamin K dependant protein in plasma that plays an essential role in regulating the coagulation cascade and inflammatory response. As a result of its importance in these roles, it has been suggested as a biomarker for prognosis of patients affected by sepsis. Sepsis is a dysregulated host response to an infection that is the leading cause of mortality in U.S hospitals and results in the most expensive cost of hospitalization. It was found that protein C concentration in non surviving sepsis patients is significantly lower (1.8 µg/mL) than survivors and healthy patients who have a protein C concentration of 3.9-5.9 µg/mL. Current methods for diagnosing sepsis rely on immunoassays which are expensive or functional assays which require multiple steps for isolation and activation of protein C. We demonstrate in this paper a low cost, single step assay for detection of protein C in blood plasma. This was done by combining isoelectric gates with barium-immobilized metal affinity trapping (IMAT). The electric field was optimized for use with IMAT using COMSOL simulation. The integrated device was tested with samples containing buffered protein C, protein C in the presence of high concentration bovine serum albumin and Alpha 1-proteinase inhibitor, and in blood plasma with spiked protein C. The stability of the measured values was tested by monitoring the intensity of a mixture of protein C with BSA and

A1PI every minute to determine that measurement after 40 minutes was optimal. The results showed that the device could be used to distinguish a reduction in protein C from 5.9 µg/mL to 3.4 µg/mL with greater than 98% confidence in plasma making it suitable for sepsis prognosis.

1. Introduction

Protein C is a vitamin K dependant protein zymogen present in plasma that plays an active role in the coagulation cascade. Its average concentration in a healthy human is in a range between 3.9-5.9 µg/mL. Protein C upon activation breaks down to form activated protein C (aPC) which inhibits coagulation and increases fibrinolysis. This interaction plays an essential role in maintaining the balance between coagulation and fibrinolysis in a healthy human [1]. APC also plays a role in decreasing inflammation by inhibiting cytokine production and neutrophil activation. Protein C deficiency in plasma has also been cited as a cause for an increased risk for venous thrombosis. This can be either due to a hereditary transmission of protein C deficiency present in 500,00 to 750,000 births worldwide or due to acquired deficiency from liver disease or vitamin K deficiency [2]. As a result of its role in regulating both coagulation and inflammation, the concentration of Protein C has been studied as a biomarker for sepsis. A recent study showed that Protein C levels decrease to a quarter of the normal range in septic patients [3] and is associated with an increased risk in mortality.

Sepsis is defined as “a life-threatening organ dysfunction caused by a dysregulated host response to infection” by the third international consensus conference organized by Society of Critical Care Medicine and the European Society of Intensive Care Medicine [4]. It has a high hospitalization cost which was estimated to be $62 billion annually in 2003 in the U.S and is the primary cause of readmission. It is the leading cause of mortality and approximately 35% of patients of all hospital

deaths are due to sepsis [5]. Furthermore, sepsis diagnosis is highly time sensitive as the risk of mortality increases by 4-9% with each hour of delay in treatment [6]. However, sepsis is a broad term wherein the clinical criteria or laboratory features that uniquely diagnose sepsis have not yet been identified. As a result, diagnosis currently relies on Sequential Organ Failure Assessment Score (SOFA) for determining the severity of sepsis. Numerous biomarkers have been suggested for the diagnosis and prognostication of sepsis patients [7]. One of these biomarkers that has been identified, particularly due to its role in maintaining the balance in the coagulation cascade and its ability to predict survival in septic patients is Protein C [3]. They report that the level of protein C was reduced to 0.41±0.22 U/mL in non survivors of sepsis and 0.53±0.24 U/ml in survivors as compared to normal individuals (0.61-1.33 U/mL). Furthermore non survivors had a sustained decrease in protein C values after 7 days to below 0.37 U/mL (1.77 µg/mL assuming an average protein C concentration of 4.8 µg/mL [8]) while that of survivors increased to 0.7±0.22 U/mL. Protein C as part of a multivariable approach in combination with cfDNA, platelet count, creatinine, Glasgow Coma Scale [GCS] score, and lactate was shown to have a stronger predictive power (AUC_P28 = 0.9) than the current diagnostic standard, SOFA (AUC_P28 = 0.86)[9]. Of these, Glasgow Coma Scale [GCS] score is a qualitative test; platelet count, creatinine and lactate are routinely evaluated and devices for rapidly detecting cfDNA are being developed [10]. However, the measurement of protein C is a more complicated process at present.

Protein C has a molecular weight of 62 kDa and an isoelectric point (pI) of 4.4-4.8 [11] and is composed of a heavy chain (41 kDa) and a light chain (21 kDa) [12]. On activation, the heavy chain consisting of the serine active site and activation peptide breaks away from the light chain forming activated protein C (aPC) which is used up as a part of the coagulation cascade. The light chain contains a y-carboxyglutamic acid domain (GLA) contains modifications of glutamate

residues by vitamin K-dependent carboxylation to form γ-carboxyglutamate (Gla). This domain has a high affinity for binding with calcium ions. At present the GLA domain is known to exist in coagulation factors II (prothrombin), VII, IX, X, proteins C, S and Z in plasma [13–15].

Due to the exclusivity of binding of the GLA domain, protein C was originally isolated from plasma using its affinity to bind to barium [16]. A precipitate of barium citrate was formed by dropwise addition of 1 M barium chloride to a solution with 0.2 M sodium citrate. Centrifugation of this precipitate formed a pellet which can be resuspended in a solution with 0.2 M ethylenediaminetetraacetic acid to extract the bound proteins, which contain a GLA domain [13]. These proteins are then further separated using ammonium sulfate fractionation, DEAE-Sephadex chromatography, dextran sulfate agarose chromatography, and preparative polyacrylamide gel electrophoresis [17] or other similar sample preparation processes that requires multiple steps [8,16]. An alternative method for the separation of protein C from platelet poor plasma, Cohn fraction Iva [18,19] and transgenic milk [20] was the use Immobilized metal affinity chromatography (IMAC) with Copper. These separations exploit the preferential adsorption of the large number of exposed histidine groups in protein C. Other studies have explored iron [19], nickel and cobalt [21] affinity chromatography. However, IMAC was only used as one of a series of steps for isolation of protein C.

Quantification of protein C was performed using one of two methods [2]. One was using immunoassays such as ELISA [16] and radioimmunoassays which have the advantage of high specificity and accuracy. The other was using functional assays which evaluate the biological activity of protein C. These methods use the separation methods described above to first isolate protein C, then stimulate its activation to form activated protein C and measure its activity using a

clotting assay that measures the increase in clotting time due to the addition of the aPC to a protein C deficient plasma sample [2,22] or using a chromogenic assay that measures the color change produced when a selective chromogenic substrate is added to aPC [23]. Among these methods, immunoassays show the most potential in the development of a bedside diagnostic measurement tool for sepsis as it is a single step process that can distinguish the decrease in protein C concentration in septic patients. However, the generation of anti protein C antibodies is expensive which has led to limited adoption of protein C as a diagnostic biomarker. A device that can leverage the low cost of IMAC, while retaining the ability to detect the concentration of protein C in a single step from a blood plasma sample would increase the usability of protein C as prognostic marker for sepsis.

Here, we demonstrate such a low-cost device that can be used for single step measurement of protein C in blood plasma. The device integrates isoelectric gates [24] as the first stage of separation with IMAC-inspired immobilized metal affinity trapping (IMAT) using barium creating a 2-stage process that separates protein C from most other proteins in solution and concentrates it for detection. The first stage of separation uses an isoelectric gate cast using buffered agarose at a pH of 5 that serves to prevent the more abundant proteins in plasma from moving further. The second stage (IMAT) uses IMAC-Select metal affinity beads chelated with barium and cast in agarose and placed over a polyester porous membrane to immobilize barium and bind protein C preferentially over other proteins in plasma that pass through the first stage. When all proteins in plasma were tagged with a nonspecific fluorescent dye, the change in fluorescence at the site of the second stage of separation was found to be indicative of the concentration of protein C. This device was tested with three types of samples – buffered protein C (Sample A), protein C with two high concentration interferents (Sample B) and protein C spiked in blood plasma (Sample C) to

demonstrate the capability of the device to distinguish protein C concentrations in the range of 0-5 µg/mL in a single step for use in sepsis prognostication.

2. Device design and working principle

Measurement of Protein C was preformed by integrating two stages of separation in the device to exclude most of the plasma proteome and is shown in Fig. 1a. The first stage was the use of an isoelectric gate at a pH of 5 to exclude proteins with a pH of 5 and above. As was previously demonstrated [24], agarose gels buffered with citrate phosphate buffer can be used to make the isoelectric gates. The second stage of separation used immobilized metal affinity trapping with barium. Beads with a chelate bound to barium were cast into an agarose gel and located on a suspended polyester membrane that forced passage of the electrophoretically transported proteins though the gel. As barium has increased affinity for proteins containing a GLA domain such as protein C, only these proteins remain bound to the agarose gel in this section while the remainder pass through with minimal binding. In addition, the gel has an ambient pH of 8.2, and if the isoelectric point of the passing protein is lower than protein C, it moves through the gel faster and which reduces the interaction between the beads and the protein. The schematic of the complete device is shown in Fig. 1b.

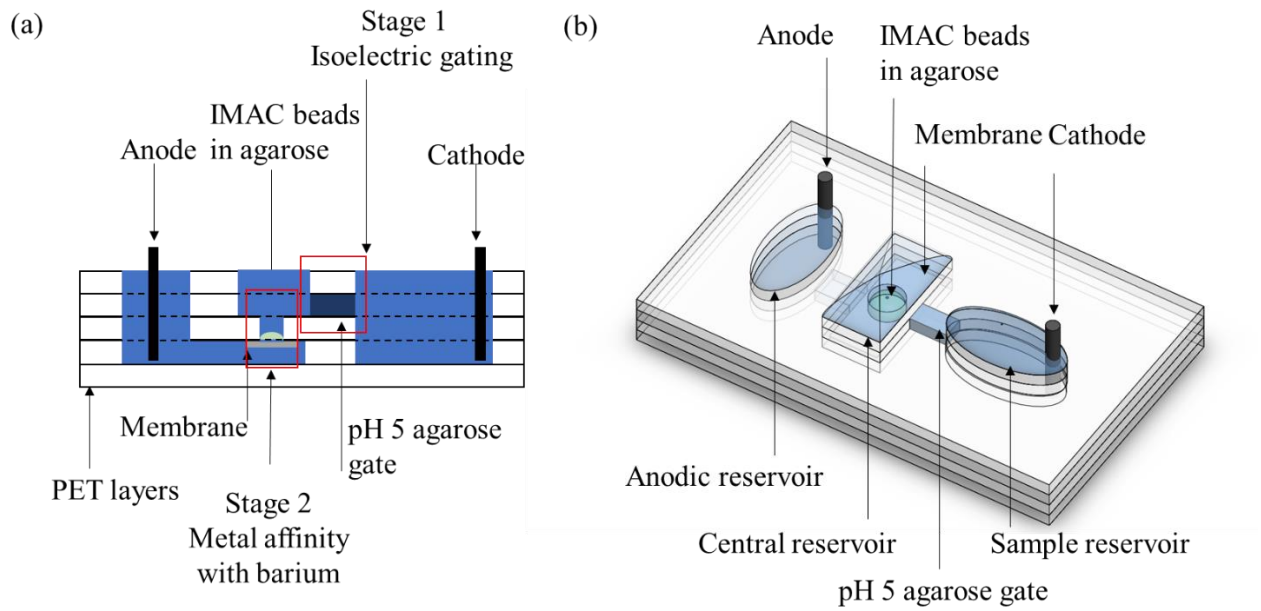

Figure 14 (a) Illustration of a cross section of the device and the two stages of separation (b) Schematic of the device showing the device with the agarose gels and buffers.

The device consists of 5 layers of polyethylene tetrapthalate (PET) adhesive tapes which were shaped into the 3 reservoirs to hold solutions. The sample reservoir was on one end of the device oriented longitudinally while the laterally oriented anodic and central reservoirs were used to hold a buffer. The sample reservoir and anodic reservoirs were elliptical with a minor axis length of 7 mm and major axis length of 14 mm. The central reservoir was a rectangle with dimensions of 14 mm x 7 mm. These dimensions were chosen to be able to hold ~180 µL of buffer which was necessary to maintain sufficient pH stability for the duration of the experiment. The shape of the central reservoir was chosen to facilitate robust adhesion of the membrane, while the shape and orientation of the two elliptical reservoirs were chosen to amplify the focusing effect of the electric field. The reservoirs were all located 5mm from each other. The 2nd layer from the bottom was used to interlink the anodic and central reservoirs. The 3rd layer consisted of a through hole with a radius of 2 cm co-centric with the central reservoir to direct protein motion through this hole and

to control the radius of the Ba-IMAT gel and ensure repeatability. A polyester membrane with dimensions of 6 mm x 13 mm was adhered to the base of the third layer and the barium bound agarose beads were placed above this membrane in the circular hole of the 3rd layer. The pH of the agarose gel used to hold the barium beads was the same the same as the pH of the buffer (pH 8.2) used in that reservoir. The sample reservoir was connected to the central reservoir in the 4th layer. This channel was used to form the isoelectric gate by pipetting agarose gel with a pH of 5 into it. Two versions of the device were fabricated with isoelectric gate widths of 0.32 cm and 0.215 cm (connecting the sample reservoir and central reservoir). Similarly, the liquid channel between anodic and central reservoirs was fabricated with dimensions of 0.5 cm and 0.3 cm respectively in the two versions of the device. The device with larger channel widths was used for experiments with plasma to allow for the higher protein load and the device with smaller channel widths was used for buffered samples which had significantly lower protein loads. The dimensions of the isoelectric gate were much smaller than the dimensions of the reservoirs to focus the electric field in these regions and increase rate of migration and separation. The resulting electric fields in the two devices have been analysed and optimized for this application as described in section 4.1. The resultant electric field in the isoelectric gate of the device when operated at 20 V with smaller channel widths was an average of 11.1-11.2 V/cm while that in the device with larger channel widths was 8-9 V/cm. This is similar to ~ 10 V/cm obtained in traditional gels operating with a 200 V power supply [9] but lower than high voltage gels.

On application of an electric field between the cathode in the sample reservoir and anode in the buffer reservoir at the other end, the proteins with an isoelectric point less than 8.2 (pH of the buffer) in the sample migrate towards the isoelectric gate where all proteins with a pI of more than 5 are trapped while the proteins with a pI less than 5 migrate through it into the central reservoir

at a slower rate. This stage of separation excludes a large fraction of proteins such as albumin (plasma concentration of 35-50 mg/mL[25], weight of 68 kDa, isoelectric point of 5.45-5.85 [33]) and most GLA domain proteins including protein S and Factor X (pI's of 5-5.5, 4.9-5.2 respectively [14]). Four GLA domain proteins pass through to interact with the barium bound IMAT beads of which both factor II and factor VII have a pI of 4.7-4.9 and 4.8-5.1 respectively [14] which is higher than protein C and moves more slowly through the isoelectric gate creating a separation in time. The proteins that pass through this stage pass through the central reservoir while interacting with the barium trapped to the beads in the gel. This gel is at a pH of 8.2, and the rate of migration of the protein through this gel is dependent on the difference between the pH of the column and the pI. The proteins that pass through the gel includes some high concentration proteins such as Alpha 1-proteinase inhibitor as well as Factor IX present in plasma at a concentration of 5 µg/mL and protein Z present at a concentration of 2.9 µg/mL are the other interfering GLA proteins. Protein C, Protein Z and Factor IX with a GLA domain have a higher affinity for barium while other proteins pass through with minimal interaction. In addition, Protein Z has an isoelectric point less than 3 [26] and factor IX has a lower pI of 4-4.5 [14] and a lower likelihood of interaction due to the higher electrophoretic force and rate of migration. As a result, protein C is most likely to interacting with barium and being trapped in this region while the remaining proteins pass through with less interaction. As a result, the final intensity of fluorescence measured at the site of the second stage of separation is expected to be primarily dependant on the concentration of protein C. A pictorial representation of the interaction of different proteins at the isoelectric gate and in the Ba-IMAT gel is shown in Fig. 2.

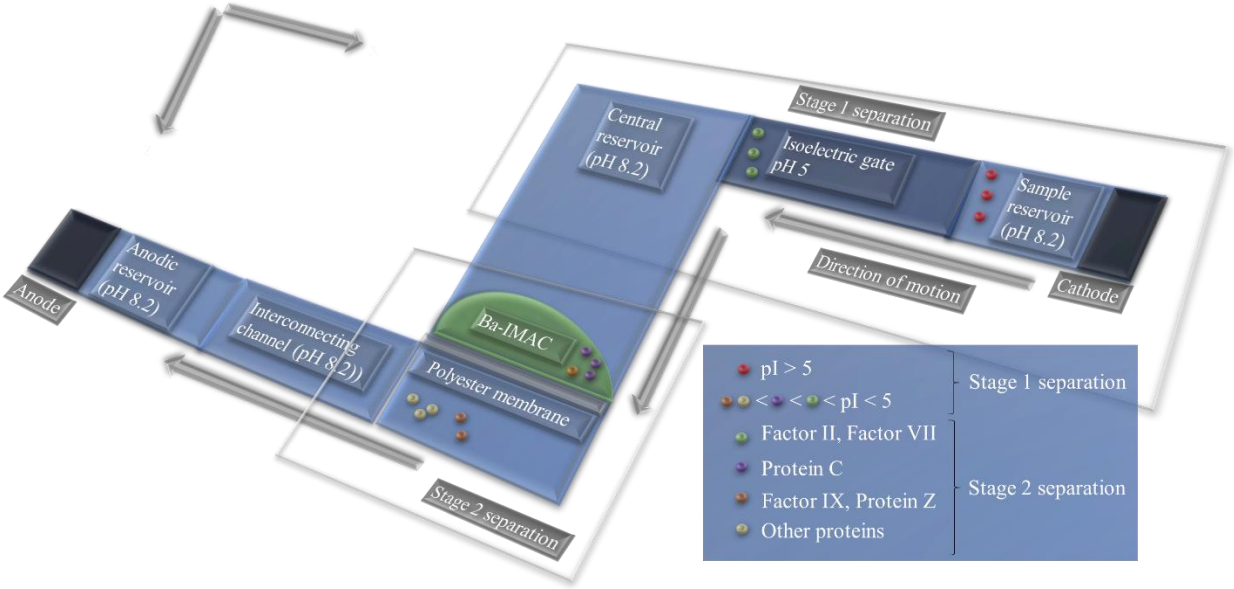

Figure 15 Schematic of protein interaction at the isoelectric gate and in the Ba-IMAT gel

3. Materials and methods

3.1 Materials

Low electroendosmosis agarose, citric acid, sodium phosphate dibasic, Tris, Hydrochloric acid, Alpha 1-proteinase inhibitor, bovine serum albumin (BSA), IMAC-Select Affinity Gel (beads in an ethanol suspension) and barium chloride were obtained from Millipore Sigma (Oakville, ON). Citrated pooled human plasma was obtained from Innovative research (Toronto, ON). Recombinant protein C concentrate was obtained from Thrombosis & Atherosclerosis Research Institute (TaARI), McMaster University. Qubit protein assay kit was obtained from Thermo Fisher Scientific. 0.005" polyethylene tetraphalate (PET) was obtained from McMaster Carr. 0.002" 7952MP transfer tape were obtained from 3M. Polyester membrane with a pore size of 5µm was obtained from Sterlitech. Graphite rods with a diameter of 0.1" were obtained for use as electrodes from Graphitestore.

Tris-HCl buffer at a concentration of 50 mM and 100 mM were prepared by titrating Tris with HCl till a pH of 8.2 was reached. Citrate phosphate buffer at a pH of 5 was prepared and mixed with the 1% agarose. This mixture was heated on a hotplate at 100°C till the solution became clear and was pipetted into the channel to fabricate the isoelectric gate. 5 µL of the gel was pipetted into the narrow channel device and 10 µL in the wide channel device. All excess gel was allowed to stay on the device in the reservoir adding an additional 2 mm of gating length present at a lower electric field.

An agarose gel containing barium bound IMAC-Select metal affinity beads was prepared by a modification of the "trial scale" protocol described by the manufacturer. To prepare 50 µL of the gel, barium was bound to the IMAC-Select metal affinity beads by incubating 25 µL of the beads suspension with 50 µL of barium chloride for 10 minutes. Following this, to remove the ethanol present in the suspension and unbound barium, washing steps were performed by centrifuging the solution for 30 s at 6000 rpm and 50 µL of the supernatant was removed. Then, 50 µL of deionized water was added and the solution was centrifuged for 30 s. The beads were equilibrated with the pH 8.2 buffer in the reservoirs by removing 50 µL of the supernatant and adding 50 µL of 50 mM of pH 8.2 Tris-HCl. The solution was centrifuged for 30 s again and 50 µL of the supernatant was removed. Finally, 25 µL of 100 mM pH 8.2 Tris-HCl with 2% agarose was added to this solution to make the final gel that was heated on a hotplate at 100 °C and pipetted into the device on the membrane.

Three types of protein samples were used to demonstrate the use of the device to measure protein C concentration. The first type of samples (Sample A) consisted of just protein C in buffer. The second type of samples (Sample B) which was used to verify the ability of the device to function

in the presence of interfering proteins consisted of a mixture of protein C, Alpha 1-proteinase inhibitor and BSA. The third type of samples (Sample C) consisted of protein C spiked in human blood plasma. Sample A were prepared by diluting the Protein C to make a 20 µg/mL master solution. 0 µL,2 µL,6 µL and 10 µL of this solution was mixed with Tris-HCl buffer to a total volume of 400 µL and 2 µL of Qubit protein assay's fluorescent dye was added to make a solution equivalent to that described in the protocol for 0 µL 1 µL, 3 µL and 5 µL samples of Protein C. Sample B used 0 µL,2 µL,6 µL and 10 µL of Protein C with 20 µL each of 10 mg/mL of BSA and 5 mg/mL of Alpha 1-proteinase inhibitor (A1PI) mixed with Tris-HCL to a total volume of 400 µL and 3 µL of fluorescent dye. The volume of dye was increased to ensure that the signal was not saturated as each µL of dye binds to a 100 µg of all proteins in the sample as given in the manufacturer's specifications. Sample C were prepared by spiking 0 µL,1 µL,3 µL and 5 µL of Protein C in 10 µL of plasma mixed with Tris-HCL to a total volume of 400 µL and 15 µL of dye. The average amount of native protein C in the plasma being used was found by ELISA (Affinity Biologicals) to be 6.8 µg/mL. As the protein volume was halved compared to the previous experiments, the resulting Protein C content corresponds to 3.4 - 5.9 µg/mL of the earlier results.

3.2 Fabrication

The device was fabricated using 5 layers of PET adhesive tapes which were patterned using Xurography and integrated using lamination as shown in Fig.3 [27]. The bottom and top layers were made from 0.005" PET. The 2nd layer from the bottom and the 4th layer from the bottom were made from 0.005" PET adhered to 0.002" transfer tape on both sides. The 3rd layer was made from PET adhered to the transfer tape on one side. The resulting cross section is shown in Fig. 3a. A schematic of the complete fabrication method used is shown in Fig.3b-i. The 3rd layer of the device was integrated with a polyester membrane on the bottom using the transfer tape. The individual

layers cut in PET using a Cricut cutting plotter and were integrated using a roller to pressure laminate the adhesive sheets together Fig. 3a-f. Prior to use, the agarose gel with IMAC-Select metal affinity beads bound to barium was pipetted into the central reservoir on the exposed portion of the membrane (Fig. 3g). The pH 5 agarose gel was then pipetted in the channel between the sample and central reservoirs forming the isoelectric gate followed by the buffers in each reservoir and the sample as shown in Fig. 3h. The device was then placed on a fluorescence microscope and graphite electrodes were introduced in the anodic and sample reservoirs of the device. The cathode in the sample chamber and the anode in the buffer reservoir. The resultant device costs less than $5 per run in plasma as shown in the cost analysis (supplementary material S2).

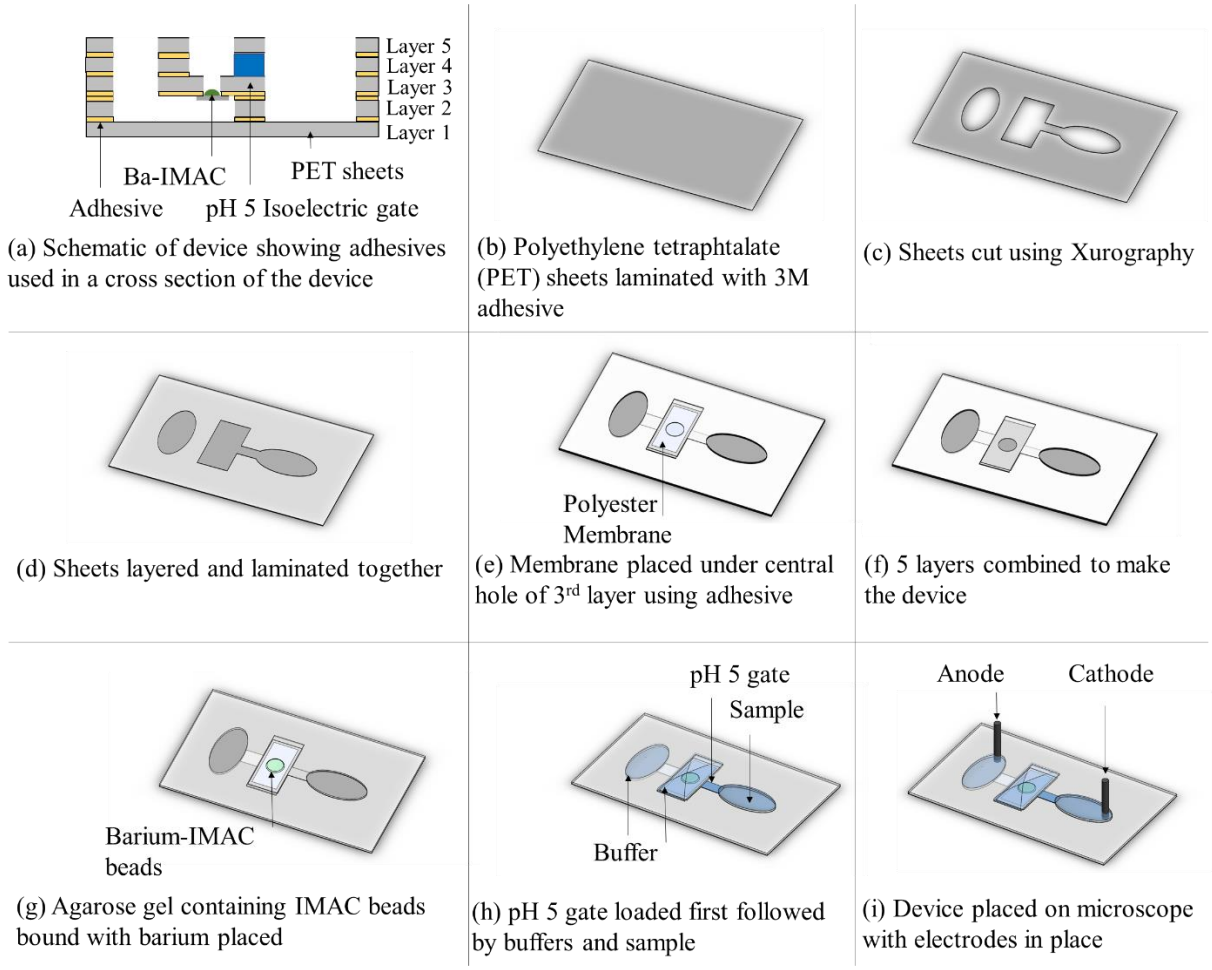

Figure 16 Schematic of the fabrication process (a) cross section of the device showing the adhesives of each layer (b-f) Patterning of each layer of PET using Cricut cutting plotter and integration of the device with polyester membrane (g) Pipetting of barium bound beads in the device (h) Placing the isoelectric gate in the channel connecting central and sample reservoirs(i) Connecting graphite electrodes.

3.3 Experimental setup

The experimental setup consists of a fluorescence microscope (Nikon Eclipse TE2000-S) on which the device was placed. The microscope was used with an excitation window of 455±25 nm and an emission window of 600±30 nm. X-Cite 360LED was used as the light source for the microscope and was operated at 30% of the maximum. The microscope was connected to a raspberry pi camera on the C-mount camera outlet and the raspberry pi was programmed to switch on the light source

1s before image capture and capture images every minute with an exposure time of 4s, an ISO of 400 and a color balance with a bias of 4: 0.1: 1 for red: green: blue, respectively. A clamp was used to hold 2 graphite rods suspended over the device connected to Keithley 2410 which was used as a power supply. The Keithley was operated with a voltage cap of 100 V and a current cap of 1 mA for protein separation with buffers and 0.75 mA for separation in plasma. This was done to limit the current produced to migration of proteins. The resultant voltage over the course of the experiment was 10-60 V increasing over time. Reaching the voltage cap in a run implied the formation of bubbles in the intersecting channels and the run was excluded from further analysis. The schematic of the experimental setup is shown in Fig. 4.

Each run was performed using a new device with freshly prepared gels which were pipetted into the assigned locations before placing the device on the microscope and placing the electrodes. The leftmost buffer reservoir was first filled with 180 µL of 50 mM Tris-HCl a part of which passes through to the bottom of the central reservoir by capillary action. It was then refreshed by 60 µL of 100 mM Tris-HCl. The central reservoir was filled with 180 µL of 50 mM Tris-HCl. The sample reservoir was filled with 120 µL of Tris-HCl and 60 µL of sample prepared as described before. The microscope was centered on the 2 cm radius agarose gel in the central reservoir and images were taken every minute for 60 minutes with buffered samples and 80 minutes for plasma samples. The electric field was applied after the first image was captured.

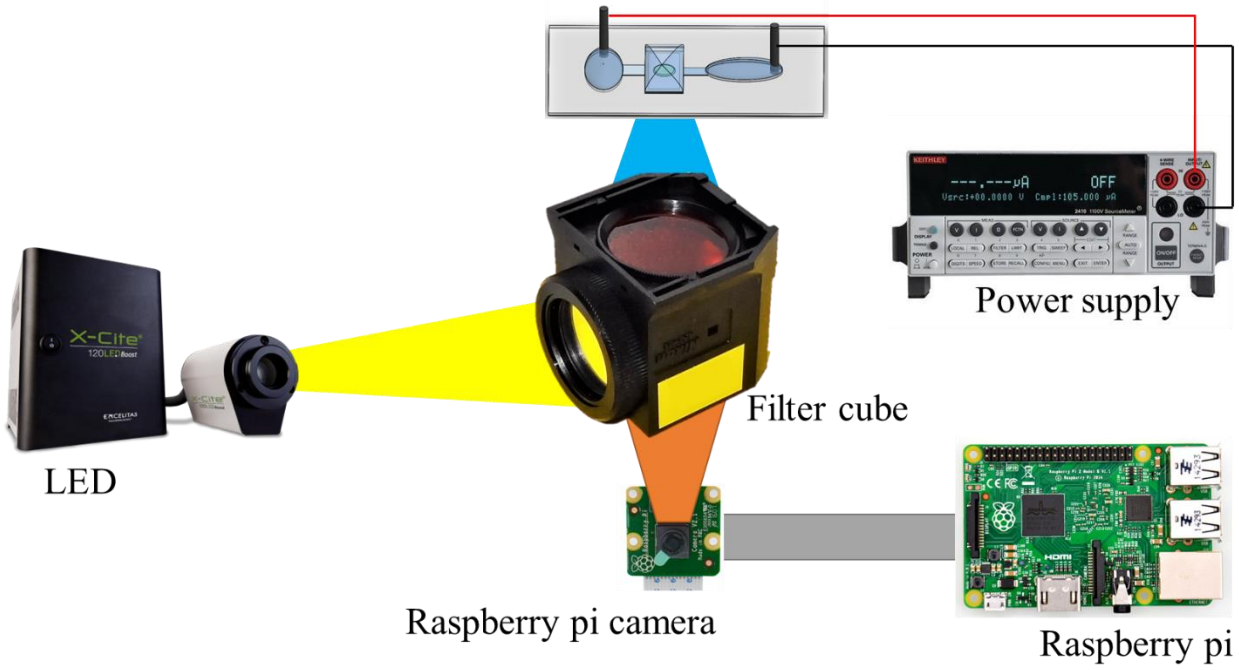

Figure 17 Experimental setup used showing filter cube with an excitation filter of 455±25nm, emission filter of 600±30nm

3.4 Image analysis

The captured images were transferred to a computer and ImageJ was used to analyse the images. A square shaped region of interest (ROI) with a side length equal to the diameter of the agarose gel was placed around the agarose gel and a second reference ROI was located in a section of the device with no solution. The second ROI was used to compensate for changes in brightness due to external factors and dispersion of light. This was particularly evident in higher intensity samples where the camera brightened the image further artificially increasing the measured intensity. The average greyscale intensity in these ROI's was measured and the difference in intensity between the measurement ROI and reference ROI was used to measure the fluorescent intensity at each time. The baseline intensity was set to 22.5±0.5 A.U, and the fluorescent intensity was plotted over time. The intensity when the first stable value was reached after half the experimental time elapsed

was considered as the measurement for that sample. A value was considered stable if 5 consecutive measurements were within 2 units of each other. This was done to allow for variability due to passage of non-binding protein through the beads. This resulted in measurement at a time of ~40 minutes (experimental time of 60 minutes) for buffered samples and ~60 minutes (experimental time of 80 minutes) for plasma samples.

4. Results and discussion

4.1 Simulation of electric field distribution

The electric field distribution in the device was calculated using COMSOL Multiphysics. The geometry was replicated, and the electric currents module was used for the calculation of the electric fields. The membrane was approximated by a single cylindrical volume with a radius of 0.5mm that had an equivalent electrical resistance. Both the narrow channel design used for buffered solutions and the wide channel design used for plasma samples were simulated. The simulation was run with the anode at 20V which was the approximate starting voltage of each experiment. The cathode was set to ground. The conductivity of 50mM Tris-HCl was approximated to be 2mS/cm[28] while that of the pH 5 buffer was 1.5mS/cm[29]. The solver used was a Newtonian fully coupled solver.

The electric field in the isoelectric gate of the narrow channel device was calculated to be 11.1-11.2 V/cm while that in the location of the Ba-IMAT gel was ~2.5 V/cm. The rest of the reservoirs had a distribution of electric fields ranging from 3 - 5 V/cm. The complete distribution is shown in Fig. 5a and 5c. The wide channel device was calculated to have an electric field of 8-9 V/cm in the isoelectric gate, ~2.5 – 3 V/cm at the location of the Ba-IMAT gel and 3 - 5 V/cm in the rest of the device. The changes in the calculated electric field were due to the larger dimensions of the

channel. This resulted in a less focused electric field, which lead to a decrease in the electric field at the isoelectric gate and a corresponding increase in the electric field at the location of the Ba-IMAT gel. These distributions were shown in Fig. 5b and 5d. The structure of the device enabled focusing of the electric field in the isoelectric gate while reducing the electric field in the Ba-IMAT gel to enable a longer residence time for protein C to bind to the barium. The electric field was then used to calculate the theoretical time needed for the protein C to pass through the device and concentrate at the Ba-IMAT gel. This was found to be 25 minutes in the absence of electroosmotic forces as shown in supplementary information 1.

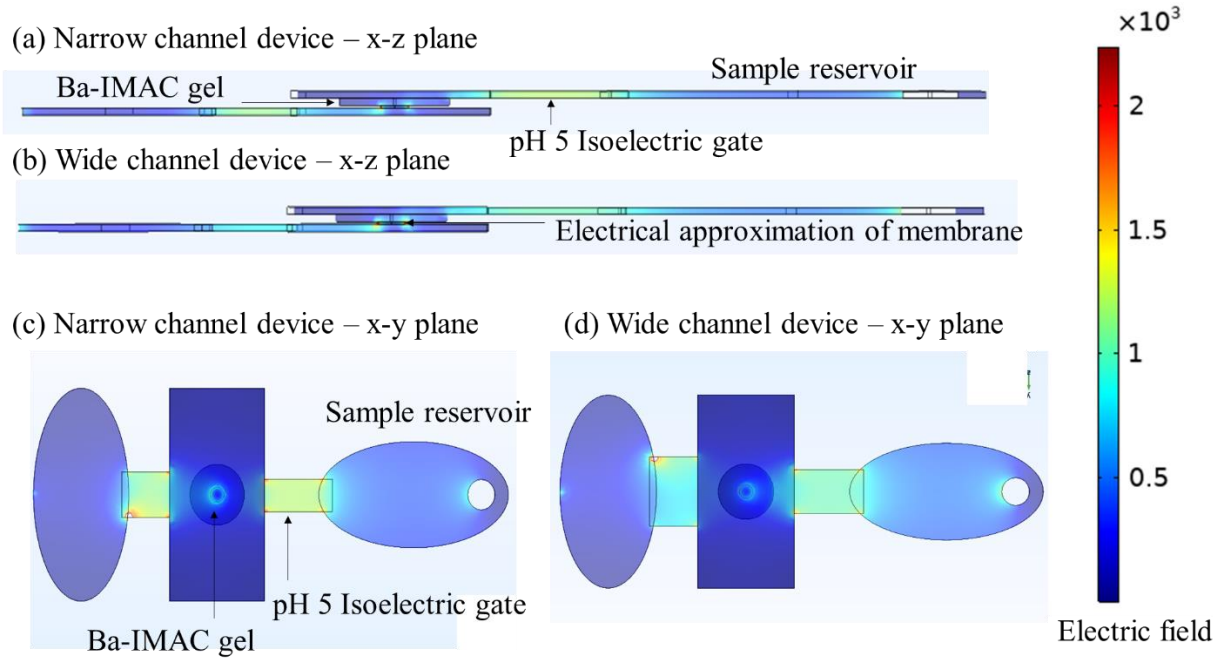

Figure 18 Distribution of electric field in the (a)(c) narrow and (b)(d) wide channel devices (a)(b) in the x-z plane (c)(d) x-y plane

4.2 Measurement of protein C in a buffered sample

The ability of the 2-staged device in trapping protein C was first characterized with a sample containing various concentrations of protein C in Tris-HCl buffer (Sample A). The device was

prepared with an isoelectric gate of pH 5 and the Ba-IMAT gel was deposited on the membrane. Following this, the buffer and sample were deposited in the respective reservoirs as described previously. On application of an electric field capped at 1 mA and 100 V, an operational voltage of 20-60 V was obtained. Images were captured with samples at concentrations of 0 µg/mL 1 µg/mL, 3 µg/mL and 5 µg/mL of protein C in buffer (Sample A). The location of image capture and images with 0 µg/mL and 5 µg/mL of protein C at 40 minutes are shown in Fig.6a. Protein C would typically take 25 minutes to reach the Ba-IMAT gel in the absence of electroosmotic flow in this device geometry as shown in supplementary information S3. To provide sufficient time for unbound protein C to pass through and stabilize the measured intensity of protein C while accounting for the reduction in flow rate of electroosmotic flow, a time of 40 minutes was chosen for measurement. These images show the increase in intensity of fluorescence emitted due to the trapping of protein C by barium chelated to the beads in the central reservoir after passing through the first stage of separation with the isoelectric gate at pH 5. The asymmetry in fluorescent intensity measured at 40 minutes with the 5 µg/mL sample is due to the distribution of the electric field lines in the central reservoir. As the electric field is much higher in the section of agarose gel closer to the sample chamber, most of the protein C is bound in that portion of the gel. The average intensity of 3 samples at each concentration after image analysis are shown in Fig.6b. The background intensity at the start of each run was 22.5±0.5 A.U. The control with the fluorescent dye and no proteins in solution had an intensity of 23.7±0.4 A.U after 40 minutes which is an insignificant difference compared to an intensity of 39.99±1.5 A.U obtained with 5 µg/mL of protein C in the sample. A two tailed t test shows greater than 99.5% confidence in differentiating between any two of these samples except between 0 µg/mL and 1 µg/mL which has an 87% confidence interval. Despite the low confidence with measuring samples at ~1 µg/mL compared with blank, the device

can be used for distinguishing samples with normal levels of protein C of 5 µg/mL from patient samples with 1-3 µg/mL which is the differentiation required for sepsis albeit in buffered samples.

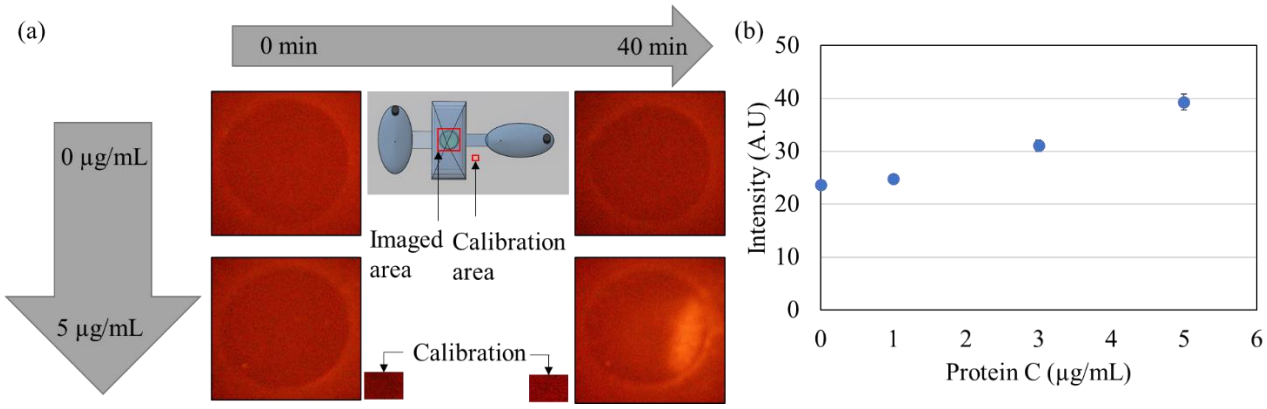

Figure 19(a) Images captured with 0 µg/mL and 5µg/mL samples of protein C at the start and after 40 minutes, including calibration for the 5µg/mL samples (b) Plot showing change in measured fluorescent intensity with protein C concentration (N=3).

4.3 Measurement of protein C in the presence of high concentration interfering agents

The use of the device to measure protein C concentration in the presence of other proteins was tested using samples of protein C in buffer mixed with 10 mg/mL of BSA and 5 mg/mL of Alpha 1-proteinase inhibitor (Sample B). This was done to verify the specificity of binding of Ba-IMAT to protein C in comparison to other proteins present at a high concentration in plasma. BSA was chosen to be analogous to human serum albumin with similar isoelectric points and weight. Alpha 1-proteinase inhibitor (A1PI) was chosen as it is a major component of plasma with an isoelectric point of 4.7 which is within the range of 4.4-4.8 of protein C, has a similar weight compared to protein C (52kDa) and is present at a higher concentration of 1.5 - 3.5 mg/mL [30] compared to 4-5 µg/mL of protein C in plasma. The device was then prepared as previously described and 60 µL of the sample was deposited in the device followed by application of the electric field with a current limit of 1 mA and voltage limit of 100 V, an operational voltage of 20-80 V was obtained. Images as shown in Fig. 7a were obtained with samples containing 0 µg/mL and 5 µg/mL of protein C

mixed with 10 mg/mL of BSA and 5 mg/mL A1PI (Sample B) at 40 minutes to show the difference in fluorescent intensity between a control containing only the interfering proteins and the intensity with the addition of protein C. Average intensity of 3 samples each with 0 µg/mL 1 µg/mL, 3 µg/mL and 5 µg/mL of protein C were plotted to obtain Fig. 7b which compares the resulting intensity in the presence of interfering proteins with that obtained from sample A containing only protein C measured in section 4.2. The results show a slight increase in fluorescent intensity measured in the control (where the concentration of protein C is zero) containing BSA and A1PI (26.9±2.79 A.U) compared to that measured in the absence of any proteins (23.7±0.44 A.U) due to low level nonspecific binding of A1PI as it passes through the gel. Additionally, there is an increase in signal measured at all concentrations of protein C compared to the respective values measured with only protein C in section 4.2. This can be attributed to less of protein C being adsorbed to the surface of the device due to the presence of BSA and A1PI at much higher concentrations. This results in more protein C being available for binding with Ba-IMAT and a resultant higher intensity. The slope of a linear regression approximation in the presence of interfering proteins (5.85 A.U/µg/mL) is better than that obtained with only protein C (3.19 A.U/µg/mL) due to the reduced loss of protein C from adsorption to the surface of the device. As a result, a 2 tailed t-test shows a greater than 99% confidence interval in differentiating any 2 samples in this device except between control and 1µg/mL that shows a 91.5% confidence, which is higher than in the case with just protein C in buffer. This shows that the device can be used for measuring protein C and differentiating between septic and non septic patients with a high accuracy even in the presence of interfering proteins.

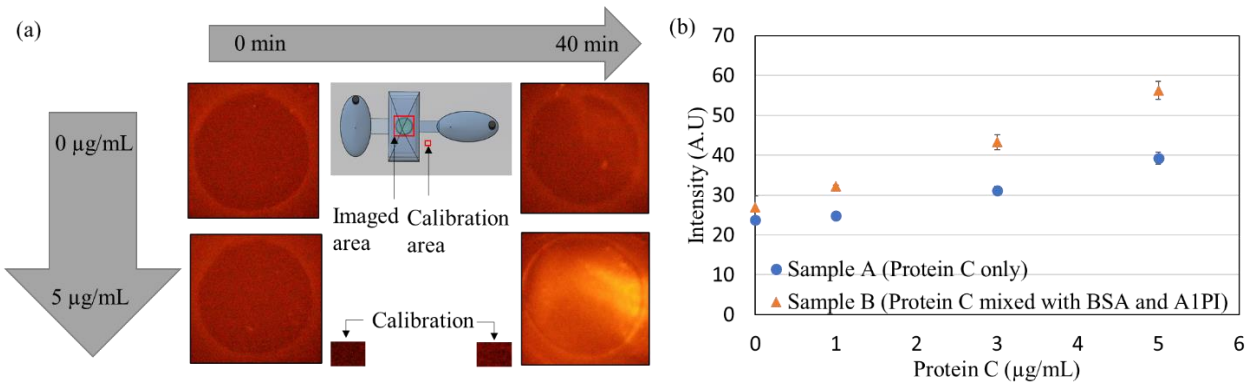

Figure 20(a) Images captured with 0 µg/mL and 5µg/mL samples of protein C in the presence of BSA and A1PI at the start and after 40 minutes, including calibration for the 5µg/mL samples (b) Plot showing change in measured fluorescent intensity with protein C concentration (N=3).

4.4 Change in intensity with time during trapping

The time stability of the intensity measurement of protein C when in a mixture with BSA and Alpha 1-proteinase inhibitor was studied to verify the stability of the measured intensity. This was done using sample solutions with 0 and 5 µg/mL of protein C mixed with 10 mg/mL of BSA and 5 mg/mL of Alpha 1-proteinase inhibitor. Three samples of each were prepared as before, and images were taken every minute with the device operated in the same condition as in section 4.3. The average intensity of the images was calculated as described previously. The average of three runs was plotted to obtain Fig. 8. The plot shows an increase in intensity with the 5 µg/mL sample due to the capture of protein C in the Ba-IMAT gel starting at ~20 minutes and stabilization of the intensity at ~35 minutes. The variation in intensity measured before 35 minutes can be attributed to the inhomogeneity of protein density in the sample reservoir causing a large variation of the rate of trapping. However, this stabilizes after 35 minutes as shown by the reduction in noise. The sample with no protein C shows no increase in intensity as the Alpha 1-proteinase inhibitor passes through rapidly while the BSA is blocked at the isoelectric gate. As a result, measurement of image intensity at the 40-minute mark can be used as a stable measurement of protein C.

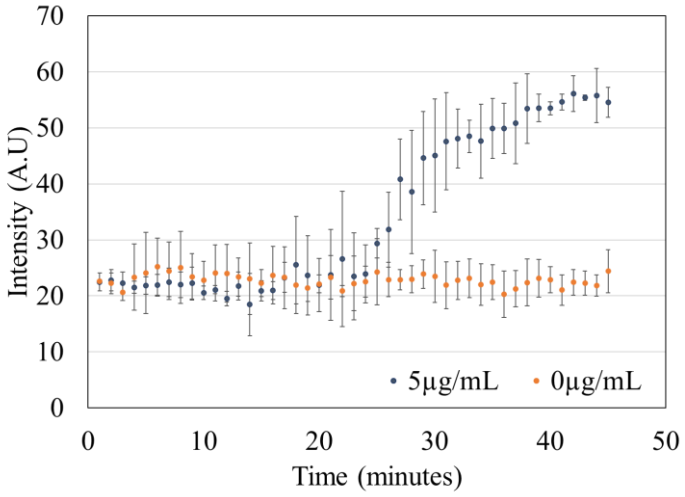

Figure 21 Change in measured intensity with time using samples containing 0 and 5 µg/mL of protein C mixed with 10 mg/mL BSA, 5 mg/mL A1PI (N=3)

4.5 Measurement of protein C in blood plasma

The device was used to measure concentration of protein C that has been added to pooled human plasma as an simulation of a real-world sample. The objective in this experiment was to verify if the device could differentiate between plasma samples when the protein C concentration is either half or a quarter of that of a healthy human (3.9-5.9 µg/mL) which is the case in sepsis non survivors. In order to prepare these samples in human plasma that may already have protein C in it, a new protocol was used. Samples were prepared with 0 µg/mL, 1 µg/mL, 3 µg/mL and 5 µg/mL of protein C spiked in plasma (Sample C) which were then used in preparation of the sample. However, due to the presence of native protein C in the pooled human plasma at a concentration of 3.4 µg/mL (measured by ELISA) and usage of half the protein volume in comparison to the previous experiments, the protein concentration in comparison to earlier experiments would be in the range of 3.4 -5.9 µg/mL.

Larger channel width devices were used with 0.75 mA and 100 V current and voltage limits on the power supply. Images were taken every minute and images after 60 minutes with the 0 µL and 5

µL sample are shown in Fig. 9a. The calibration for the 5 µg/mL sample at 60 minutes shows the increase in background brightness when exposed to high intensity sample, which was corrected for in the graphed values. The average of intensities measured for each of the protein C concentrations is plotted in Fig. 9b and compared to results obtained with Sample B (protein C mixed with BSA and A1PI). When corrected for the initial protein C content in the plasma as measured using ELISA, the intensity measured at each concentration lies close to the interpolated intensity from Sample B with a maximum error of 13%. This is due to the difference in interfering agents. The interference in the mixture with A1PI and BSA is primarily due to the excess of A1PI. However, the interference in plasma is due to the passage of other GLA domain proteins and nonspecific binding of other proteins which affects the binding characteristics of the Ba-IMAT gel. The binding of other GLA domain proteins passing through the Ba-IMAT beads is less than that of protein C due to the difference in pI as described in section 2. Of the GLA domain proteins passing through, protein Z has the lowest pI of less than 3 [26] as a result of which its residence time in the vicinity of the Ba-IMAT beads is the lowest resulting in minimal binding. Factor IX has a pI of 4-4.5 [14] which is slightly lower than protein C, resulting in reduced residence time and possibly some binding with Ba-IMAT. Factor II and Factor VII have a higher pI of more than 4.7 and migrate more slowly through the isoelectric gate of pH 5, taking longer than the experimental time to reach the Ba-IMAT gel and probably do not play a role in the measurement.

The dilution of protein C due to spiking reduced the range of measurement from 0 – 5 µg/mL in the previous experiments to 3.4 – 5.9 µg/mL in plasma. Nevertheless, the device could differentiate protein C concentrations with a confidence of greater than 93% between any 2 concentrations which were ~ 1 µg/mL apart. The objective of the device is to be able to differentiate between samples with protein C halved or reduced to a quarter of the original 5µg/mL concentration in

septic patients for which the device has a greater than 98% confidence in plasma. A limit of detection defined as three times the standard deviation of the control (0 µg/mL spiked in plasma) was found to be 0.35 µg/mL spiked in plasma.

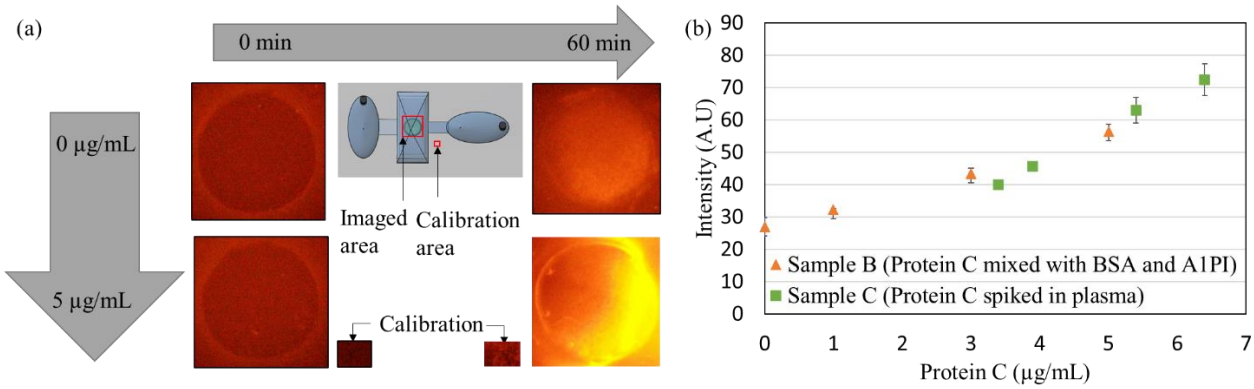

Figure 22(a) Images captured with 0 µg/mL and 5µg/mL samples of protein C spiked in human plasma at the start and after 60 minutes, including calibration for the 5µg/mL samples (b) Plot showing change in measured fluorescent intensity with protein C concentration for various samples (N=3).

5. Conclusion

A low-cost device that can be used for single step measurement of protein C in human plasma was demonstrated as an intial step in the development of a POC device for sepsis. The device integrates isoelectric gates with IMAC inspired Ba-IMAT in a microfluidic device fabricated using PET sheets. We first used simulations to study the variation in electric field to optimize conditions for using Ba-IMAT to trap protein C. Then, we demonstrated the use of barium bound IMAT beads to bind to protein C in the presence of a high concentration of interfering agents such as A1PI and BSA which showed an improvement in detection compared to just protein C due to reduced surface

adsorption of protein C. Then, we show the stability of the measurement by viewing the change in intensity with time and show that a measurement 40 minutes after applying the electric field provides a stable measurement of intensity. The testing time could potentially be further enhanced by optimizing device geometry to increase residence time of protein C during IMAT while reducing transit time in the reservoirs. Finally, we demonstrate the detection of protein C spiked in plasma which shows a maximum error of 13% compared to the three-protein mixture despite the differing interfering agents. The device also showed sufficient capability to distinguish between the measured concentrations of protein C with 93% confidence and greater than 98% confidence in determining a reduction of protein C from 5.9 µg/mL to 3.4 µg/mL (unspiked plasma) which was necessary for sepsis prognosis. This device could then be integrated with alternative strategies to eliminate gel loading before the experiment to simplify workflow and a portable fluorescence imaging system to replace the currently used microscope for use as a of low cost, single step POC system for sepsis prognosis.

6. Author information

Corresponding Author
* selvaga@mcmaster.ca

Author Contributions

SD and PRS formulated the concept and experimental protocols with inputs from AEF. DJD and PCL provided protein C samples and provided inputs on biomarkers and protein behavior. SD wrote the paper with revisions and inputs from PRS, AEF, PCL and CCCTBG.

7. Acknowledgment

This work was supported by the Natural Sciences and Engineering Research Council of Canada (NSERC) and Canadian Institutes for Health Research (CIHR) through the Collaborative Health Research Program. PRS also acknowledges support from the Canada Research Chairs Program as well as the Discovery Accelerator Supplement grant.

8. References

[1] J.G. Dib, K. Zarikian, The role of activated protein C in sepsis, Hosp. Pharm. 39 (2004) 558–563. https://doi.org/10.1177/001857870403900610.

[2] R.A. Marlar, D.M. Adcock, Clinical evaluation of protein C: A comparative review of antigenic and functional assays, Hum. Pathol. 20 (1989) 1040–1047. https://doi.org/10.1016/0046-8177(89)90221-9.

[3] A.E. Fox-Robichaud, L.A. McIntyre, A. Turgeon, R. Green, R. Zarychanski, S. Bagshaw, I. Stiell, A. Worster, B. Rowe, M. Emond, D. Dwivedi, P.C. Liaw, The precise pilot trial: Temporal changes in thrombin generation, protein C levels and activated protein C generation in early septic shock, Am. J. Respir. Crit. Care Med. 181 (2010) 6146. http://ajrccm.atsjournals.org/cgi/reprint/181/1_MeetingAbstracts/A6146?sid=8cb89aaf-c3c2-47cb-8276-ae5c8d143d17%5Cnhttp://ovidsp.ovid.com/ovidweb.cgi?T=JS&CSC=Y&NEWS=N&PAGE=fulltext&D=emed10&AN=70844387%5Cnhttp://sfx.scholarsportal.info/uhn?sid=OVID:embas.

[4] M. Singer, C.S. Deutschman, C.W. Seymour, M. Shankar-Hari, D. Annane, M. Bauer, R. Bellomo, G.R. Bernard, J.-D. Chiche, C.M. Coopersmith, R.S. Hotchkiss, M.M. Levy, J.C. Marshall, G.S. Martin, S.M. Opal, G.D. Rubenfeld, T. van der Poll, J. Vincent, D.C. Angus, The Third International Consensus Definitions for Sepsis and Septic Shock (Sepsis-3)., J. Am. Med. Assoc. 315 (2016) 801–10. https://doi.org/10.1001/jama.2016.0287.

[5] C. Rhee, R. Dantes, L. Epstein, D.J. Murphy, C.W. Seymour, T.J. Iwashyna, S.S. Kadri, D.C. Angus, R.L. Danner, A.E. Fiore, J.A. Jernigan, G.S. Martin, E. Septimus, D.K. Warren, A. Karcz, C. Chan, J.T. Menchaca, R. Wang, S. Gruber, M. Klompas, for the C.D.C.P.E. Program, Incidence and Trends of Sepsis in US Hospitals Using Clinical vs Claims Data, 2009-2014, JAMA. 318 (2017) 1241–1249. https://doi.org/10.1001/jama.2017.13836.

[6] Sepsis Alliance, Sepsis fact sheet, 2020.

[7] L. Jacobs, H.R. Wong, Emerging infection and sepsis biomarkers: will they change current therapies?, Expert Rev. Anti. Infect. Ther. 14 (2016) 1–13. https://doi.org/10.1080/14787210.2016.1222272.

[8] P. Comp, R. Nixon, C. Esmon, Determination of functional levels of protein C, an antithrombotic protein, using thrombin-thrombomodulin complex, Blood. 63 (1984) 15–21. https://doi.org/10.1182/blood.V63.1.15.15.

[9] P.C. Liaw, A.E. Fox-Robichaud, K.-L. Liaw, E. McDonald, D.J. Dwivedi, N.M. Zamir, L. Pepler, T.J. Gould, M. Xu, N. Zytaruk, S.K. Medeiros, L. McIntyre, J. Tsang, P.M. Dodek, B.W. Winston, C. Martin, D.D. Fraser, J.I. Weitz, F. Lellouche, D.J. Cook, J. Marshall, Mortality Risk Profiles for Sepsis, Crit. Care Explor. 1 (2019) e0032. https://doi.org/10.1097/cce.0000000000000032.

[10] J. Yang, P.R. Selvaganapathy, T.J. Gould, D.J. Dwivedi, D. Liu, A.E. Fox-Robichaud, P.C. Liaw, A microfluidic device for rapid quantification of cell-free DNA in patients with severe sepsis, Lab Chip. 15 (2015) 3925–3933. https://doi.org/10.1039/C5LC00681C.

[11] W.M. Canfield, L.H. Ericsson, E.W. Davie, J. Stenflo, J.W. Suttie, C.M. Jackson, L.H. Ericsson, E.W. Davie, E. Marciniak, W. Kisiel, K.G. Mann, W. Kisiel, W.M. Canfield, W. Kisiel, K.G. Mann, P.W. Sexton, P.C. Comp, F.J. Walker, Protein C, Methods Enzymol. 80 (1981) 320–332.

[12] C. Gelfi, P.G. Righetti, P.M. Mannucci, Charge heterogeneity of human protein C revealed by isoelectric focusing in immobilized pH gradients, (1985) 373–376.

[13] D. Josic, L. Hoffer, A. Buchacher, Preparation of vitamin K-dependent proteins, such as clotting factors II, VII, IX and X and clotting inhibitor Protein C, J. Chromatogr. B Anal. Technol. Biomed. Life Sci. 790 (2003) 183–197. https://doi.org/10.1016/S1570-0232(03)00082-5.

[14] R.G. Discipio, E.W. Davie, Characterization of Protein S , a 7-Carboxyglutamic Acid Containing Protein from Bovine and Human Plasma "', 18 (1979).

[15] A. Ichinose, H. Takeya, E. Espling, S. Iwanaga, W. Kisiel, E.W. Davie, Amino acid sequence of human protein Z, A vitamin K-dependent plasma glycoprotein, Biochem. Biophys. Res. Commun. 172 (1990) 1139–1144. https://doi.org/10.1016/0006-291X(90)91566-B.

[16] A. Jean, C. Boyer, C. Rothschild, M. Wolf, DETERMINATION OF PROTEIN C BY AN IMMUNOENZYMATIC ASSAY, Protein C Biochem. Med. Asp. Proc. Int. Work. C Biochem. Med. Asp. Proc. Int. Work. (1985).

[17] W. Kisiel, Human Plasma Protein C- ISOLATION, CHARACTERIZATION, AND MECHANISM OF ACTIVATION BY alpha-THROMBIN, J. Clin. Invest. 64 (1979) 761–769.

[18] H. Wu, D.F. Bruley, Homologous human blood protein separation using immobilized metal affinity chromatography: Protein C separation from prothrombin with application to the separation of factor IX and prothrombin, Biotechnol. Prog. 15 (1999) 928–931. https://doi.org/10.1021/bp9901015.

[19] H. Wu, D.F. Bruley, Chelator, metal ion and buffer studies for protein C separation, Comp. Biochem. Physiol. - A Mol. Integr. Physiol. 132 (2002) 213–220. https://doi.org/10.1016/S1095-6433(01)00550-5.

[20] J.. Dalton, D.. Bruley, K.. Kang, W.. Drohan, SEPARATION OF RECOMBINANT HUMAN PROTEIN C FROM TRANSGENIC ANIMAL MILK USING IMMOBILIZED METAL AFFINITY CHROMATOGRAPHY, 1997.

[21] L.K. Korah, K.A. Kang, Preliminary study for the protein C purification using mini-antibodies produced from recombinant E.coli, in: Oxyg. Transp. to Tissue XXV, 2003: pp. 171–176.

[22] G. Owen, D.I. P-thrombin-sepharose, A functional assay of protein C in human plasma,

Blood. 63 (1984) 671–675.

[23] R.A. Marlar, J.N. Gausman, Laboratory testing issues for protein C, protein S, and antithrombin, Int. J. Lab. Hematol. 36 (2014) 289–295. https://doi.org/10.1111/ijlh.12219.

[24] S. Damodara, D.J. Dwivedi, P.C. Liaw, A.E. Fox-Robichaud, P.R. Selvaganapathy, Single step separation and concentration of biomarker proteins using agarose based miniaturized isoelectric gates for point of care diagnostics, Sensors Actuators, B Chem. 330 (2021). https://doi.org/10.1016/j.snb.2020.129265.

[25] T. Peters Jr, All about albumin: biochemistry, genetics, and medical applications, Academic press, 1995.

[26] K. Kaneko, T. Yamanobe, K. Nakagomi, K.I. Mawatari, M. Onoda, S. Fujimori, Detection of protein Z in a renal calculus composed of calcium oxalate monohydrate with the use of liquid chromatography-mass spectrometry/mass spectrometry following two-dimensional polyacrylamide gel electrophoresis separation, Anal. Biochem. 324 (2004) 191–196. https://doi.org/10.1016/j.ab.2003.09.018.

[27] A. Mohammadzadeh, A.E.F. Robichaud, P.R. Selvaganapathy, Rapid and Inexpensive Method for Fabrication and Integration of Electrodes in Microfluidic Devices, J. Microelectromechanical Syst. (2019) 1–9. https://doi.org/10.1109/jmems.2019.2914110.

[28] J.. Fullarton, A.J. Kenny, A Rapid System for Preparative Electrophoresis Depending on Isoelectric Buffers of Low Conductivity, Bot. Mar. 23 (2009) 147–149. https://doi.org/10.1515/botm.1980.23.1.63.

[29] J.R. Rumble, ed., CRC Handbook of Chemistry, and Physics, 98th Editi, CRC Press/Taylor & Francis, Boca Raton, FL., 2018.

[30] Z. Wang, T.L. Hilder, K. Van Der Drift, J. Sloan, K. Wee, Structural characterization of recombinant alpha-1-antitrypsin expressed in a human cell line, Anal. Biochem. 437 (2013) 20–28. https://doi.org/10.1016/j.ab.2013.02.006.

[31] E.M. Johnson, D.A. Berk, R.K. Jain, W.M. Deen, Hindered diffusion in agarose gels: Test of effective medium model, Biophys. J. 70 (1996) 1017–1023. https://doi.org/10.1016/S0006-3495(96)79645-5.

[32] H.P. Erickson, Size and shape of protein molecules at the nanometer level determined by sedimentation, gel filtration, and electron microscopy, Biol. Proced. Online. 11 (2009) 32–51. https://doi.org/10.1007/s12575-009-9008-x.

S1 Supplementary information 1 – Theoretical time for protein motion

In the absence of electroosmotic flow, the force balance on each protein is given by

$$\boldsymbol{qED = fV}$$

Where q is the charge on the protein, theoretically predicted based on the functional groups on protein C. This was obtained from https://www.protpi.ch/Calculator/ProteinTool/

D is the diffusivity ratio which is the additional resistance to flow due to the structure of the gel and size of the protein and was approximated based on the size of protein C in agarose to be 0.85[31]

V is the velocity that is being calculated

f is the stokes drag acting on the particle obtained from

$$\boldsymbol{f = 6\pi\eta r}$$

Where

Where η is the kinematic viscosity

r is the stokes radius of the protein, approximated to be 3nm[32]

When applied to protein C, with a theoretical pI of 5.9191, The theoretical velocity at a pH difference of 0.2 and 3.4 that corresponds to an ambient pH of 5 and 8.2 for protein C with a pI range of 4.4 - 4.8 are shown below.

pH (pH difference)	charge (C)	stokes drag (N)	Location	Electric field	velocity (mm/s)
6.2 (+ 0.2)	-3.9E-19	5.65E-11	Isoelectric gate	1.1 V/cm	6.52E-03

9.3 (+ 3.4)	-6.8E-18	5.65E-11	Central reservoir (pre membrane)	0.5 V/cm	0.06
			Central reservoir (gel)	0.25 V/cm	0.0255
			Sample reservoir	0.35 V/cm	0.042

Time needed to travel through

The sample reservoir = 14 mm / 0.042 mm/s = 333.3 s = 5.55 minutes

The isoelectric gate = 5 mm / 6.52E-03 mm/s = 766.87 s = 12.78 minutes

The central reservoir = 4 mm / 0.06 mm/s + 3mm / 0.0255mm/s = 360 s = 6 minutes

Total = 24.33 minutes in the absence of electroosmotic flow

S2 Supplementary information 2 - Cost analysis of the device

Cost of a PET sheet 0.005” – 27” x 10ft – CAD $6

(McMaster Carr)

Area of sheet used per device - 1.5” x 1” per layer –3 layers

Cost of PET per device – CAD $0.0083

Cost of 3M tape – 600mm x 900mm - $9.5

Cost of 3M per device – 5 layers – CAD $0.009

Fluorescent dye used – qubit protein assay - $444 for 500 assays that use 3µL each

= $0.866 per assay

We use 15µL per run = CAD $4.33

https://www.thermofisher.com/order/catalog/product/Q33211#/Q33211

IMAC affinity beads – 25mL for CAD $485

25µL used per run = CAD $0.485

Barium chloride, citric acid, sodium phosphate dibasic, tris, hydrochloric acid - <$0.01 per device

Instrumentation cost

Cost of xurography using cricut explore - $350

Results

Setup cost = $350 for small scale production

Total cost per device = Cost of materials + Cost of reagents

= 0.0083 + 0.009 + 4.33 + 0.485

= CAD $4.83

Chapter 4: Development of automated aliquoting in thread based microfluidic sensing

Full Citation: Damodara, S., Zhu, Y. & Selvaganapathy, P.R. Patterned threads as solid-state reagent storage and delivery medium for automated periodic colorimetric monitoring of the environment. Microfluid Nanofluid 25, 93 (2021). https://doi.org/10.1007/s10404-021-02496-x

Patterned threads as solid-state reagent storage and delivery medium for automated periodic colorimetric monitoring of the environment

Sreekant Damodara[1], Yujie Zhu[1], P.Ravi Selvaganapathy[1*]

[1]Department of Mechanical Engineering, McMaster University, Hamilton, CANADA

Abstract

Environmental monitoring requires periodic measurement of parameters such as pH, heavy metals, nitrates and phosphates in field settings, autonomously. Microfluidic devices have been considered for environmental sensing due to its inherent advantages of lower volume, faster sensing and low-cost fabrication. Various sensing methods including colorimetric, fluorescence and electrochemistry have been studied. Among them, colorimetric sensing is attractive due to its simple instrumentation and wide range of selective reagents. Nevertheless, it is limited by the use of liquid reagents which necessitates the use of energy demanding valves and pumps that limit the lifetime of colorimetric systems in the field. Here, we demonstrate that threads can be used for solid state reagent storage in the dried form to facilitate autonomous measurement. When integrated together with a microfluidic device, the system was shown to control the volume of sample exposed to the stored reagent on a thread for a controlled sample-reagent interaction and demonstrating color change that can be measured using a simple, low-cost system that minimizes energy cost by reducing the number of pumps and valves necessary. We develop a new approach to pattern and separate the dried reagents using paraffin wax to allow the thread to slide smoothly into the microfluidic device while preventing the sample from wetting the remaining thread allowing experiments to be performed at different timepoints. We demonstrate this platform for periodic measurement using pH and nitrites as examples of environmental monitoring which is

extendable to other colorimetric analytes for periodic autonomous monitoring. We show that the device operates in a range of 1 – 5 mg/mL of nitrite and pH range of 6 - 7.4 which covers the regulatory range in many countries.

Keywords – Environmental monitoring, automated sensing, colorimetric sensing, thread microfluidics, low-cost sensing

1. Introduction

The sustainable development goals (SDG 6) for 2030 announced by WHO lists access to clean water as being a vital target to be achieved in many countries around the world as it reports that unsustainable stress on water resources could put upto 45% of global gross domestic product (GDP) and 52% of the world's population at risk. The development of integrated water resources management (IWRM) was recommended as an essential part of the agenda [1]. A large part of IWRM is the development of monitoring and reporting mechanisms for water quality. To reach the global targets for water monitoring requires frequent and rapid monitoring of water quality in remote areas with limited access to laboratory services and manpower. A system that can automate the monitoring process and periodically monitor the water quality without human intervention would help meet these goals. Among the numerous analytes that are used to measure water quality, nitrite is one of the most studied analytes. It is a naturally occurring form of nitrogen and is found in low concentrations in water. An increase in its concentration can cause eutrophication of the water and lead to increased mortality of aquatic life [2]. Recommended limits for nitrite content in water range from 1mg/L in the US [3], to 3 mg/L as recommended by Health Canada [4] and WHO [5]. As a result, nitrite concentration has been assessed using a variety of methods including capillary electrophoresis [6], chemiluminescence [7], fluorescence [8], electrochemistry [9], high

performance liquid chromatography [10] and spectroscopic methods [11,12] among others. Chemiluminescence paired with flow injection analysis (FIA) [7] and absorbance after the Greiss reaction with sequential injection analysis (SIA) devices for automated monitoring [13] have been used. However, both FIA and SIA devices require the use of a combination of pumps paired with microcontrollers and numerous time synchronized valves which results in a complicated system. Microfluidic alternatives [14,15] reduce the power requirements for the components enabling longer periods of remote detection but are still by power use of the various components such as pumps and valves.

pH is another frequently studied analyte in determining water quality. While pH has limited health impact, a pH of more than 10 or less than 4 is an important indicator in measuring the corrosivity and disinfection of water. As drinking water is chlorinated, a pH above 8 indicates insufficient disinfection of the water while a low pH of under 6.5 is corrosive to plumbing, contaminating the water [16]. Furthermore, the current increase in atmospheric carbon dioxide leads to an increase in acidity of water bodies which needs to be monitored for its effects on aquatic life. The most common methods for measuring pH are electrochemical [17] and optical sensor based measurements [18–21]. Electrochemical and spectrometric sensors are widely used for pH measurement due to their high sensitivity and ability to continuously monitor pH level when deployed in remote locations without manual intervention. Electrochemical sensors are limited by requiring frequent calibrations to avoid artifacts which can cause sensor drift. These are associated with both residual liquid junction potentials and variations in asymmetry potentials [21]. Microfluidic electrochemical sensors resolve this through the use of calibration samples that are regularly used to correct for the drift, but this adds additional complexity due to the additional pumps and valves which increases the cost of the device and reduces the duration over which

automated sensing can occur. Spectrometric and colorimetric sensors avoid the issues with sensor drift but require the storage and transportation of liquid reagents which limit the period of operation [22]. In addition, both types of sensors are limited by the power demands of the components used when deployed in remote locations. This includes the pumps for the calibration samples in electrochemical sensors and the sensing reagents used in colorimetric/spectrometric sensors, valves operated to regulate fluid flow and power requirements of the electrochemical/optical sensor used. The need for pumps and valves originates from the storage, transportation and aliquoting needs of liquid reagents. The devices currently developed for remote monitoring have a high resolution for both pH and nitrite sensing. pH sensing has been demonstrated with a resolution of 0.001-0.004 pH units [19,21] and nitrite sensing with a LOD of 0.2 μM. This is necessary for some applications which require sensitive detection of changes in the environment. However, this sensitivity results in an increase in cost of the device. For applications that can be resolved at a lower sensitivity, there are only a few technologies available for automated remote monitoring due to the need for pumps and valves that need to be integrated. Monitoring water quality in remote areas with limited access to electricity could be improved through the development of a low-cost device that can continuously monitor the analyte of interest using a solid state reagent for colorimetric sensing that would reduce the power demand and enable longer term monitoring.

Low-cost microfluidic devices in combination with the colorimetric markers to detect analytes in water presents an opportunity for the development of low power automated and periodic monitoring of analytes in water. Some of the devices developed for low cost measurement use paper microfluidic devices [23] or hydrogels [24] paired with mobile phone cameras or an imaging system for colorimetric testing. These devices leverage the low cost, easy manufacturability, and

availability of numerous fabrication methods to make devices that can rapidly measure nitrite concentrations. However, these low-cost colorimetric testing methods are designed for a single use by a person on the field and require the deposition of specific volumes of sample. While self-metering paper devices have been developed, they still require personnel to operate [25]. Thread based microfluidic devices [26] share many of the advantages of paper microfluidic device including low cost, portability and ease of manufacturing. In addition, there are a few other advantages including a wide variety of materials and a higher wet strength [27]. However, traditional thread-based sensing uses threads as a medium for transporting liquids like in traditional capillaries. The testing reagent is placed on a segment of the thread and the sample is wicked to that segment by capillary forces which results in a diluted signal. In addition, the formats currently available for thread-based devices are not suitable for automated periodic monitoring as a sample needs to be manually deposited for each test using currently available devices. Microfluidic automated colorimetric systems have not been demonstrated using threads.

In this work, we show that patterned threads can be used as a solid-state reagent storage and aliquoting system that can be automated for periodic monitoring. The use of solid-state reagent storage would reduce the transportation costs associated with transportation and aliquoting of liquid samples while also reducing the power costs associated with pumps and valves associated with fluid control within the device. The patterned threads were integrated with a PDMS microfluidic device and paired with a simple imaging system. The resulting device was used to expose individual segments of the thread (with known quantities of reagent stored on it) to specific volumes of sample in an automated and controlled interaction repeatedly and consistently. We show the versatility of this device for monitoring different analytes by measuring the concentration of nitrite from 1 to 5 mg/L and pH ranging from 6 to 7.6. A nitrite range of 1 to 5 mg/L was chosen

based on the regulatory limits of nitrite content in water [3,5]. The range of pH was chosen as a pH of less than 8 is necessary for effective disinfection with chlorination and a pH of less than 6.5 can increase corrosion of plumbing and cause gastrointestinal irritation [16].This versatile platform can be adapted for monitoring other analytes of importance in the environment.

2. Device design and working principle

The development of a thread-based microfluidic device for automated and periodic monitoring of analytes requires integration of sample processing operations such as metering of the testing reagent and sample fluid. This was achieved by using a patterned thread as a solid-state container for storing and transporting dried testing reagent. Threads enable the storage of a larger volume of reagent in comparison to paper microfluidic devices of the same dimension due to the complex 3D structure and higher porosity which enables the packaging of higher amount of testing reagent in small volumes. Microfluidic containers for reagents are created on threads by patterning segments of the thread with hydrophobic materials that seep into it and prevent fluidic connection (wicking) between adjacent hydrophilic unpatterned segments. The form factor of the thread itself provides ideal confinement of fluids in the radial direction and the uniform size of the thread provides a consistent microfluidic volume for absorption and serves to aliquot reagents precisely. These advantages were leveraged to fabricate discrete compartments for reagent storage in threads separated by segments of either paraffin wax or another hydrophobic solution. The 1-D format of the thread allows sequencing of the reagents as well as spatial localization that is useful when introducing multiple reagents one after another or performing periodic tests one after another. As the thread is flexible, reagents dried on it can be stored in a more compact form when it is rolled

into a spool. Also, using stitching techniques they can be inserted into any compliant material such as an elastomer.

Leveraging these features, the patterned thread was then integrated into a PDMS device fabricated using a 3D printed mold as shown in Fig. 1(a) to satisfy two objectives. The first objective was to create a sealed environment and expose a single segment of the patterned thread at a time. The second objective was to control the volume of solution that was exposed to the segment. To accomplish these objectives, a cross channel arrangement was chosen consisting of a main channel for sample transport and an intersecting thread channel through which the patterned thread loaded with reagents was passed. The first objective was met by setting the width of thread channel to be slightly less than the free width of the thread and sealing the base of the PDMS device using a deformable silicone membrane. When a wax patterned thread was introduced into the thread channel, due to the larger diameter of the wax patterned regions, each wax barrier slightly deforms the silicone membrane as shown in the schematic of the cross section in Fig. 1(b) forming a waterproof seal. The segment between these seals acts as discrete, sealed compartments which was can then be exposed to the sample. The second objective was met by modulating the shape of the main channel at the intersection region. A diamond shaped intersection between the main and thread channels was found to minimize bubble entrapment, minimize dead volume and enabled control of the reagent volume delivered by varying the lengths of the sides of the diamond. It also reduced diffusion of the reagent stored in the thread into the remaining sample channel. The sample channel used was 2 mm wide and diverges at the intersection to be 5 mm wide forming the testing chamber. The change in width from 2 mm to 5 mm was over 4 mm. As a patterned thread with segments of 1cm was integrated into the PDMS device for sensing, a maximum width of 5 mm

was chosen to enable exposure of the sample to a single thread segment at a time while ensuring that the wax barriers block contamination of adjacent reagent segments.

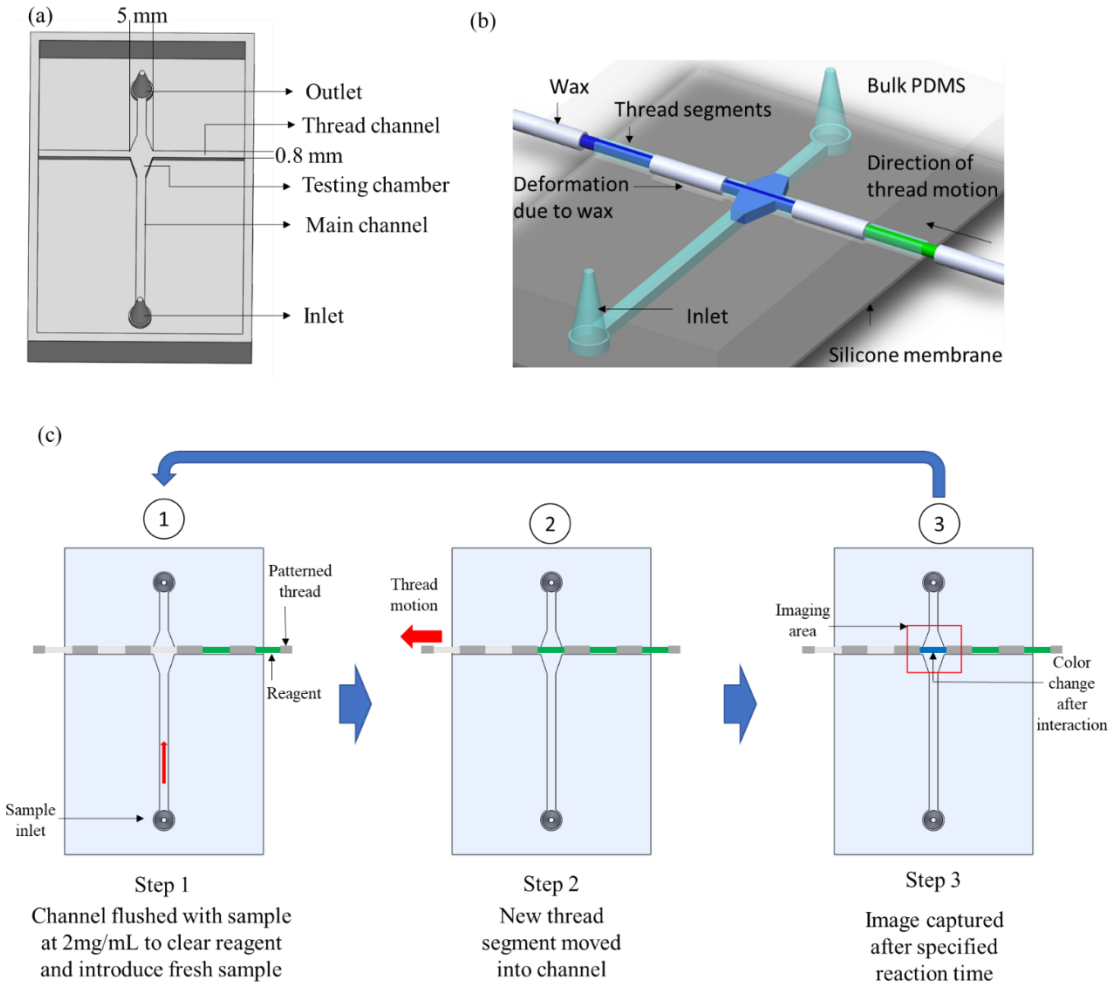

Figure 23 (a) Mold used for the fabrication of the microfluidic device (b) Fabrication of compartments in a patterned thread by deformation of silicone membrane to store reagents (c) Schematic showing the use of patterned threads for solid-state reagent storage and delivery in an automated and periodic system.

By controlling the length of the exposed thread segment to control the volume of reagent and the volume of sample exposed by using the geometry of the device, a controlled colorimetric reaction can be produced in the testing chamber. The resulting color change is then dependent mainly on the concentration of analyte in the sample. The protocol for such an application is illustrated in

Fig. 1(c). A patterned thread was dipped in a testing reagent to introduce a fixed volume of reagent into each segment of the patterned thread (colored green in Fig. 1(c)) and then inserted into the PDMS device using a needle. The wax boundaries seal the testing chamber isolating and exposing a single segment of the thread to the sample channel. The sample when injected through the main channel consists of an analyte of interest that generates a color change when exposed to the reagent in the thread. As both the volume of sample in the testing chamber and the length of the exposed thread segment are controlled, the resultant color change (green to blue in Fig. 1(c)) is dependent on the concentration of analyte. This color change could then be quantified by capturing an image after a fixed time interval. To perform another analysis, the device is flushed, and thread moved by a certain distance by winding it so that a new reagent segment on the thread is exposed to the sample in the testing chamber. This cycle can be repeated to periodically monitor the concentration of analyte in the sample.

3. Materials and Methods

3.1 Materials

The thread used in the device was 100% size 2 cotton purchased from Amazon with a diameter of 1.3 mm and ~20 tpi. PDMS (Sylgard 184) was obtained from Dow Corning, USA. Medium grade silicone sheets with a thickness of 1/32” were obtained from McMaster Carr. Real world water sample was obtained from local lake (Cootes Paradise) Hamilton, Canada. Paraffin wax with a melting point of 65 °C which was used for wax patterning, sodium nitrite with a purity of ≥99% which was used for preparation of sodium nitrite solution, anhydrous citric acid with a purity of ≥99.5% purity and sodium phosphate dibasic with a purity of ≥99% which were purchased from Sigma-Aldrich for buffer preparation. Commercial grade sensing reagent for nitrite and pH

manufactured by API fishcare that are used for macroscale sensing in aquariums, melamine sponge (Mr.Siga, China) and Neverwet (Rust-oleum, USA) were purchased from Amazon.

3.2 Fabrication

The device was fabricated in two stages. The first step was the development of patterning techniques to segment the length of the thread into discrete, defined microvolumes. This was followed by the fabrication of a microfluidic sample analysis device and integrating the patterned thread into it, to expose the sample to an individual segment of the thread without interfering with other segments.

3.2.1 Thread patterning

A patterned thread was used to control the volume of testing reagent that was absorbed into the thread for the assay. Two methods for patterning were developed. One method used a hydrophobic coating to change the contact angle of segments of the thread to make it unfavorable for wicking. This was done by fabricating a stamp containing sections of melamine sponge adhered to a glass slide as shown in Fig. 2(a) which was then spray coated with the Neverwet hydrophobic solution soaking the sponge. The stamp was then manually placed on a thread and a gentle pressure was applied to transfer the solution from the sponge sections onto the thread, creating hydrophobic segments in the thread. By making the spacing between the hydrophobic segments uniform and precise, the thread can be patterned such that the space between the hydrophobically patterned regions on the thread can serve as microvolume containers capable of storing precise quantities of reagents. This method was used to fabricate wicking barriers without affecting the flexibility and dimensions of the thread. It should be noted however that the coating took 12 hours to cure and is

a temporary coating. Frequent contact and movement over time would reduce the life of the coating and might allow fluidic contact between adjacent thread segments.

Alternatively, molten wax was also used as an ink to form the wicking barriers. This was done by placing both the wax and the thread to be patterned on a hotplate set to the temperature. A 3D polylactic acid (PLA) printed stamp, shown in Fig 2(b), was dipped in the molten wax and rapidly pressed on the thread to deposit the wax. The volume of transferred wax depends on the geometry of the stamp. The thread was heated to ensure that the wax wicks into the thread and the wicking length of wax at 75 °C was measured to be ~0.5 cm in each direction from the features on the stamp. A gap of 2 cm was used between successive features on the stamp to obtain unpatterned segments that were 1 cm long. This process was repeated to create wax boundaries with a known spacing. Wax patterning creates a reliable and inert boundary but increases the stiffness of the thread. The presence of wax coated areas also increases the diameter of the wire in the waxed segments as the wax does not completely seep into the thread before solidifying.

Once patterned, the thread was loaded by immersing it in the reagent for 1-2 minutes. The extended immersion ensures that all the hydrophilic (unpatterned) segments of the thread are fully saturated with the reagent. As is shown later in the paper, as the length of the hydrophilic segments can be controlled by the stamp used which inturn controls the volume of the reagent stored in each segment.

3.2.2 Microfluidic sample analysis device

A microfluidic device was fabricated in PDMS using soft lithography with a 3D printed PLA mold (Figure 2(c)). The PDMS device was then wet bonded to a silicone membrane by spreading a thin layer of PDMS on the base and baking the two parts together at 85 °C (Figure 2(d)). A thread

patterned using wax and loaded with the testing reagent (Figure 4(e)) was then inserted into the PDMS device using a needle. The wax barriers on the thread deform the silicone membrane forming waterproof seals between adjacent thread segments containing reagents forming the completed device as shown in Figure 4(f). Additional images are shown in Fig. S1 that show the seal when the device was operated.

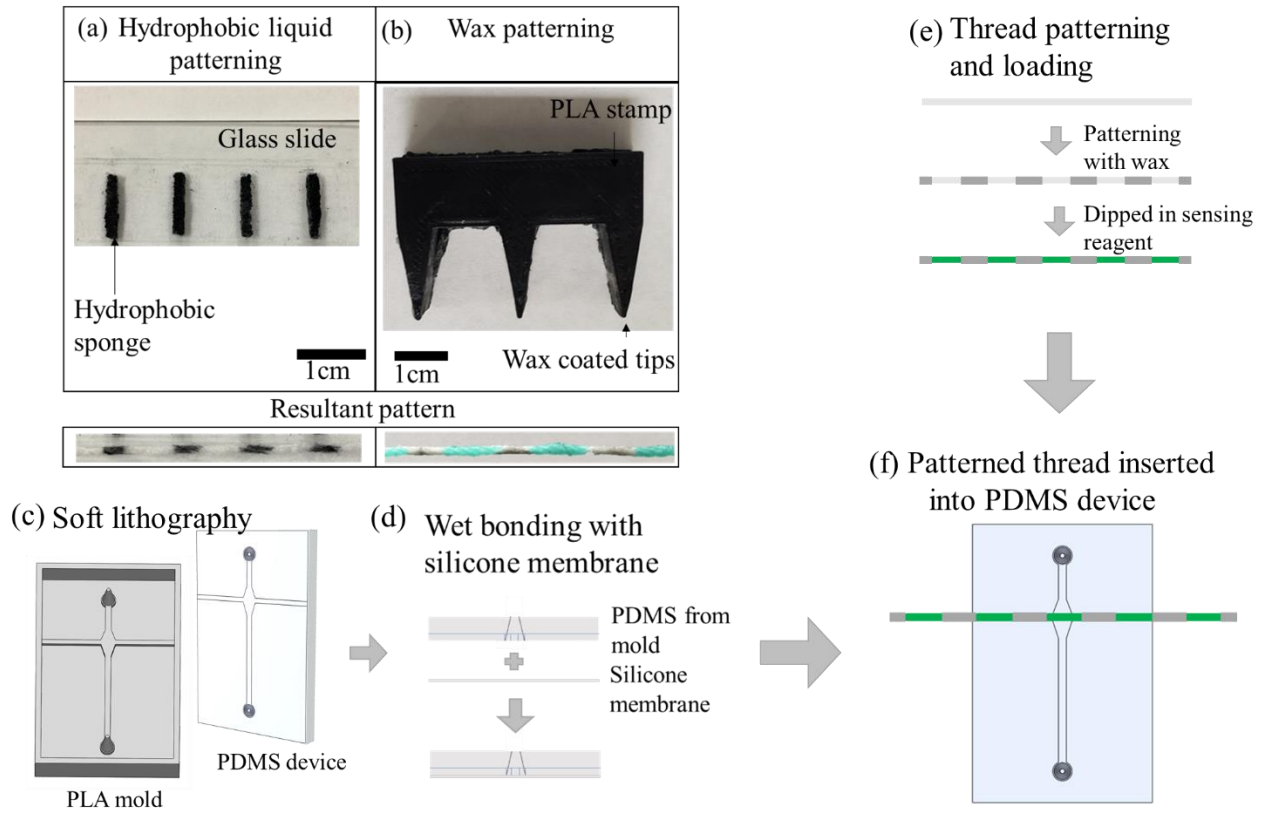

Figure 24 (a) The sponge stamp made using hydrophobic solution filled sponge on a glass slide and the resultant thread pattern (b) 3D printed PLA stamp used to wax pattern a thread with nitrite testing reagent deposited between grey wax barriers. Fabrication of the composite PDMS-thread device. (c) Soft lithography using a PLA mold (d) Wet bonding of the PDMS to a silicone membrane (e) Wax patterning and loading testing reagent on the thread (f) Insertion of patterned thread into PDMS forming individually sealed thread segments.

3.3 Experimental method and setup for colorimetric imaging

The PDMS-thread composite device was placed in an imaging box made using a black, opaque acrylic to control the lighting as shown in Fig. 3. A light source was placed at the bottom and a PDMS block was placed between the light source and device to prevent liquid from seeping into the light source inadvertently. The device was then connected to a syringe pump using luer lock connectors and liquid from the output was collected in a petri dish and discarded. A Nikon D800 camera was mounted on the ceiling of the box and connected via USB to a laptop. A software 'Digicamcontrol' was used to control the camera to take images with the box fully closed.

Automated and periodic measurement using commercial colorimetric dyes was performed by filling 5mL syringes with the necessary samples. The presence of nitrite was tested at concentrations of 1, 2 and 5 mg/L using solutions freshly made from sodium nitrite. pH was measured using solutions at pH 6.0, 6.2, 6.4, 6.8, 7.2 and 7.4 made using a combination of citric acid and sodium phosphate dibasic and verified using a pH meter to be within ±0.05. The syringe was then connected to the sample channel of the device and was perfused into the sample channel at a flow rate of 1 mL/min mimicking the typical flow of sample into the device. While a syringe pump was used in the demonstration for convenience, a low cost, low power pump or natural fast flowing streams in water bodies could be used without detriment to the functioning of the device as the accuracy of flow rate is inconsequential to the purpose of flushing remnant dye in the testing chamber and infusing a fresh sample. The device was flushed with the sample solution, several times the priming volume of the device, to remove any reagents from the prior measurement. After flushing, the pump was stopped, and the next thread segment was moved into the testing chamber to expose the reagent loaded on it to the sample in the device. The dried reagent in the thread aliquoted by the length of the thread segment then slowly dissolves and diffuses into the sample

volume in the testing chamber while the thread simultaneously absorbs the sample solution. This interaction with the sample in the chamber produces a consistent color change both in the thread as well as in the testing chamber. After a fixed exposure time (3 minutes for nitrite and 30 seconds for pH), an image of the testing chamber was taken, and the chamber was flushed again till all the testing reagent and previous sample was expelled. For periodic measurements, this operation can be repeated, and the next thread segment can be moved into the central chamber and exposed. DI water was used to flush the chamber every 3 runs. Testing with environmental samples were performed by filtering the water sample obtained from the shore of cootes paradise through a No.1 Whatman filter paper to remove the sediment and other solid particulates from the water. This was necessary as colorimetric imaging is sensitive to the hue of the water which would be affected by floating particulate matter.

To provide a benchmark for using threads in colorimetric sensing, cut threads segments with a length of 1cm were used to identify the ideal color change that could be obtained on threads with complete control over the reagent and sample volumes. This was done by dipping the thread segments in the testing reagents for nitrite and pH till they were saturated. Then, the threads were dried and placed in a petri dish. Following this, different volumes of sample containing nitrite at concentrations of 0.4, 1, 2 and 5 mg/L were added. The threads were then allowed to react for 3 minutes for nitrite before being transferred into separate chambers in a 3D printed mold for measurement. The 3D printed mold was used to hold the threads close together without contact and ensure uniform lighting across all the thread segments. The color change obtained with different volumes of nitrite was then measured from the captured images.

3.3.1 Imaging

A Nikon D810 DSLR in an opaque black box was used for imaging. A custom white balance was setup in the camera to compensate for the inherent bias in LED lighting and maintain a neutral balance in all images except for images used to check the effects of diffusion. A blue tinted white balance was used in those experiments. Raw “tiff” images were obtained from the camera. The color change in cut thread segments was measured using reflected light from the threads as the threads are opaque and color change was measured at the center of each thread. The inbuilt flash of the DSLR camera was used as the light source. An exposure time of 0.25 s, ISO 1000 and f/4.2 were used. Transmittance measurement was used for the PDMS-thread composite device as the PDMS was reflective and prevented reflectance measurement. An LED lamp placed under the device was used as the light source and the color change in the solution in the immediate vicinity of the thread was measured. The color change in the thread itself could not be used with transmittance measurement as the light source silhouettes the thread reducing the sensitivity. The nitrite color change was measured with an exposure time of 1/50 s, with an aperture of f/3.3 and ISO 32. The pH color change was measured at an exposure time of 1/100 s with an aperture of f/3.3 and ISO 64.

3.3.2 Data analysis

The obtained images were analysed using ImageJ by converting to the HSB color space. In the HSB color space, the image is split into three channels, each representing the hue, saturation, and brightness of the pixels in the original image. Hue is an angle from 0-360° that represents 0° at red, green at 120° and blue at 240°. The average hue in a fixed area near the thread (transmittance) or on the thread (reflectance) was measured to denote the color change.

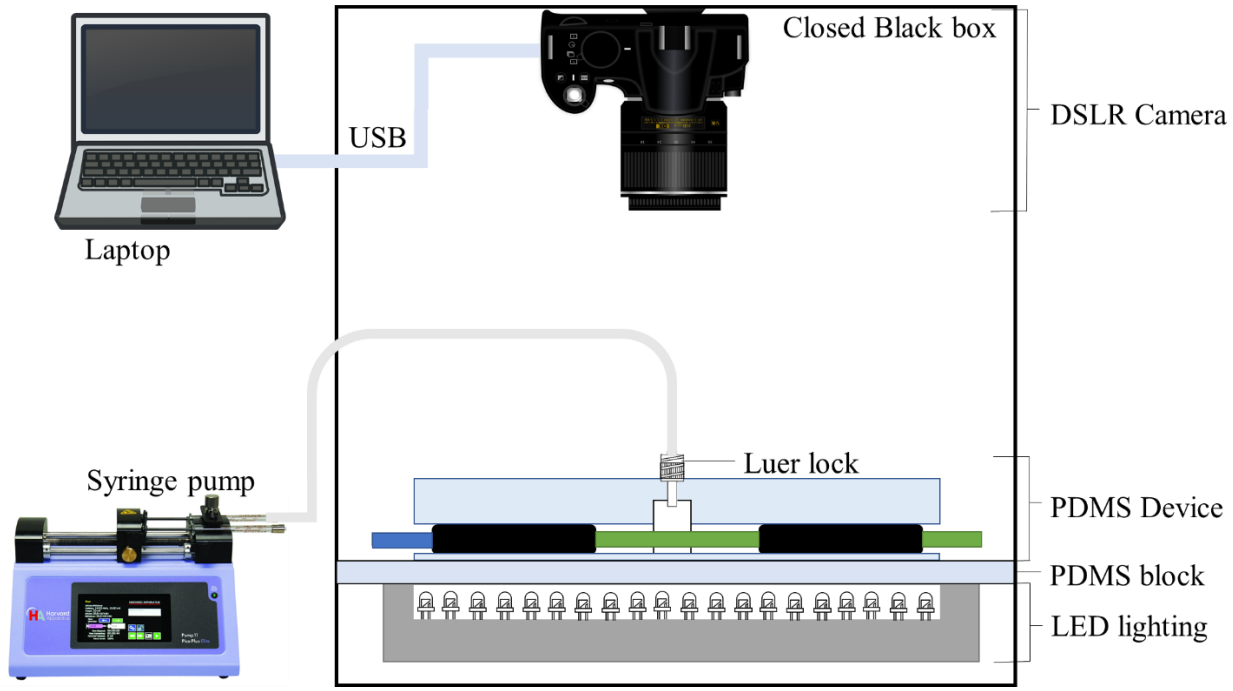

Figure 25 Experimental and imaging setup used for demonstrating automatic and periodic sensing

4. Results and Discussion

4.1 Aliquoting reagents using thread segments

The volume of reagent available in the testing chamber of the PDMS-thread device has to be controlled to produce the consistent and optimal color change for the given range of analyte concentration. The linear nature of threads enabled the use of the patterned lengths of the thread as a unique method of aliquoting the reagent volume, while also improving the ease of transport and storage. To demonstrate the ability of a patterned thread segment to aliquot specific volumes of reagent by controlling its length, the volume of liquid that can be trapped in each length of thread was quantified by cutting the thread into segments of 1, 2 and 3 cm in length. The threads were then weighed to an accuracy of 0.1 mg. The cut threads were then immersed in DI water and

gentle pressure was applied to ensure complete wetting of the threads. The threads were then weighed again, and the difference in weight was used to determine the volume of liquid held in that thread segment. This was repeated thrice for each length of thread to obtain a graph of the volume absorbed by different lengths of the cotton thread which is shown in Fig. 4(a). Next, threads were cut with an additional length of 2 cm and patterned with wax (1 cm) on each side at 75 °C as shown in Fig. 4(b). The additional 2 cm were added to allow the wax to wick through the thread, as wax wicks 0.5 cm in both direction from each point of application. The resultant trapped fluid volume was compared to the unpatterned thread to obtain Fig. 4(a). The patterned threads store slightly larger volumes of liquid compared to the same lengths of their unpatterned counterparts, which can be attributed to variation in wicking length of wax at 75 °C. The volume of fluid stored however, is consistent and predictable at each length of thread showing that fluid can be aliquoted with a patterned thread. The trendline when extended to zero length produces a non-zero intercept due to the additional surface area at the ends of the device for capillary absorption which facilitates additional absorption capacity that is independent of length. This method of using a 3D printed mold was found to be suitable to fabricate hydrophobic barriers with a length of 1 cm which separate reagent loadable segment of lengths 1cm, trapping a volume of 25 µL using this cotton thread.

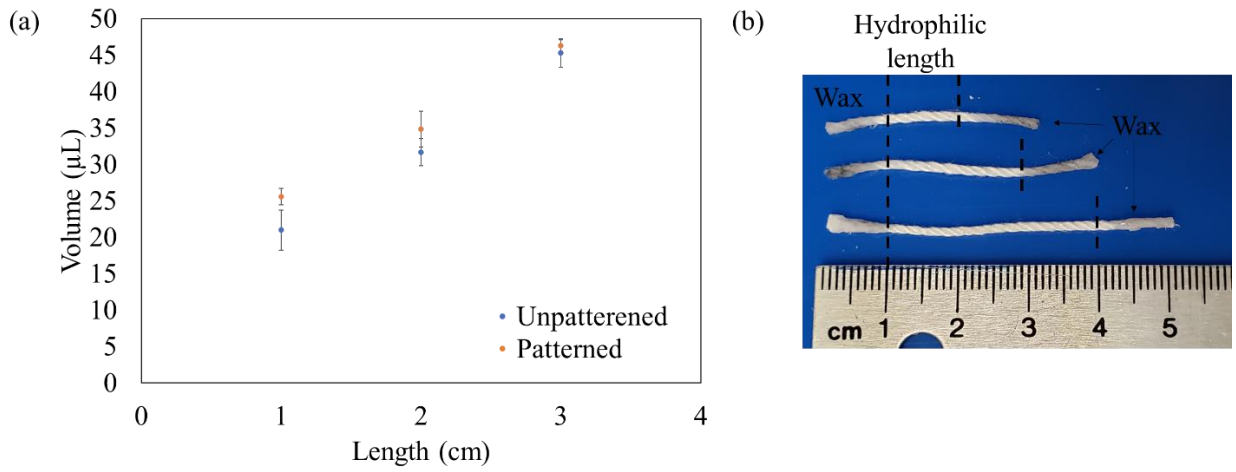

Figure 26 (a) Volume of liquid trapped in different lengths of thread with associated error bars (± 1σ) (n=3) (b) Images of patterned threads with hydrophilic lengths of 1, 2 and 3 cm.

4.2 Color change in cut thread segments

The color change in cut thread segments was measured to provide a baseline measurement for the ideal color change that could be obtained by controlling the volumes of both reagent and sample. This was done by testing different sample volumes to obtain the largest color change for a thread deposited with a known volume of reagent. The reagent volume was standardized by using a saturated 1 cm long thread segment, corresponding to a volume of 25 µL. The reagent loaded thread segments were first dried for ~2hours at room temperature. Then, 3 samples at a concentration of 5mg/L and volumes of 10,30,50,70 and 90 µL were deposited on the cut thread segments. The change in color at each sample volume was measured by capturing the light reflected from the threads as previously described and analyzed using ImageJ to obtain a correlation between the sample volume deposited and the resulting color change shown in Fig. 5(a). The color changed from an initial hue of 138° to 167° on addition of 10 µL of sample. The color change increased to 208° on addition of 50 µL of sample which was 2.4 times the change in hue with 10 µL of sample. At higher volumes, there was limited increase in the color change. A

hue of 221° was measured when 90 µL of sample was deposited which was only 1.18 times the change in hue with 50 µL of sample. This was due to a combination of limited reagent volume and limited reaction time of 3 minutes. The increase up to 50 µL was a result of the availability of unreacted reagent in the testing chamber, However, at higher sample volumes, a majority of the easily available reagent was used up except for some that was deeply trapped in the thread and slowly diffused resulting in a slight increase at higher sample volumes. As a result, the thread that was nearly saturated showed an increase from 208° at 50 µL to 221° at 90 µL. As there is little advantage to using higher sample volumes, a sample volume of 50 µL was chosen for the next test.

Solutions with concentrations of 0, 1, 3 and 5 mg/L were used to test the color change in the range necessary for testing nitrite quality in water the upper limit of which ranges from 1-3 mg/L around the world. The threads were prepared by dipping in the nitrite detection reagent and dried for ~2 hours at room temperature before adding 50 µl of the sample solution. Images were then taken as described in the methods section to obtain Fig. 5(b) which consists of three measurements at each concentration. The results show that these concentrations can be distinguished from each other using this method. The limit of detection was found to be 0.35 mg/mL based on the standard deviation of the blank.

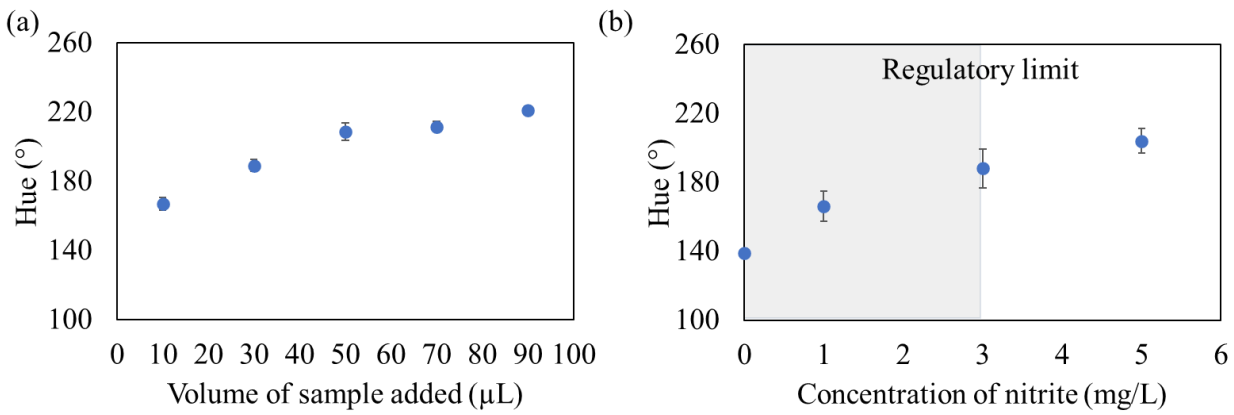

Figure 27 Color change with associated error bars (± 1σ) obtained with (a) different volumes of sample with 5mg/L of nitrite in cut thread segments (b) with 50µL of different concentrations of nitrite solution.

4.3 Dissolution of Solid-State Reagents

Controlling the sample volume in the PDMS-thread device was done by designing a suitable geometry of the testing chamber in the device. The volume of the testing chamber was designed to be 48 µL to approximate the saturation volume of 50 µL found above for color change in nitrite measurement. In addition, the diffusion of stored reagent from the thread into the device was imaged to show that the reagent-analyte interaction in the testing area at the time of imaging. The diamond shaped geometry narrows before continuing into the main channel to control the interaction of the reagent to the volume present in the diamond shaped testing chamber for the duration of the experiment by reducing convective flow and outward diffusion. This was tested by following the same protocol as described for nitrite testing in the methods section using a sample of DI water with the nitrite testing reagent on the thread. However, instead of a single image after 3 minutes, images were taken every 10 sec for 3 minutes in the area shown in Fig. 6(a). Images were taken with a blue biased white balance and converted to the HSB color space. The hue channel was used after the contrast was increased to visualize the extent of diffusion of the dye. This was possible as the green dye was visible as areas of lower intensity (darker) on a light

background. A sequence of images was taken over 3 minutes after the dye was introduced in the testing chamber and presented in Fig 6(b). These images show the initial diffusion of dye in the sample solution close to the thread (hue of 120°) and in the testing chamber initially compared to a background hue of 180° in the rest of the sample channel. The diffusion of dye into the solution reduces the hue over time, and the measured hue was used as an indicator of the extent of diffusion. The hue measured at the exit of the testing chamber remains stable at ~150° while that measured 5 mm from the exit decreases over time from an initial measurement of 176° to164° over 3 minutes as shown in Fig. 6(c) indicating diffusion of dye from the thread to a distance of 5 mm, which results in both an introduction of an additional 15 µL of sample solution (improves hue change) and diffusion of reagent over a larger volume (worsens hue change).

The response time of the device was characterized by measuring the change in hue of samples with 5 mg/mL of nitrite over 5 minutes. Images were taken every 30 seconds using a neutral white balance. The change in hue measured adjacent to the thread is shown in Fig. 6(d) which shows that the change in hue stabilizes after 180 s due to a combination of additional sample (slight increase in hue), reaction time (increase in hue) and diffusion of reagent (decrease in hue). In addition, the measured hue is noisy before 180 s as localized concentrations are non-uniform within the testing chamber, resulting in a large variation in measured hue. Although the time needed for the complete reaction of nitrite and the reagent for the macro-scale protocol was stipulated to be 5 min by the manufacturer, 3 minutes was found to be ideal for the PDMS-thread device as it was found to balance between reaction time and diffusive effects. The time for measurement pH is 30 sec as per the manufacturer's protocol, which is well within the diffusion limitations of the device. With these caveats, the design was found to be sufficient for the experiments demonstrated in this paper

and the ratio of sample to reagent use was controlled by the dimensions of the sample testing chamber.

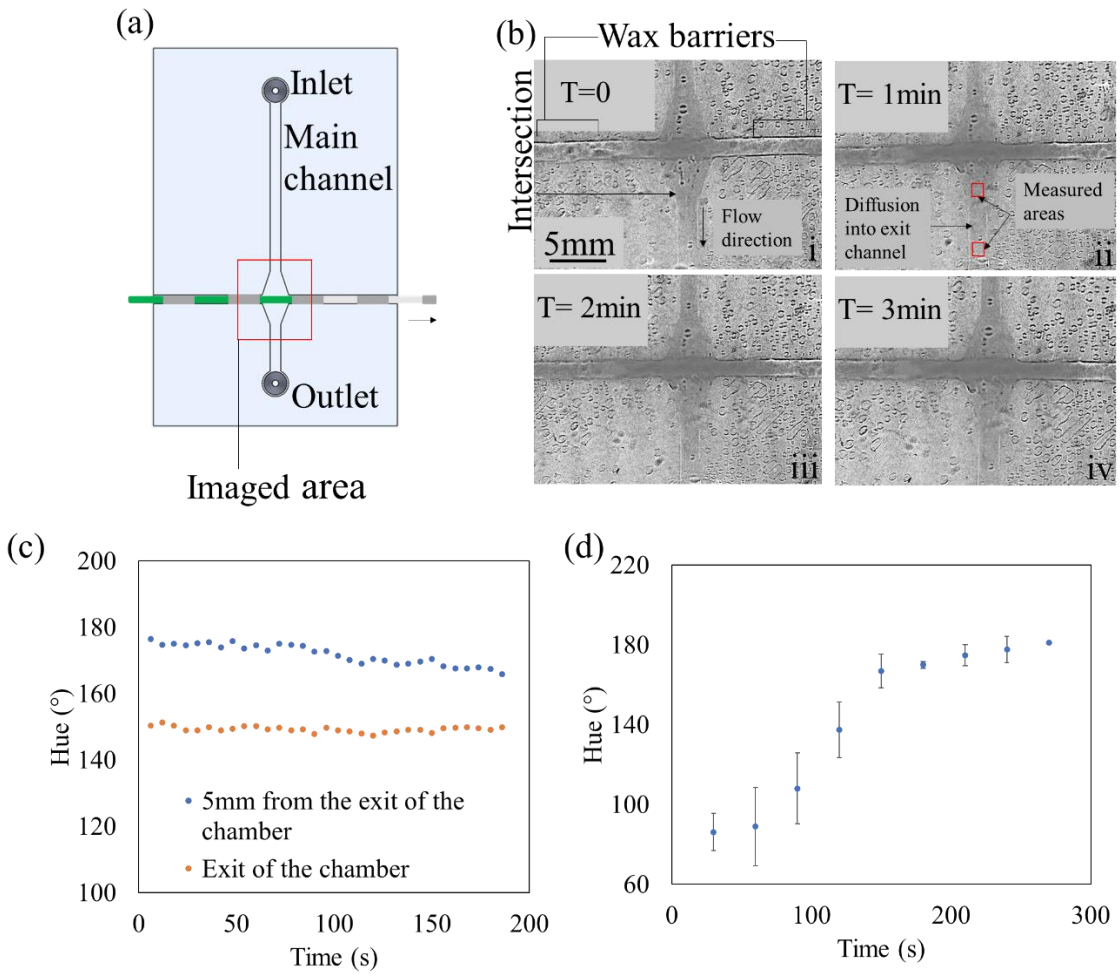

Figure 28 (a) Schematic showing the section of the device that was used for imaging color change (b) Diffusion of testing reagent over time (i)showing an overlay with the diamond shaped testing area (ii,iii) Diffusion of the reagent from the thread into the diamond shaped testing area after 1 and 2 minutes respectively (iv) Start of diffusion of the reagent into the narrow main channel (c) Hue measured in two areas of the channel (d) Change in hue over the experimental time with associated error bars (± 1σ)

4.4 Measurement of nitrite in the microfluidic-thread device

The use of an automated system for control of sample volume and reagent during the measurement of nitrite concentration in water was demonstrated using the microfluidic device. The efficacy of this method was then compared to the measurement obtained earlier where known sample volumes were pipetted onto 1cm cut threads. The demonstration was performed using a cotton thread patterned with 1cm long hydrophilic segments separated by wax barriers which was loaded by dipping in the reagent (approximate volume of 25 µL) and drying followed by integration into the microfluidic device through needle insertion. The sample was injected into the testing chamber (~48 µL) and maintained in position for 3 min. The images of the testing chamber taken after 3 min for concentrations of 0 and 3 mg/L of nitrite concentration is shown in Fig. 7(a). In order to perform the next test, the device was flushed with a sample and the thread was moved by winding it through the device to expose a new segment with the reagent to the new sample and the process repeated. The hue measured at different concentrations was plotted and compared to the results obtained using cut thread segments in Fig. 7(b). The limit of detection using the standard error of the regression was found to be 0.11 mg/mL which is significantly better than that using cut threads (0.61 mg/mL), potentially due to the use of transmission imaging which eliminates the noise from the reflection of the light source. The use of transmission imaging also changes the baseline for 0 mg/mL to 105° compared with 139° in reflective imaging while also reducing the peak from 204° compared to 183° for transmission imaging. In addition, the results with transmission imaging show a more linear change in hue with concentration showing that the microfluidic device was capable of accurately aliquoting both sample and reagents injecting and mixing them in the testing chamber in an automated manner for the detection of nitrite in a range of 1-5 mg/L in the absence of other ions in solution.

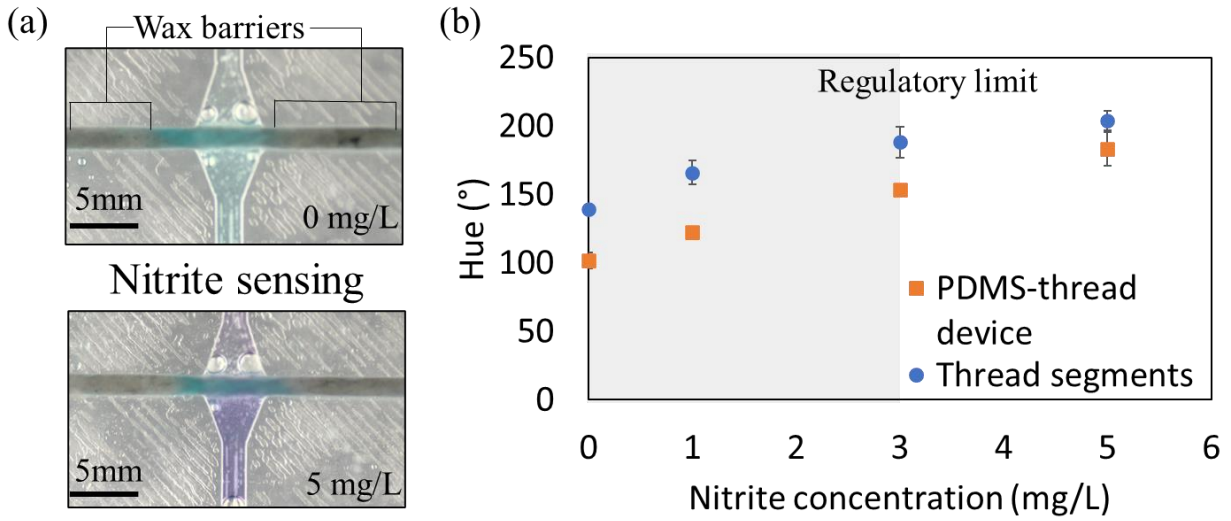

Figure 29 (a) Images obtained for nitrite sensing using the composite PDMS-thread device at 0 and 5 mg/L (b) Graph plotting the hue of the light transmitted through the solution with associated error bars (± 1σ) when measuring nitrite concentration

4.5 Nitrite measurement on environmental samples in the microfluidic-thread device

The device was then tested with a filtered sample obtained from a local pond (Cootes Paradise, Hamilton, Canada) to test for the effects of other naturally occurring ions on measurement accuracy. As nitrite rapidly oxidizes to nitrate, there was no natural nitrite in the sample. As a result, the experiments were performed using the environmental sample spiked with nitrite by adding appropriate quantities of sodium nitrite to the sample water to obtain concentrations of 0,1,3 and 5 mg/L. The protocol described in the previous section was followed and the results of the experiment with the real-world sample were compared with those obtained with DI water as shown in Fig. 8 which compares the hue obtained with these samples compared to those obtained with DI water. A 2-sided unpaired t-test comparing the measurements at each concentration shows that they do not present a statistically significant difference at a 95% confidence interval. This implies that the device can be used for testing real-world samples without manually dispensing samples.

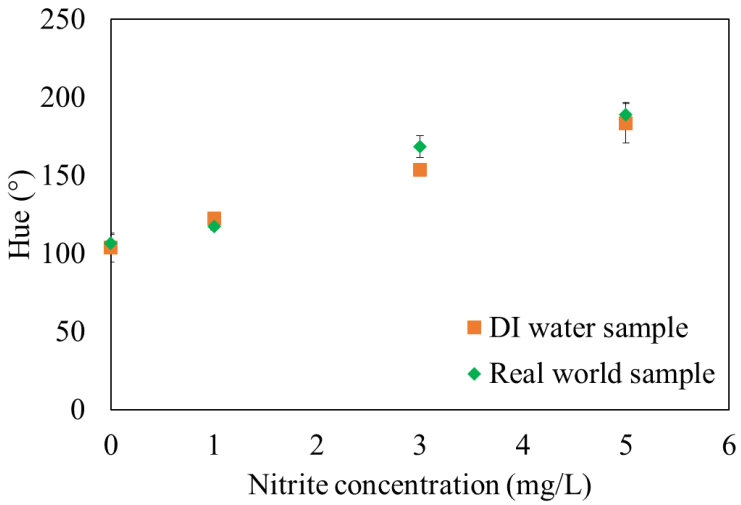

Figure 30 Results with associated error bars (± 1σ) obtained from the test with spiked real-world samples compared with those obtained from spiked DI water

4.6 Periodic and automated testing of nitrite in the PDMS-thread device

Periodic and automated testing requires repeated testing of a sample solution after fixed periods of time. This was done using the PDMS-thread device following the previously described procedures. The device was flushed with a sample solution containing 5 mg/L of nitrite in DI water and a new thread segment exposed by moving the thread every 3 minutes. Images were taken every 15sec and plotted to show the change in color over a time of 10 minutes including two sample changes. The results as shown in Fig.9 demonstrates the repeatability of measurement when using simple flushing to purge the chamber. The peak hues measured are 177.27±4.23° which is not statistically different from the 183.3±12.48° measured earlier using DI water with 5 mg/mL of nitrite. This shows that measurement within 3 minutes using the PDMS-thread device can be done periodically using an automated system that leverages the aliquoting methods described.

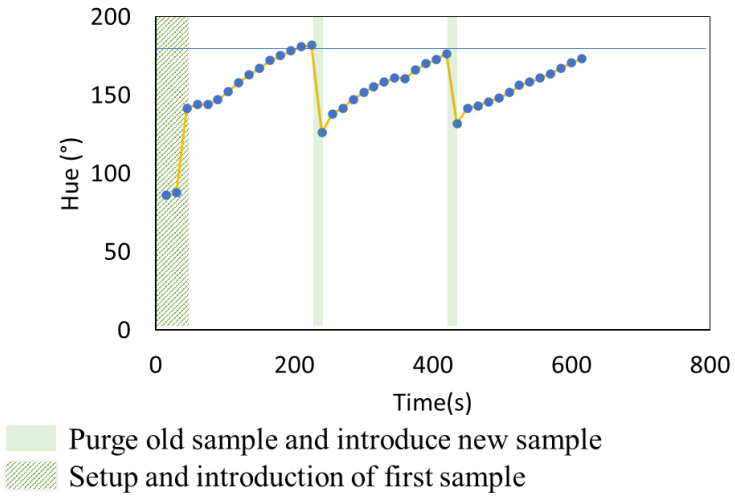

Figure 31 Plot showing measurement of 3 samples over 10 minutes, each with a concentration of 5mg/mL

4.7 Measurement of pH in the PDMS-thread device

The device can also be used for the measurement of other water quality markers such as pH which have existing colorimetric testing reagents. Samples at a pH of 6, 6.4, 6.8, 7.2 and 7.6 were prepared by using a combination of citric acid, and sodium phosphate dibasic. The wax segmented thread was dipped in the pH sensing reagent to aliquot and dried before being inserted in the device. Then, the protocol was followed as described in the previous sections with images taken 30 s after interaction between the sample and reagent. Fig. 10(a) shows the images obtained after 30 seconds using samples at pH 6.8 and 7.2. Fig. 10(b) shows a plot of the hue measured in the immediate vicinity of the thread using transmittance imaging. This results in an average change of 7.3° of hue per 0.4 change in pH. In addition, even at the pH values with the lowest difference between 6 and 6.4, a two tailed t-test shows a confidence of 96.2%, which is sufficient for automated monitoring of water quality.

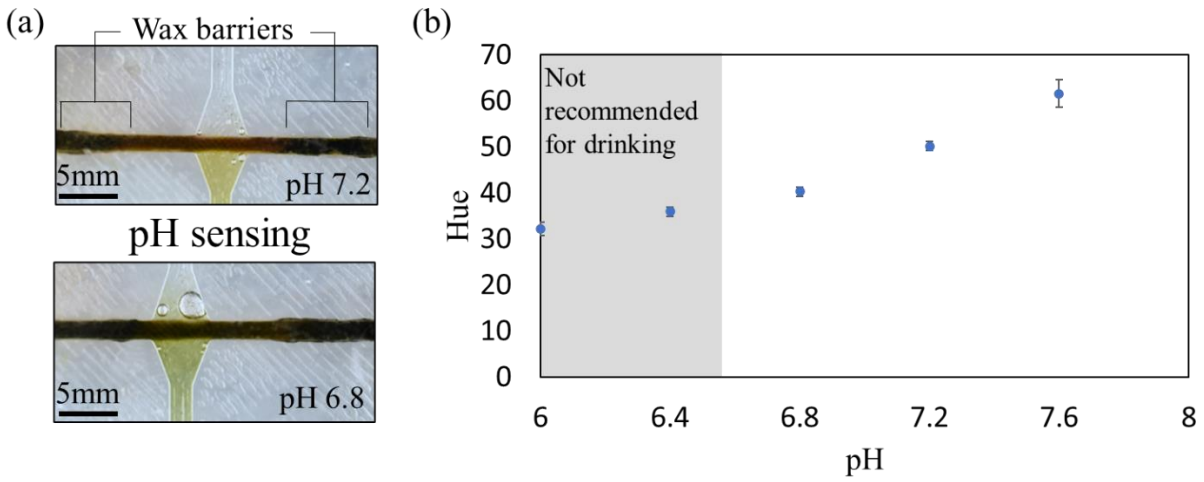

Figure 32(a) Images captured after 30s exposure of the pH sensitive dye to samples at a pH of 6.8 and 7.2 (b) The change in hue with change in pH from 6 to 7.6

5. Conclusion

We report the development of an integrated PDMS-thread device that uses a patterned thread for the solid-state storage of a reagent and the use of different lengths of thread as an effective method for controlling reagent volume. We also show the control of exposed sample volume by using the geometry of the device to expose a fixed volume of the sample to the reagent in the given time. We then demonstrate the use of the integrated device by measuring nitrite concentration in a range from 1 to 5 mg/L of nitrite that covers the minimum nitrate recommendations that range from 1mg/mL in Canada/US to 3mg/mL by WHO. We also test pH in range of 6 to 7.6 as a pH below 6.5 would corrode plumbing and cause gastrointestinal irritation while a higher pH of upto 8.5 has been reported in natural raw water and has minimal influence on health. We compare the efficacy of color change obtained in the integrated device with automated aliquoting to that obtained when samples are manually measured and deposited on 1cm long threads and obtain a slightly higher sensitivity due to the better baseline obtained as a result of transmittance-based imaging. We also

show that the device works with spiked real samples obtained from Cootes paradise, Canada and demonstrate the sequential processing ability of the device for periodic monitoring. A cost analysis conducted as shown in supplementary information 2 showed that a portable version of the device could be fabricated at a cost of $80 without a microfluidic pump $220 with the pump. The individual cost of each assay could be reduced to less than $0.11 and the power consumed by the device would be under 1W. The resultant fabricated device is a low cost and portable automated, periodic colorimetric monitoring system for nitrite and pH. In addition, due to the simplicity of the device, we believe that the principle can be extended to numerous other analytes with known reagents capable of exhibiting a color change on exposure. This would enable more robust monitoring of water reservoirs and wastewater releases into the environment and save on both fabrication and personnel cost for more extensive monitoring towards the attainment of the sustainable development goals (SDG 6).

Author declarations

This work was supported by the Natural Sciences and Engineering Research Council of Canada (NSERC) and Canadian Institutes of Health Research (CIHR) through the Collaborative Health Research Program. PRS also acknowledges support from the Canada Research Chairs Program as well as the Discovery Accelerator Supplement grant.

Declaration of Competing Interest

The authors declare that they have no known competing financial interests or personal relationships that could have appeared to influence the work reported in this paper.

Author's contributions

YZ, SD and PRS formulated the concept and experimental protocols. SD performed the investigation with inputs from PRS. SD wrote the paper with revisions and inputs from PRS.

References

[1] UN Water, Sustainable Development Goal 6: synthesis report 2018 on water and sanitation, United Nations, New York, New York, United States of America, 2018.

[2] H. Kroupova, J. Machova, Z. Svobodova, Nitrite influence on fish: a review, Veterinarni Medicina. 50 (2012) 461–471. https://doi.org/10.17221/5650-VETMED.

[3] Nitrite/Nitrate fact sheet, Water Quality Association, 2013.

[4] Federal-Provincial-Territorial Committee on Drinking Water (Canada), Canada, Health Canada, Canada, Water and Air Quality Bureau, Guidelines for Canadian drinking water quality: guideline technical document - nitrate and nitrite, 2013. https://central.bac-lac.gc.ca/.item?id=H144-13-2-2013-eng&op=pdf&app=Library (accessed May 29, 2021).

[5] J.K Fawell, Speijers, GJA, Nitrate and nitrite in drinking-water, Background document for development of WHO Guidelines for Drinking-water Quality, (2011).

[6] M.C. Barciela Alonso, R. Prego, Determination of silicate, simultaneously with other nutrients (nitrite, nitrate and phosphate), in river waters by capillary electrophoresis, Analytica Chimica Acta. 416 (2000) 21–27. https://doi.org/10.1016/S0003-2670(00)00865-5.

[7] P. Mikuška, Z. Večeřa, Simultaneous determination of nitrite and nitrate in water by chemiluminescent flow-injection analysis, Analytica Chimica Acta. 495 (2003) 225–232. https://doi.org/10.1016/j.aca.2003.08.013.

[8] L. Wang, L. Dong, G.-R. Bian, L.-Y. Wang, T.-T. Xia, H.-Q. Chen, Using organic nanoparticle fluorescence to determine nitrite in water, Anal Bioanal Chem. 382 (2005) 1300–1303. https://doi.org/10.1007/s00216-005-3250-0.

[9] B. Šljukić, C.E. Banks, A. Crossley, R.G. Compton, Copper Oxide – Graphite Composite Electrodes: Application to Nitrite Sensing, Electroanalysis. 19 (2007) 79–84. https://doi.org/10.1002/elan.200603708.

[10] H. Kodamatani, S. Yamazaki, K. Saito, T. Tomiyasu, Y. Komatsu, Selective determination method for measurement of nitrite and nitrate in water samples using high-performance liquid chromatography with post-column photochemical reaction and chemiluminescence detection, Journal of Chromatography A. 1216 (2009) 3163–3167. https://doi.org/10.1016/j.chroma.2009.01.096.

[11] A. Büldt, U. Karst, Determination of Nitrite in Waters by Microplate Fluorescence Spectroscopy and HPLC with Fluorescence Detection, Anal. Chem. 71 (1999) 3003–3007. https://doi.org/10.1021/ac981330t.

[12] J. Chen, S. Pang, L. He, S.R. Nugen, Highly sensitive and selective detection of nitrite ions using Fe3O4@SiO2/Au magnetic nanoparticles by surface-enhanced Raman spectroscopy, Biosensors and Bioelectronics. 85 (2016) 726–733. https://doi.org/10.1016/j.bios.2016.05.068.

[13] Z. Legnerová, Automated simultaneous monitoring of nitrate and nitrite in surface water by sequential injection analysis, Water Research. 36 (2002) 2777–2783. https://doi.org/10.1016/S0043-1354(01)00513-9.

[14] A.D. Beaton, V.J. Sieben, C.F.A. Floquet, E.M. Waugh, S. Abi Kaed Bey, I.R.G. Ogilvie, M.C. Mowlem, H. Morgan, An automated microfluidic colourimetric sensor applied in situ

to determine nitrite concentration, Sensors and Actuators B: Chemical. 156 (2011) 1009–1014. https://doi.org/10.1016/j.snb.2011.02.042.

[15] A.D. Beaton, C.L. Cardwell, R.S. Thomas, V.J. Sieben, F.-E. Legiret, E.M. Waugh, P.J. Statham, M.C. Mowlem, H. Morgan, Lab-on-Chip Measurement of Nitrate and Nitrite for In Situ Analysis of Natural Waters, Environ. Sci. Technol. 46 (2012) 9548–9556. https://doi.org/10.1021/es300419u.

[16] WHO, Background document for development of WHO Guidelines for Drinking-water Quality, (2003).

[17] M.T. Ghoneim, A. Nguyen, N. Dereje, J. Huang, G.C. Moore, P.J. Murzynowski, C. Dagdeviren, Recent Progress in Electrochemical pH-Sensing Materials and ConFigurations for Biomedical Applications, Chem. Rev. 119 (2019) 5248–5297. https://doi.org/10.1021/acs.chemrev.8b00655.

[18] A. Steinegger, O.S. Wolfbeis, S.M. Borisov, Optical Sensing and Imaging of pH Values: Spectroscopies, Materials, and Applications, Chem. Rev. 120 (2020) 12357–12489. https://doi.org/10.1021/acs.chemrev.0c00451.

[19] V.M.C. Rérolle, C.F.A. Floquet, A.J.K. Harris, M.C. Mowlem, R.R.G.J. Bellerby, E.P. Achterberg, Development of a colorimetric microfluidic pH sensor for autonomous seawater measurements, Analytica Chimica Acta. 786 (2013) 124–131. https://doi.org/10.1016/j.aca.2013.05.008.

[20] M.P. Seidel, M.D. DeGrandpre, A.G. Dickson, A sensor for in situ indicator-based measurements of seawater pH, Marine Chemistry. 109 (2008) 18–28. https://doi.org/10.1016/j.marchem.2007.11.013.

[21] X. Liu, Z.A. Wang, R.H. Byrne, E.A. Kaltenbacher, R.E. Bernstein, Spectrophotometric Measurements of pH in-Situ: Laboratory and Field Evaluations of Instrumental Performance, Environ. Sci. Technol. 40 (2006) 5036–5044. https://doi.org/10.1021/es0601843.

[22] A.M. Nightingale, A.D. Beaton, M.C. Mowlem, Trends in microfluidic systems for in situ chemical analysis of natural waters, Sensors and Actuators B: Chemical. 221 (2015) 1398–1405. https://doi.org/10.1016/j.snb.2015.07.091.

[23] N. Lopez-Ruiz, V.F. Curto, M.M. Erenas, F. Benito-Lopez, D. Diamond, A.J. Palma, L.F. Capitan-Vallvey, Smartphone-Based Simultaneous pH and Nitrite Colorimetric Determination for Paper Microfluidic Devices, Anal. Chem. 86 (2014) 9554–9562. https://doi.org/10.1021/ac5019205.

[24] J. Nam, I.-B. Jung, B. Kim, S.-M. Lee, S.-E. Kim, K.-N. Lee, D.-S. Shin, A colorimetric hydrogel biosensor for rapid detection of nitrite ions, Sensors and Actuators B: Chemical. 270 (2018) 112–118. https://doi.org/10.1016/j.snb.2018.04.171.

[25] B.M. Jayawardane, W. Shen, I.D. McKelvie, S.D. Kolev, Microfluidic paper-based analytical device (μPAD) for the determination of nitrite and nitrate, Analytical Chemistry. 86 (2014) 7274–7279. https://doi.org/10.1021/ac5013249.

[26] X. Li, J. Tian, W. Shen, Thread as a Versatile Material for Low-Cost Microfluidic Diagnostics, ACS Appl. Mater. Interfaces. 2 (2010) 1–6. https://doi.org/10.1021/am9006148.

[27] M. Reches, K.A. Mirica, R. Dasgupta, M.D. Dickey, M.J. Butte, G.M. Whitesides, Thread as a Matrix for Biomedical Assays, ACS Appl. Mater. Interfaces. 2 (2010) 1722–1728. https://doi.org/10.1021/am1002266.

Supporting information 1 – Sealing of the thread channel using wax patterned thread

The wax barriers used to pattern the thread were used to seal the thread channel and expose a single section of the thread at a time. This was tested using samples of 0 and 5 mg/mL when images were taken after 3 minutes of exposure to the sample. The color of the unexposed sections of the thread remained unchanged while those of the exposed section changed showing that the sample was not allowed to percolate into the unexposed thread section. The location of the images on the device is shown in Fig. S1a and the images of the wax barrier in two samples each with 0 and 5 mg/mL are shown in Fig. S1b. The consistent color of the unexposed section despite three minutes of exposure in the testing chamber shows and flushing steps shows that the wax barrier based deformation of silicone is sufficiently watertight for the flow rates used in the experiment.

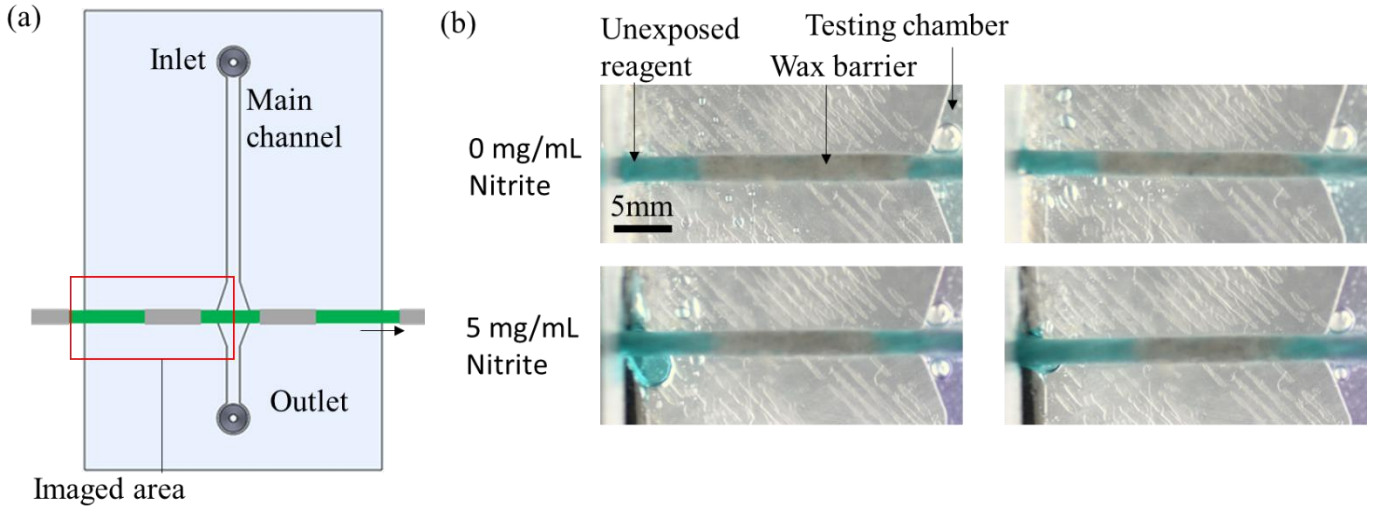

Supporting information 2 – Cost and power draw of the device

PDMS device – 20 Kg for USD$2600

https://krayden.com/buy/sylgard-184-silicone-elastomer-kit-clear-19-9-kg-kit-44lbs.html

Cotton thread - $6 for a 200+ yard spool (Amazon.ca)

Paraffin wax (Sigma-Aldrich) – 12Kg for CAD592

https://www.sigmaaldrich.com/CA/en/product/aldrich/327204?context=product

Nitrite test kit - CAD$16 for 50mL

PDMS - 50g - CAD$8.2

Cost for a portable package

Raspberry pi zero W - USD$15

https://www.pishop.ca/product/raspberry-pi-zero-w/

Raspberry pi camera - USD$36

https://www.pishop.ca/product/raspberry-pi-8mp-camera-board-v2/

3D printed support - PLA 100g – USD4.8 + Printing cost

https://shop3d.ca/products/dremel-3d-1-75mm-pla-filament?_pos=3&_sid=6863a61e4&_ss=r&variant=1996259360778

Stepper motor for thread control - $16

https://www.amazon.ca/Twotrees-Nema17-Stepper-17HS4401S-Printer/dp/B08C2KDY6R/ref=sr_1_5?dchild=1&keywords=stepper+motor&qid=1630532858&sr=8-5

Pump (resolution unimportant) - CAD$244*

https://www.dolomite-microfluidics.com/product/peristaltic-pump/

*Can be replaced with natural flow

Per test cost

Cotton thread	- 30cm - CAD$0.001
Paraffin wax	- 2g – CAD$0.1
Nitrite testing reagent	- 25µL – CAD$0.008

Power usage

Raspberry pi camera + Raspberry pi zero	- 100mA idle to 170mA@ 5.19V – 0.882W
Pump	- 0.12 W
Total power use	– 1W when taking a picture, 0.639 W on idle.

Chapter 5: cfDNA measurement using thread microfluidic devices

Single step measurement of circulating free DNA for sepsis prognosis using a thread based microfluidic device

Sreekant Damodara[1], Jaskirat Arora[2], Patricia C. Liaw[2], Alison E. Fox-Robichaud[2], P. Ravi Selvaganapathy[1]*

[1]Department of Mechanical Engineering, McMaster University, Hamilton, CANADA

[2]Department of Medicine, McMaster University, Hamilton, CANADA

Abstract

Sepsis is a "life-threatening organ dysfunction caused by a dysregulated host response to infection" which affects more than 1.5 million people annually in the U.S alone. However, diagnosis and prognosis of sepsis is challenging, and numerous biomarkers have been studied to improve this. One such biomarker is the cell free DNA (cfDNA) in plasma. During sepsis, there is a significant increase in cellular death resulting in an increase in total plasma cfDNA which could be used as an in indicator of severity of sepsis. It was found that the cfDNA content in sepsis patients entering ICUs who were likely to survive had a cfDNA concentration of 1.16± 0.13 µg/mL compared to 4.65 ± 0.48 µg/mL of non survivors. Current methods for measuring cfDNA content in plasma such as UV absorbance, fluorescent spectrometry, quantitative PCR (qPCR) or digital PCR (dPCR) were designed to amplify and measure low concentrations of specific DNA making them unsuitable for the use in measuring total cfDNA content in plasma. Here, we have developed a POC device that used a thread-silicone device as a medium to store a fluorescent dye eliminates the need for preparatory steps, external aliquoting and dispensing of reagents, preconcentration and external mixing while reducing the cost of detection. The device was paired with a portable imaging system that can be operated with just 100mA current supply. The device was

demonstrated for use in the quantification of buffered cfDNA samples in a range of 1 – 6 µg/mL with a sensitivity of 5.43 AU/µg/mL and with cfDNA spiked in plasma with a range of 1 – 3 µg/mL and a sensitivity of 5.7 AU/µg/mL. The results showed that the device could be used as a low cost, rapid and portable POC device for differentiating between survivors and non survivors of sepsis within 20 minutes.

1. Introduction

Sepsis is a "life-threatening organ dysfunction caused by a dysregulated host response to infection" [1]. It affects more than 1.5 million people and killing at least 250,000 each year in the US alone [2] and is the leading cause of mortality in the U.S with an estimated 35% of all hospital deaths attributed to sepsis in 2003. The risk of mortality increases by 4 – 9% for every hour that treatment is delayed[3]. However, diagnosis and prognosis of sepsis is exceptionally challenging due to the diverse range of conditions could result from it. As a result, numerous biomarkers have been studied for their use in sepsis diagnosis and prognosis. One of the well studied biomarkers is circulating free DNA (cfDNA) which was found to show a correlation to the ongoing process of sepsis [4]. cfDNA molecules are transient fragments of DNA released from neutrophils, eosinophils and macrophages as a result of necrosis [4][5]. They are also released by neutrophils when they release extracellular traps (NETs) via a death mechanism, known as NETosis. This releases extracellular chromatin wrapped around histones and numerous granular proteins and enzymes. Citrullination of these histones by peptidyl arginine deiminase-4 relaxes and releases cfDNA into the circulation to engulf invading microbes. They are present in minimal levels in healthy humans as they are regularly cleared by phagocytosis. However, in septic patients, there is rapid cellular death and increased apoptosis. As a result, cfDNA concentration was found to be

a prognostic indicator for overall morbidity and mortality, as cfDNA content in surviving patients on admission (1.16 ± 0.13 μg/mL) was similar to that of healthy volunteers (0.93 ± 0.76 μg/mL), while that of non-survivors (4.65 ± 0.48 μg/mL) was notably higher [6]. It has also been studied as a part of a panel of biomarkers in addition to protein C, platelet count, creatinine, Glasgow Coma Scale [GCS] score, and lactate. The panel was shown to have a stronger predictive power for mortality risk in the 28 days following measurement than SOFA)[7] which is the currently established standard for sepsis care [1].

Current methods for measuring the concentration of cfDNA, with a size of about 167 bp [8] in plasma includes the use UV absorbance, fluorescent spectrometry, quantitative PCR (qPCR) and digital PCR (dPCR). Most of these techniques were not designed with quantification of cfDNA in mind and have been adapted as they were already available in the laboratory. These factors make them unsuitable for POC rapid quantification of cfDNA at the bedside. For example, fluorescent spectrometry which typically has a detection limit of pg/mL has been integrated with electrophoretic concentration for measuring cfDNA concentration in plasma [6] in a laboratory setting. RT-qPCR with a fluorophore-based assay has been used for detection with a LOD of 0.02 pg/mL in large sample volumes [9]. Miniaturized RT-PCR with a detection limit of 1 ng/μL was demonstrated using 20μL samples with automated loading of samples[10]. However, RT-PCR has found limited use as it is more time-consuming than detection directly with fluorescent dyes [8]. Digital PCR and digital droplet PCR (ddPCR) disperse the sample volume into multiple smaller testing units to artificially increase concentration and improve the detection limit [11]. This was used to detect the presence of a mutant cfDNA at a concentration 1000-fold less than was detectable using RT-PCR. The amplification-based methods are designed for identification of extremely small amounts of DNA (such as pathogenic DNA) present in the sample and are highly

sensitive. However, in the case of sepsis, most of the cfDNA is the patients own DNA and the exact sequence of the DNA is not as important as its quantification [12]. Furthermore, the concentration of the DNA is in the µg/mL rather than pg/mL or ng/mL making amplification unnecessary. A device specifically designed for measuring total cfDNA in plasma has previously been demonstrated that used the difference in electrophoretic mobility between an agarose gel and a solution to accumulate cfDNA at the agarose gel interface. The resulting cfDNA was quantified using fluorescence microscopy with 10 minutes of sample preparation time and 5 minutes of concentration in an electric field [6]. However, the use of a gel in this device required it to be loaded just prior to use which may not be possible in a point of care setting. Furthermore, it was an active device requiring external power supply to concentrate the cfDNA.

A simple device that can eliminate the need for preparatory steps, external aliquoting and dispensing of reagents, preconcentration and external mixing while reducing the cost of detection and offering sufficient resolution to measure the difference between 1 to 6 µg/mL of cfDNA would be extremely valuable as a tool to measure cfDNA at the bedside and facilitate its use as a prognostic biomarker for sepsis. The device should be designed to distinguish between survivors of sepsis (~1 µg/mL) and non survivors of sepsis (>4 µg/mL). In this paper, we present such a POC device that meets these requirements by using threads. Thread microfluidic devices were used due to the low cost, ease of fabrication, wide range of materials to choose from, better wet strength than paper microfluidic devices, anisotropic wicking, and pre-established chemical modification toolkit from the fabric industry [13]. The thread-based device was used as a medium for storing a fluorescent dye eliminating the need for preparatory steps and externally dispensing reagents. The device uses capillary forces within the thread for aliquoting the sample and deformation of the thread under pressure to mix the samples. This was paired with a low cost and

portable imaging system for measuring the fluorescent intensity at a sensitivity required for measurement in the range of 1 – 6 µg/mL in buffered solutions and spiked in plasma.

2. Device design and working principle

The POC device that was developed consisted of two discrete subsystems. The first consists of a thread based microfluidic device that was used for storing the dye, aliquoting the sample and enhancing the mixing between the dye and sample. The second subsystem was composed of a portable fluorescence imaging system that provided sufficient illumination and filters to detect the fluorescence dye at the required resolution.

The thread based microfluidic device consisted of a polyester twisted thread that was inserted into a silicone tube. This composite device has three distinct characteristics that are useful for POC applications. Firstly, maintaining the number of twists per length is important in thread-based devices as the gap between the fibers in the twisted thread determine its storage capacity and its wicking ability. In the composite device, the silicone tube that has an inner diameter that is slightly smaller than the normal cross-sectional diameter of the twisted thread helps maintain the twists per centimetre (tpcm) of the thread (Fig. 1a). Briefly, the elastic silicone tube is expanded to insert the thread. Subsequently, the required tpcm is programmed into the embedded thread by twisting and untwisting as appropriate. In this case the natural tpcm of the polyester thread is 6. Twisting further will produce a higher tpcm and untwisting it will produce a lower one which can be used to modulate fluid transport in the thread. The silicone tube compresses the embedded thread uniformly and the frictional force of that contact overcomes the torsional spring force in the thread that has been twisted further which helps maintain the programmed tpcm over long periods of time.

Secondly, the capillary action of the hydrophilic thread draws in a fixed sample volume as it is a function of the length of the thread and the number of twists per unit length of thread (twists per cm - tpcm) both of which are tightly controlled in this device as compared with an unconstrained thread. The geometry of the thread also increases the wicking rate along the length of the device in comparison to isotropic porous media. Thirdly, the introduction of the thread into the tube increases the scattering coefficient of the device. The 3D translucent thread structure can be approximated by Mie theory by assuming the internal structure of the device as a series of spheres of different sizes[14]. Using a thread introduces a number of layers over which Mie scattering could occur in comparison to an empty tube. This increases the number of fluorescent dye molecules the excitation light could interact with which increases the emitted fluorescence and hence, the signal measured at the camera This improves the detection limit of the device which enables the detection of cfDNA without preconcentration. However, a more comprehensive study is required to identify the parameters of the thread on which this improvement is dependant. A cross section of the device is shown in Fig. 1b that shows the numerous surfaces over which scattering can occur.

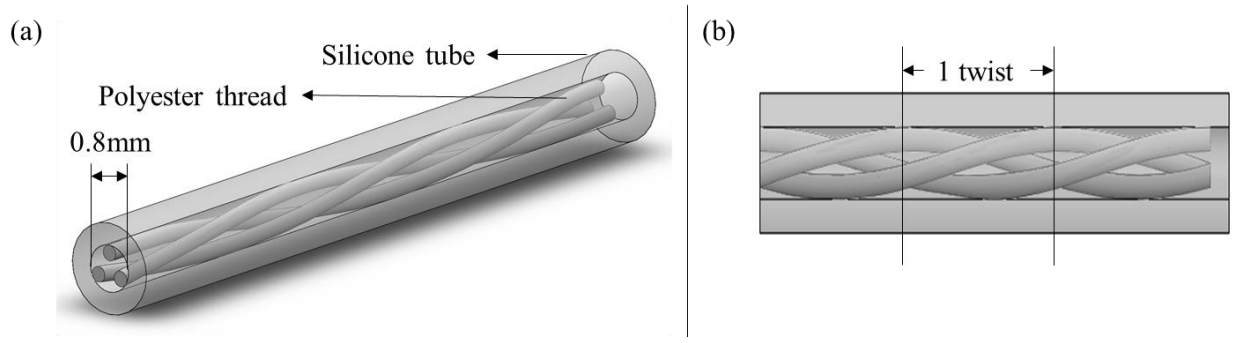

Figure 3*(a) Schematic of the thread-silicone device used as the substrate for measuring cfDNA (b) Cross section of the thread-silicone device showing numerous surfaces for Mie scattering*

3. Materials and methods

3.1 Materials

Silicone tube to serve as the sheath for the thread was purchased from Cole-Parmer. Polyester thread that was at the core of the device was purchased from amazon. Optical filters and dichroic mirror used to build the imaging setup were purchased from Edmund optics. A 470 nm LED was purchased from Thorlabs and 3D printing filament (PLA) used to print the housing for the imaging setup was purchased from Ultimaker. Buffered cfDNA samples were obtained from the Thrombosis & Atherosclerosis Research Institute (TaARI). Citrated pooled human plasma was obtained from Innovative research. Picogreen dsDNA asaay kit was obtained from Thermofisher Scientific. The 20x concentrate of TE buffer from the Picogreen dsDNA assay kit was diluted using DI water to obtain 1x TE buffer which was used as the control.

3.2 Fabrication

The polyester thread was composed of three intertwined strings with 6 twists per cm (tpcm) of thread and a free diameter of 1 mm. The thread was inserted into a silicone tube with an inner diameter of 0.8 mm using a needle compressing the thread to a diameter of 0.8 mm. The friction between the thread and tubing was used to hold the twists of the thread in place when the tpcm was changed manually. Sections with a length of 1cm were then cut from the composite and used as the substrate for measurement. A front end and a tail end for the device were arbitrarily chosen and 0.5 µL of undiluted picogreen dye was pipetted into the device from the front end of the device. Typically, the dye loaded device was used within 30 minutes of fabrication although longer durations between dye loading and experimentation are possible.

3.3 Imaging setup

The fluorescence imaging system consisted of a 3D printed black box affixed with the required lenses and cameras. A Raspberry pi camera was installed at the top of the black box, and a Thorlabs 470 LED with a peak wavelength of 470nm was installed at the left side of the black box. An excitation filter with a wavelength of 472 ± 10nm and a diameter of 12.5 mm was placed in front of the LED. An emission filter with a wavelength of 520 ± 10nm with a diameter of 25 mm was placed in front of the Raspberry pi camera. A dichroic mirror with a passing wavelength of 490 nm was placed at a 45° angle to reflect the LED light onto the sample and allow passage of the emitted light to the camera. A schematic of the imaging setup is shown in Fig. 2a. A drawer was used to introduce the sample to this camera while blocking out external lighting. The drawer was designed as a fixture to ensure repeatable positioning of the microfluidic device and was lined with silicone sheet to prevent contamination between samples.

The Raspberry pi camera was connected to a Raspberry pi controller and a python code was used to capture the image with an ISO of 50, and a white balance ratio of red:green:blue of 0:1:1. A shutter speed of 1s was used for the buffered samples of cfDNA which was reduced to 0.75 s for plasma due to a higher background signal. All other automatic filters of the camera were disabled. A power supply was connected to the LED to obtain an input current of 100 mA.

The resulting images were transferred and analysed using ImageJ. The images were split into R-G-B channels and the intensity of the green channel at the end of the device where the dye was deposited was measured.

3.4 Experimental protocol

During the experiment, a drop of the sample was placed at the tail end of the device, allowed to wick-in and excess sample removed by shaking. The time between the addition of the dye and the sample was found to have no effect on measured intensity within 30 minutes. Longer times were not tested but should be possible as the dye was dried within 30 min. Since the dye and sample were loaded from opposites ends, the physical distance separating them prevents any appreciable mixing of the dye with excess sample. The tube was then squeezed in the middle to deform it which causes the sample to flow into the dried dye region enabling resuspension of the dye and its eventual mixing with the sample (Fig 2c). The device was then allowed to incubate for 20 minutes following which it was placed in the slot in the 3D printed drawer which was then placed in the imaging setup as shown in Fig. 2b. A current of 100mA was supplied to the LED and a program written in python was used to capture the image with the raspberry pi camera. The intensity was measured 1mm from the front end of the device in a centrally located square of side 0.5 mm

Buffered cfDNA samples obtained from TaARI were obtained by purification using DNA blood mini kit from Qiagen and measured using standard spectrophotometric methods to determine the amount of cfDNA present. Plasma cfDNA samples were obtained by diluting the buffered cfDNA samples using citrated pooled human plasma. The resulting samples contained 50% plasma and 50% of the cfDNA concentration in buffer resulting in a lower range for testing plasma samples. Buffered cfDNA samples with a concentration of 1.6, 3.2 and 5.9 µg/mL were used in the testing of the device.

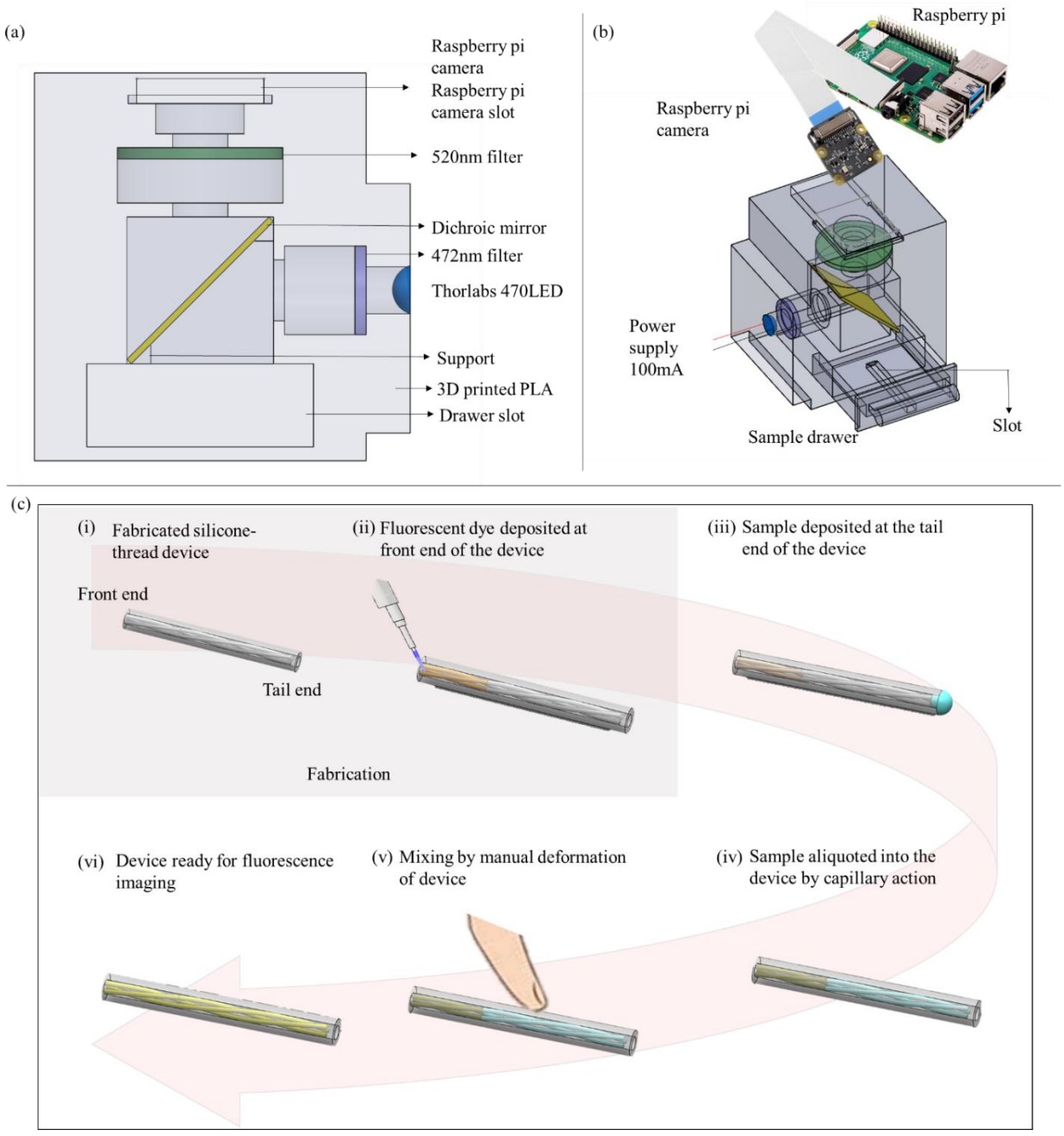

Figure 34(a) Schematic of the 3D printed imaging setup showing the locations of the filters and dichroic mirror (b) Experimental setup used for measuring cfDNA (c) Process flow to setup the thread-silicone device for measurement

4. Results and discussion

4.1 Aliquoting using the thread-tube device

Aliquoting defined sample volumes without extensive or intricate effort by the user is an important element of any POC device. In this device, the defined length (1 cm) along with an accurate control of the twists in the thread enabled accurate definition of the aliquot volume of the sample passively. Various experiments were performed to characterize the effect of the device length and the tpcm of the embedded thread in the volume aliquoted by simply weighing the device before and after absorption of water. Three devices each were prepared with lengths of 1 cm, 2 cm, and 3 cm and an embedded polyester thread with 6 tpcm. DI water samples were placed at the tail end of the device and allowed to absorb passively. The difference in the weight of the device before and after absorption was measured and shown in Fig. 3a. Similarly, three additional devices with a length of 2 cm and containing embedded thread with 5, 6 and 7 twists per cm (tpcm) were fabricated. DI water absorption in these devices was used to characterize the effect of the twists in the thread on the capacity to aliquot different volumes as shown in Fig. 3b.

The results show that the volume of fluid absorbed increases with increase in length as the polyester thread is hydrophilic and draws in fluid by capillary action to saturate the thread. Threads with longer length have more capacity to absorb. It should be noted that extending the trendline to zero length produces an intercept of 1.17 µL which is due to the end effects which facilitate additional absorption capacity. Longer threads also take longer time to fill. Therefore, a device length of ~ 1 cm is optimal to aliquot ~ 4 µL of sample which is sufficient for the purposes of cfDNA analysis.

The effect of tpcm on the volume absorbed was different from that of the length. Twists less than 5 tpcm were not feasible in the current format of the device. The volume absorbed remains constant

for twists up to 6 tpcm. Further increase in twist leads to a drop in the volume absorbed. This decrease is due to the fibers of the thread being brought closer together due to the increased twist which reduces the volume available for the liquid to wick in. This behaviour was predicted based on a theoretical description of fluid flow in threads [15]. It should be noted that the twist beyond the range of 5-7 tpcm could not be maintained for long durations without constraint due to restoring spring forces in the thread. The frictional forces exerted by the silicone tube were not sufficient to withstand the spring forces and enabled the thread to slowly move back to the allowable range of tpcm. The variation in absorbed volume due to twisting of the thread was minimized by using thread with 5 -6 tpcm. The absorbed volume could be reduced by regulating the characterizing and controlling the twists per cm in the range of 6 -7 tpcm. Controlling both the length and the twists per cm of the thread enabled the use of threads to aliquot the volume of sample using capillary forces. While the current devices were prepared by manual twisting with rudimentary control of thread twisting, automated twisting of the thread would enable more precise control of fluid aliquoting in threads.

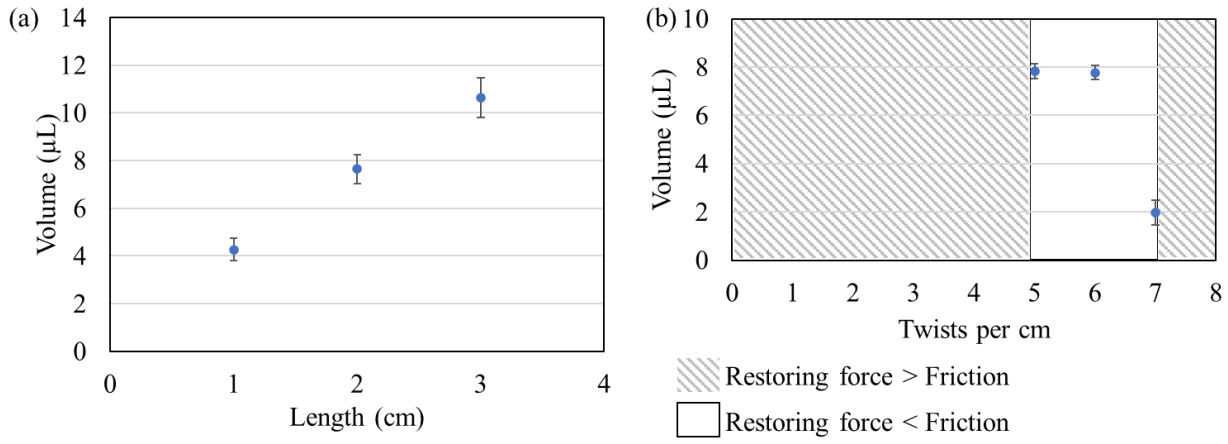

Figure 35 Dependence of volume absorbed into the thread-composite device on (a) length of the device (b) twists per cm of the thread (n=3)

4.2 Optimization of excitation light intensity in buffered samples

Since there is considerable background intensity in the device and the measurement setup, various excitation light intensities were investigated to determine the optimized value for measurement with highest sensitivity. The raspberry pi camera was setup as previously described with a shutter speed of 1s. Three samples each with TE buffer and buffered cfDNA at a concentration of 5.9 µg/mL were measured 20 minutes after the application of the sample. The intensity of the excitation light was modulated by varying the current applied to the LED. The current was set to three distinct values – 75 mA, 100 mA, 125 mA. The fluorescent intensity was measured in each of these illuminations and plotted in Fig. 4. The fluorescent intensity obtained with the TE buffer was considered as the background and the additional intensity due to the cfDNA was plotted in green. The results show a large increase in the background with each increase in current due to the increase in diffuse reflection from the thread. However, the added intensity due to cfDNA increases from 75 mA to 100 mA but decreases when further increased to 125 mA. This is because of saturation of the image from the background, which reduces the further increase from cfDNA

concentration. A lower shutter speed would be necessary to operate at a high illumination. However, this would increase the heat at the LED. As a result, a current of 100 mA was chosen to operate the LED with a shutter speed of 1s on the raspberry pi.

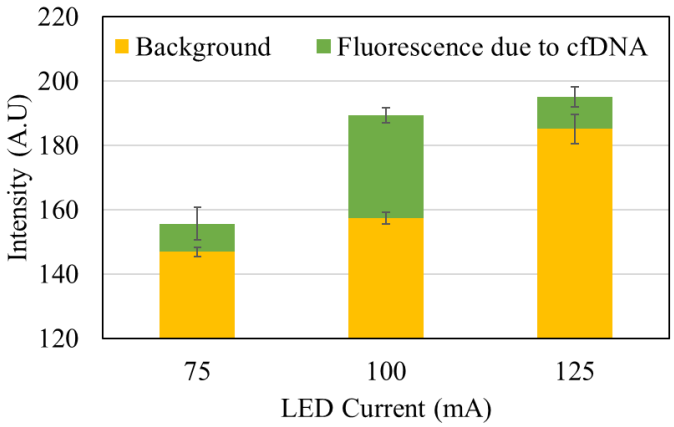

Figure 36 Effect of illumination controlled by the LED current on fluorescent intensity

4.3 Use of thread increases sensitivity

The detection of cfDNA using the portable system was first demonstrated by measuring the concentration of cfDNA in buffered samples. The buffered samples were obtained by isolating cfDNA from patient samples which were loaded into standard TE buffers. Three samples with concentrations of 1.6, 3.2 and 5.9 µg/mL of cfDNA were obtained with their concentrations confirmed by standard spectrophotometric methods as described in section 3.4. These samples were loaded on to the device and mixed using thread deformation as per protocol following which the intensity of the fluorescence close to the tail end was measured after 20 min. The results were then compared to images obtained by following the same protocol using a silicone tube except without a thread. Fig 5a shows the images obtained with 5.9 µg/mL of cfDNA in comparison to the control and the location of the imaging area used. The light in the imaging area is uniform at

the front end of the thread where the measurement is made and non uniform toward the tail end of the device resulting in a reduced intensity in that part of the image. The intensity was measured 1mm from the front end of the device in a centrally located square of side 0.5 mm. The ends of the device were avoided when measuring to reduce artifacts from evaporation affecting the measurement.

The average intensity measured with three samples at each concentration in the thread-based device were plotted to obtain Fig. 5b that shows the linear change in measured intensity with cfDNA concentration. The background intensity with and without the thread were measured using TE buffer by following the same protocol as with the cfDNA samples and resulted in average intensities of 157.6 AU and 99.67 AU respectively. The increase in background with the thread is due to the additional nonspecific background fluorescence of the thread. A comparison of the fluorescence signal obtained due to the variation in cfDNA concentration with and without the thread is shown if Fig. 5c by plotting the average increase in fluorescence intensity above the background in three samples at each concentration. The results show that the change in intensity with cfDNA concentration is linear in both formats and is significantly higher in the presence of the thread due to the increase in scattering of the incident light within the device. The slope improved from 1.6 AU/µg/mL to 5.43 AU/µg/mL which was more than a three-fold increase in sensitivity. As a result, the device had a greater than 97% confidence in differentiating between any two of the measured datapoints without any preconcentration steps compared to the greater than 50% confidence of the device without threads. As a result, the thread-silicone format device can be used to easily distinguish each of these concentrations from each other with a high confidence which is not possible in the format without a thread.

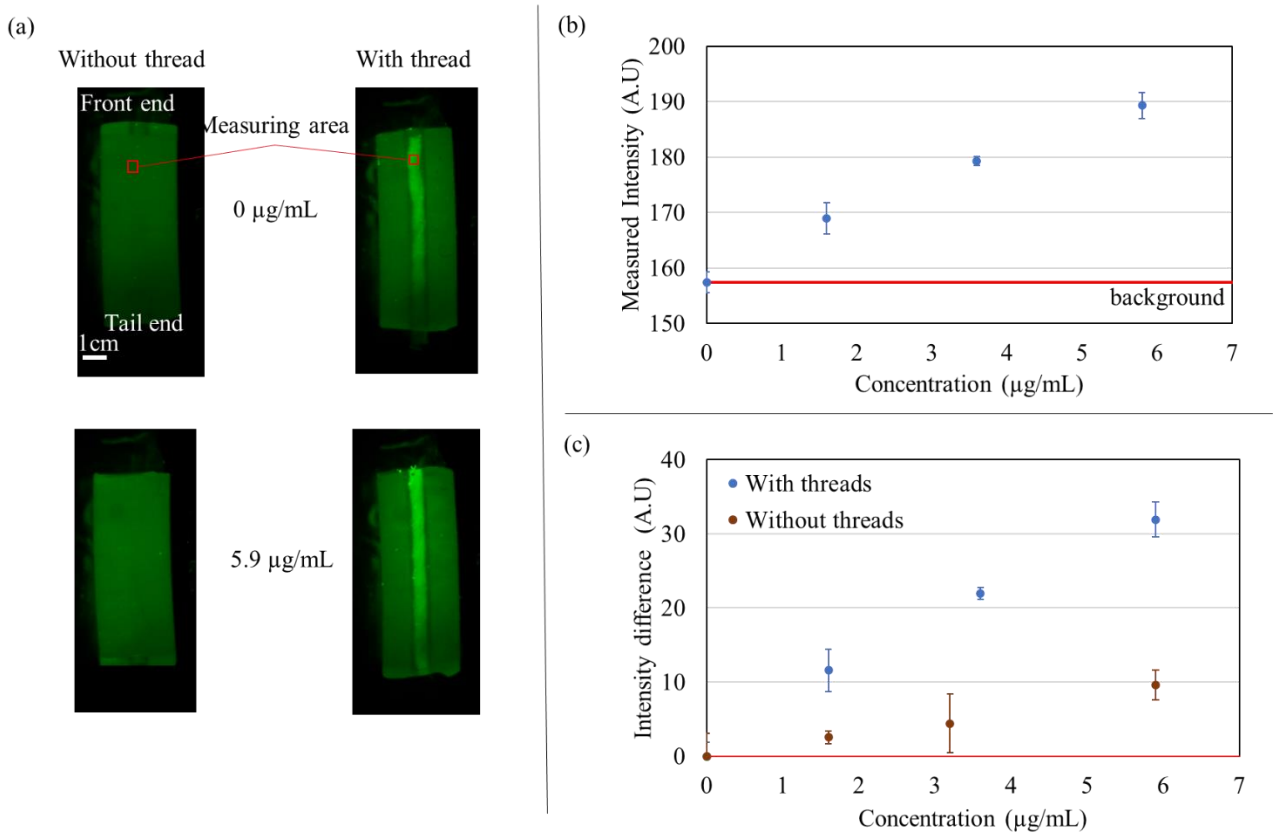

Figure 37(a) Images obtained with 5.9 µg/mL of cfDNA compared to the background (0 µg/mL) (b) Intensity of cfDNA measured in the thread-silicone device (c) Comparison of the increase in intensity due to cfDNA in devices with and without the thread.

4.4 Volume independence of cfDNA measurement

The capability of the device to aliquot a constant volume from a larger sample and prevent the dispersion of the fluorescent dye into the excess sample volume was tested by measuring the fluorescent intensity obtained when exposed to different volumes of sample. Three samples each with volumes of 5, 6 and 7 µL at a concentration of 5.9 µg/mL of cfDNA were placed on the tail end of the device. The device was then gently shaken within 2- 5 seconds to remove excess sample. This was enough time for the thread to be fully wetted by the sample. The fluorescence intensity was then measured using the protocol described in section 3.4 and the intensity plotted to obtain Fig. 6. The average intensity measured with different volumes have a range of 4 AU and are not

significantly different from each other. This was expected as the sample was deposited at the farthest point from the dye at the tail end and the excess was removed before the predeposited dye could diffuse through from the front end of the thread. As a result, no fluorescent dye was lost when the excess sample was removed. This shows that using capillary action for aliquoting in a thread result in a consistent volume of fluorescent dye interacting with a constant sample volume for a repeatable reaction irrespective of volume deposited making it ideal for point of care applications.

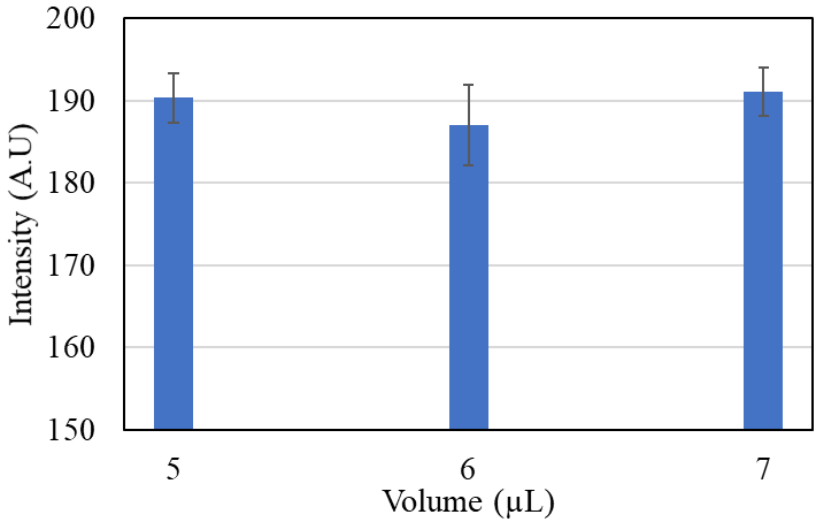

Figure 38 Volume invariance of measured intensity tested using 5, 6 and 7 µL of 5.9 µg/mL of buffered cfDNA

4.5 Determining minimum assay completion time

As the dye gets dissolved and mixed with the sample it interacts with the DNA which then diffuses over the entire thread section to reach equilibrium concentration everywhere. The time that it takes to equilibrate depends on the length of the thread device. In order to determine the time for completion of this process so that reliable and stable measurement can be taken, the change in fluorescent intensity at the tail end as a function of time was measured. Measurements were

conducted every 5 minutes for 20 minutes on three different devices each loaded with a sample with cfDNA concentration of 5.9 µg/mL. The first measurement was made within 1 minute of depositing a 5µL sample volume at the tail end of the device. The measured intensity was plotted with respect to time in Fig. 7. The results show a significant increase in intensity within 1 minute of deposition from the background (157.6) and a rapid increase in fluorescent intensity within 10 minutes followed by a stable intensity with minimal increase over the rest of the time. The protocol for picogreen dye identifies 15 minutes as the incubation time for a sample with the dye. The measured 10 minutes is slightly faster than the protocol, potentially due to the low sample volume and rapid mixing by deformation of the tube. These experiments indicate that an assay time of 10 mins from the addition of the sample is sufficient to measure intensity in the device. This is much shorter than any of the PCR based methods and is faster than the comparable fluorescence measurement technique for total cfDNA content that needs 15 minutes from sample mixing to measurement [6]. The short assay time enables the use of this device for rapid and frequent measurement of cfDNA which is necessary for use as a prognostic biomarker.

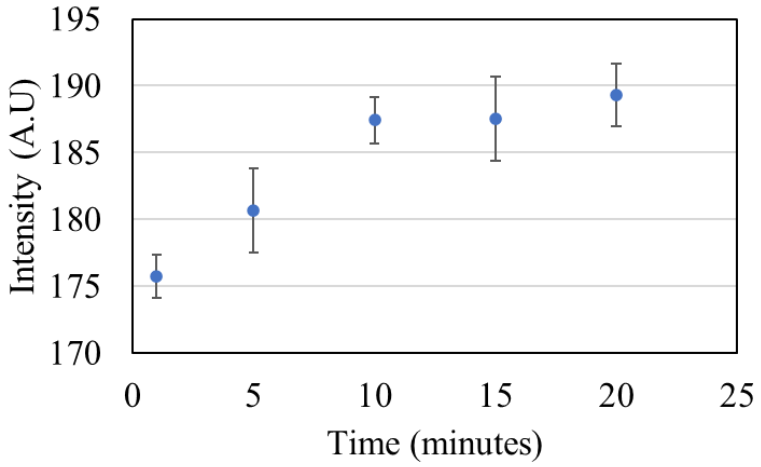

Figure 39 Changes in fluorescent intensity at tail end of the device with time and progress of the assay.

4.6 cfDNA measurement in plasma

The capability of the device to measure cfDNA in a complex medium was tested by using samples with cfDNA spiked in plasma. The buffered cfDNA used in previous experiments was mixed in a 1:1 ratio with pooled citrated human plasma which resulted in halving of the concentrations to 0.8, 1.6 and 2.95 µg/mL. The experiments were run by following the protocol described in section 3.4 with a 75 mA current supplied to the LED. The current used is less than with buffered samples due to the high background from other components in plasma which resulted in a saturated signal at 100mA. Three samples were measured at each of these concentrations and plotted to obtain Fig. 8. A slope of 5.7 AU/µg/mL was obtained which was similar to the 5.43 AU/µg/mL obtained with buffered cfDNA samples. This showed that the sensitivity of the device was not reduced due to the additional interfering agents present in plasma. The device had a greater than 95% confidence in differentiating between 0.8, 1.6 and 2.95 µg/mL samples and a greater than 85% confidence in differentiating between 0 and 0.8 µg/mL of cfDNA. The lower confidence was due to the higher noise of the background due to the presence of numerous interfering agents in plasma In comparison to the previously developed device for the measurement of total cfDNA in plasma, we obtained a p-value of 94.5e-4 with α of 0.01 to differentiate between 5.9 µg/mL and 1.6 µg/mL compared to a reported p-value of 3.7e-4 for a difference between 5 µg/mL and 1 µg/mL with the same α despite the lack of a concentration step. This shows that while the performance of the proposed device is slightly worse, it is sufficient to differentiate between patients with a high risk of mortality (>4.65 µg/mL) from survivors (~1 µg/mL) with a high confidence.

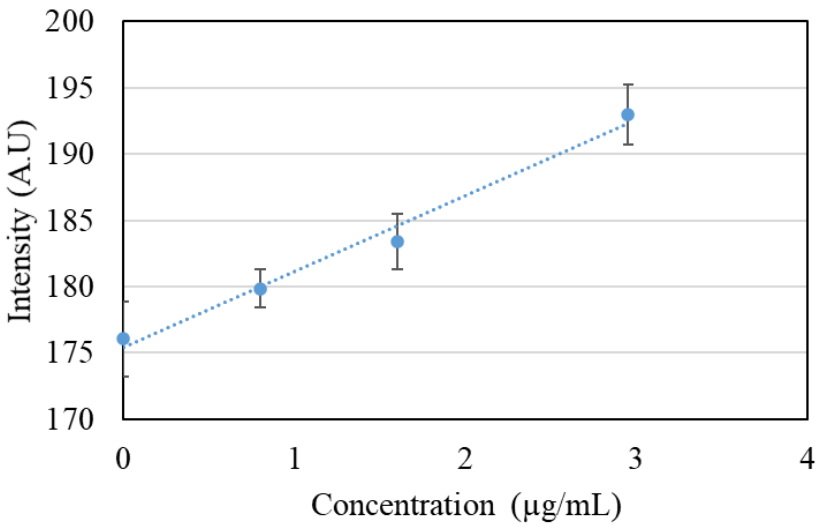

Figure 40 Change in intensity with concentration of cfDNA in 50% diluted plasma samples

5. Conclusion

A low-cost rapid measurement device for the measurement of cfDNA was demonstrated. The device consisted of a substrate made from thread trapped in a silicone tube and a portable fluorescence imaging setup for measuring the change in intensity due to the binding of a fluorescent dye with cfDNA. The samples were aliquoted using capillary flow and it was demonstrated that the volume of sample did not affect the measured intensity. This was demonstrated with volumes of 5, 6 and 7 µL of sample. The system was then used to demonstrate the advantage of additional scattering due to the thread by comparing the intensity obtained with 1.6, 3.2 and 5.9 µg/mL of cfDNA in devices with and without the thread. The results showed an increase in sensitivity from 1.6 to 5.43 AU/µg/mL which enabled the use of the device for measuring cfDNA concentration without preconcentration. The change in intensity over time was measured to show that the intensity is stabilized within 10 minutes of deposition of the sample and would be the minimum time required for the assay. The device was then demonstrated for use in plasma samples spiked with cfDNA. Plasma samples consisting of a 1:1 mixture of citrated plasma

and buffered cfDNA with a resulting concentration of 0.8, 1.6 and 2.95 µg/mL were measured. The device showed a greater than 95% confidence in distinguishing between the 0.8, 1.6 and 2.95 µg/mL samples and a slope of 5.7 AU/µg/mL which was comparable to that obtained with buffered cfDNA showing minimal effect due the presence of interfering agents in plasma. The device is a low cost, portable POC device that could be used for distinguishing patients who are likely to have a high risk of mortality (cfDNA concentration > 4.65 µg/mL) from those who are likely to survive (cfDNA concentration ~ 1 µg/mL).

6. References

[1] M. Singer, C.S. Deutschman, C.W. Seymour, M. Shankar-Hari, D. Annane, M. Bauer, R. Bellomo, G.R. Bernard, J.-D. Chiche, C.M. Coopersmith, R.S. Hotchkiss, M.M. Levy, J.C. Marshall, G.S. Martin, S.M. Opal, G.D. Rubenfeld, T. van der Poll, J. Vincent, D.C. Angus, The Third International Consensus Definitions for Sepsis and Septic Shock (Sepsis-3)., J. Am. Med. Assoc. 315 (2016) 801–10. https://doi.org/10.1001/jama.2016.0287.

[2] Centers for Disease Control, Protect Your Patients From Sepsis, (2016). https://www.cdc.gov/sepsis/pdfs/HCP_infographic_protect-your-patients-from-sepsis_508.pdf.

[3] Sepsis Alliance, Sepsis fact sheet, 2020.

[4] L. Jacobs, H.R. Wong, Emerging infection and sepsis biomarkers: will they change current therapies?, Expert Rev. Anti. Infect. Ther. 14 (2016) 1–13. https://doi.org/10.1080/14787210.2016.1222272.

[5] A. Rhodes, M. Cecconi, Cell-free DNA and outcome in sepsis., Crit. Care. 16 (2012) 170.

https://doi.org/10.1186/cc11508.

[6] J. Yang, P.R. Selvaganapathy, T.J. Gould, D.J. Dwivedi, D. Liu, A.E. Fox-Robichaud, P.C. Liaw, A microfluidic device for rapid quantification of cell-free DNA in patients with severe sepsis, Lab Chip. 15 (2015) 3925–3933. https://doi.org/10.1039/C5LC00681C.

[7] P.C. Liaw, A.E. Fox-Robichaud, K.-L. Liaw, E. McDonald, D.J. Dwivedi, N.M. Zamir, L. Pepler, T.J. Gould, M. Xu, N. Zytaruk, S.K. Medeiros, L. McIntyre, J. Tsang, P.M. Dodek, B.W. Winston, C. Martin, D.D. Fraser, J.I. Weitz, F. Lellouche, D.J. Cook, J. Marshall, Mortality Risk Profiles for Sepsis, Crit. Care Explor. 1 (2019) e0032. https://doi.org/10.1097/cce.0000000000000032.

[8] Z. Xu, Y. Qiao, J. Tu, Microfluidic technologies for cfDNA isolation and analysis, Micromachines. 10 (2019). https://doi.org/10.3390/mi10100672.

[9] K. Patsch, N. Matasci, A. Soundararajan, P. Diaz, D.B. Agus, D. Ruderman, M.E. Gross, Monitoring dynamic cytotoxic chemotherapy response in castration-resistant prostate cancer using plasma cell-free DNA (cfDNA), BMC Res. Notes. 12 (2019) 1–7. https://doi.org/10.1186/s13104-019-4312-2.

[10] R. Zhang, H.Q. Gong, X. Zeng, C. Lou, C. Sze, A microfluidic liquid phase nucleic acid purification chip to selectively isolate DNA or RNA from low copy/single bacterial cells in minute sample volume followed by direct on-chip quantitative PCR assay, Anal. Chem. 85 (2013) 1484–1491. https://doi.org/10.1021/ac3026509.

[11] B.J. Hindson, K.D. Ness, D.A. Masquelier, P. Belgrader, N.J. Heredia, A.J. Makarewicz, I.J. Bright, M.Y. Lucero, A.L. Hiddessen, T.C. Legler, T.K. Kitano, M.R. Hodel, J.F.

Petersen, P.W. Wyatt, E.R. Steenblock, P.H. Shah, L.J. Bousse, C.B. Troup, J.C. Mellen, D.K. Wittmann, N.G. Erndt, T.H. Cauley, R.T. Koehler, A.P. So, S. Dube, K.A. Rose, L. Montesclaros, S. Wang, D.P. Stumbo, S.P. Hodges, S. Romine, F.P. Milanovich, H.E. White, J.F. Regan, G.A. Karlin-Neumann, C.M. Hindson, S. Saxonov, B.W. Colston, High-throughput droplet digital PCR system for absolute quantitation of DNA copy number, Anal. Chem. 83 (2011) 8604–8610. https://doi.org/10.1021/ac202028g.

[12] D.J. Dwivedi, L.J. Toltl, L.L. Swystun, J. Pogue, K.L. Liaw, J.I. Weitz, D.J. Cook, A.E. Fox-Robichaud, P.C. Liaw, Prognostic utility and characterization of cell-free DNA in patients with severe sepsis, Crit. Care. 16 (2012). https://doi.org/10.1186/cc11466.

[13] M. Reches, K.A. Mirica, R. Dasgupta, M.D. Dickey, M.J. Butte, G.M. Whitesides, Thread as a Matrix for Biomedical Assays, ACS Appl. Mater. Interfaces. 2 (2010) 1722–1728. https://doi.org/10.1021/am1002266.

[14] S.L. Jacques, Erratum: Optical properties of biological tissues: A review (Physics in Medicine and Biology (2013) 58), Phys. Med. Biol. 58 (2013) 5007–5008. https://doi.org/10.1088/0031-9155/58/14/5007.

[15] B. Das, A. Das, V.K. Kothari, R. Fangueiro, Development of mathematical model to predict vertical wicking behaviour.part I: flow through yarn, J. Text. Inst. 102 (2011) 957–970. https://doi.org/10.1080/00405000.2010.529281.

Chapter 6: Conclusions and future directions

Conclusion

This thesis was motivated by the need for portable and rapid diagnostic assays to improve the quality of care for sepsis patients. Sepsis a life-threatening organ dysfunction caused by a dysregulated host response to infection and is characterized by a wide variety of symptoms making it challenging to diagnose. The current diagnostic method is a scoring system called SOFA that requires the measurement of partial pressure of oxygen, platelet count, bilirubin levels, blood pressure, dopamine/ epinephrine/ norepinephrine dosage, Glasgow coma scale, creatinine, and urine output. This requires laboratory assays that are time consuming and need to be performed off site. However, diagnosis is a dichotomous result which does not fully account for disease severity. Prognosis draws on the full range of relevant and available information to model the possible outcomes for an individual and is crucial to providing effective treatment based on individual requirements. Numerous biomarkers such as Procalcitonin (PCT), C-reactive protein (CRP), TNF-α, cfDNA, protein C and PAI 1 have been found to be useful, either by themselves or as a panel for improving the quality of prognosis. Currently, the most used technique for measurement of these biomarkers is an immunoassay using antibodies specific to that biomarker. However, the production of these antibodies is expensive, resulting in a high cost to run the assay. In addition, commercially available immunoassays require trained personnel and expensive equipment. As a result, the use of these biomarkers to improve the quality of patient prognosis has been limited. A recent study found that a panel of biomarkers that included cfDNA, protein C, platelet count, creatinine, Glasgow Coma Scale [GCS] score, and lactate had a high accuracy in predicting patient outcome. Of these, lactate and creatinine have commercially available techniques for bedside measurement. The development of devices for rapid and portable

measurement of protein C and cfDNA would enable the use of this panel for improving diagnostic care and providing a more accurate prognosis of sepsis patients.

The development of a device for low cost and rapid measurement of protein C was done in two stages. The first was the development of isoelectric trapping using a xurographic chip. Agarose gel was shown to be an alternative to current polyacrylamide-based gel separation techniques but with larger pore sizes that enabled faster migration of proteins. Slab gel-based methods are additionally limited by the total protein load that can be separated and the requirement for high voltages. Alternative solution-based separations such as cIEF and dIEF are faster but also use high voltages for separation and require complicated fabrication techniques which increases cost and reduces portability. The utility of a patterned xurographic substrate to shape the sizes of the reservoirs and gates was demonstrated by the focusing of the electric field in the gates to maintain an average electric field of 44 V/cm in the gates with an operating voltage of 15V. This enabled a reduction in the separation time to under 20 minutes while operating at a voltage that can be delivered using a portable apparatus. Tunability of the agarose gel by using commonly available buffers enabled the targeted separation of proteins from a mixture without the need for a specifically targeted dye that greatly reduces the cost of separation compared to currently available assays and was demonstrated by targeted separation of ovomucoid from egg white. Targeted separation is particularly challenging in the case where the components in a mixture span a wide range of concentrations and the targeted protein is at a significantly lower concentration than interfering components. Additional processing steps are currently used to reduce the protein load from the interfering proteins prior to separation which could be avoided using the combination of isoelectric gates and xurographic patterning developed in this device. This was demonstrated by separating protein C at a concentration of 1 - 5 µg/mL from a mixture with 5 mg/mL of BSA. The

development of a targeted separation technique without using a targeted tag would reduce costs compared to the currently used techniques which is necessary for the use of proteins as prognostic markers. The reduction in number of preparatory steps due to the elimination of preprocessing to remove interfering proteins would simplify workflow in testing and enable the use of the device with minimal training.

While the device presents numerous advantages to currently available techniques in the applications demonstrated, it is limited by the resolution of the isoelectric gates used and the complexity of the matrix. The highest resolution gates demonstrated have a pH gap of 0.4 units, as a result of which a matrix containing multiple proteins with an isoelectric point within 0.4 pH units of each other could not be separated. This was the case for the separation of protein C from other components in human plasma such as Alpha 1-proteinase inhibitor which has a similar pI but is present at a much higher concentration in plasma. This led to the development of a second stage of separation that used the affinity of protein C for Barium.

Immobilized metal affinity chromatography (IMAC) is a macroscale separation technique used to separate proteins with affinities to specific metals. It is traditionally used to bind to proteins that have Histidine groups that bind to copper, nickel, zinc or cobalt and Cysteine groups which show affinity to iron. Miniaturized IMAC has previously been demonstrated using frits that were photolithographically made to trap the metal ion selective beads in place. However, the use of photolithography increases the cost of each device which reduces its applicability for biomarker assays. A lower cost alternative was demonstrated by fabricating a miniaturized packed bead column that leverages the layered structure of a xurographic device to use a polyester membrane to hold the beads which were trapped in an agarose gel in place. The applicability of IMAC was

then extended from traditional metals such as copper, nickel, zinc or cobalt to Barium. Affinity to Barium is present only in proteins that contain a γ-carboxyglutamate (GLA) group and has previously been used to separate these proteins from plasma in multi-stepped macroscale techniques but not for IMAC separations. γ-carboxyglutamate group is only present in a few proteins in plasma - coagulation factors II (prothrombin), VII, IX, X, proteins C, S and Z in plasma. A combination of an isoelectric gate at a pH of 5 with Ba-IMAT was shown to be sufficient to separate protein C from the other proteins in plasma to a degree where the presence of 0 – 5 µg/mL of protein C spiked in plasma could be differentiated which was sufficient for the prognosis of sepsis using protein C. The demonstration of a microfluidic process with no preparatory steps to separate and measure the concentration of a -GLA domain protein in plasma using its affinity to Barium is a cost-effective method that can greatly aid in the prognosis of sepsis. Further, as the process can be tuned to target the other -GLA domain proteins by optimizing the characteristics of the device and the important role of the -GLA domain proteins in the coagulation cascade, the extension of this technique to the other proteins could prove to be a value source of prognostic information to understand the status of the coagulation cascade.

While the previously developed device is effective for the separation of -GLA domain protein biomarkers, the techniques used, and challenges faced in the measurement of DNA based biomarkers are different. cfDNA is currently measured using PCR UV absorbance, fluorescent spectrometry, quantitative PCR (qPCR) or digital PCR (dPCR) which are unsuitable for the prognosis of sepsis as they do not measure the total cfDNA content and are expensive, multi stepped processes that are designed for measuring cfDNA concentrations in the range of ng/mL or lower. What is needed for sepsis is the development of a portable device that can measure the total cfDNA content in the range of µg/mL with minimal cost and preparation.

The development of this device started with the development of a colorimetric thread based microfluidic device that could store specified amounts of a testing reagent in a dried form and aliquot the required volumes of the testing reagent/dye and the test sample in an automated manner. Storage of the testing reagent in the dried form enables easy transportation compared to liquid samples and eliminates the need for manual dispensing of the reagent simplifying the end use of the device. This was done by developing patterning methods that used a hydrophobic solution or wax to form discrete segments in the thread. The length of each thread segment was controlled and used to aliquot the volume of reagent exposed to the sample. As the reagent was dried on the thread, it could be rehydrated at the time of use simplifying and improving the reliability of the sensing reaction compared to manual dispensing of the reagent with traditional colorimetric tests. The patterned thread was integrated into an integrated PDMS-thread device that exposed individual sections of the patterned thread to a known volume of sample using the geometry of the PDMS device. This eliminated the need for complex external control of the sample volume further simplifying measurement compared to traditional methods that require external systems to aliquot specific quantities of sample into comparable devices. An imaging setup was developed that used a DSLR camera in an opaque acrylic box to control the lighting at the time of imaging. The resultant setup was prototyped by the measurement of nitrite concentration using the color change produced because of a controlled reaction between the automated aliquoting of volumes of reagent and sample. It was shown in a range of 0 – 5 mg/L which covers the maximum amount of allowable nitrite that ranges from 1mg/mL in the US to 3mg/mL by WHO and Health Canada. A similar setup was also shown to work for the measurement of pH in a range of 6 to 7.6.

The integrated PDMS-Thread device was then further miniaturized for the detection of cfDNA by integrating threads in a silicone tube and using the capillary action of the thread to aliquot the

sample. The control of volume using thread length that was developed in the previous format was further developed with control of volume using thread length and tpcm being used to automate aliquoting of the cfDNA sample. The PDMS device used in the previous device was miniaturized to a silicone tube and used to control the tpcm of the thread. This eliminated the need for an external pump and reduced the sample volume. The fluorescent dye (reagent) was pipetted at one end of the device and sample introduced at the other end was aliquoted by using a 1 cm device with a 6 tpcm thread. A portable fluorescence imaging setup was developed based on the colorimetric acrylic box that was previously used. The DSLR camera, light source and acrylic box that were used for the previous format was miniaturized using a raspberry pi camera paired with a 3D printed PLA box and a 470nm LED. The opaque exterior was 3D printed in two sections and a drawer used to introduce the sample into the imaging area to replace the opening of the acrylic box. Fluorescence filters and a dichroic mirror were assembled to form a filter cube. The resulting setup was then used for the detection of cfDNA in a range of 1 – 5.9 µg/mL in a buffer. The volume independence of the measured intensities was shown, and the device characterized by finding the minimum experimental time and lighting conditions. Finally, cfDNA was measured in buffered samples and in samples spiked in plasma to show that there was a measurable change in fluorescence intensity between samples with and without cfDNA.

In summary, devices for the detection of protein C and cfDNA in plasma were developed which could be used to improve the quality of patient prognosis as a part of a panel of biomarkers. In the process, technologies were developed for the rapid separation of proteins that either have a unique isoelectric point or specific affinity to metal ions. A combination of both was necessary for the measurement of protein C. With some modifications, these techniques could be extended for the measurement of other proteins in plasma as is detailed in the future directions. In the development

of a rapid measurement system for cfDNA, the use of a patterned thread for storage and aliquoting of reagents and samples was shown. Parameters for controlling fluid volume stored in threads were established. Threads integrated with silicone were shown to be an optimal solution for capillary driven aliquoting that eliminated the need for preprocessing steps and enabled single stepped measurement of cfDNA in plasma. Both systems were developed for fluorescence measurement using nonspecific dyes which enables future integration into a combined system. A portable fluorescence imaging and measurement setup was demonstrated for the measurement of cfDNA which could be further extended into an integrated system. These applications are described in further detail in the future directions.

Future directions

The tools developed in the thesis present low-cost alternatives for the measurement of cfDNA and protein C using nonspecific dyes through the development of microfluidic isoelectric trapping and Ba-IMAT for protein separation, the development of thread microfluidic devices for automated aliquoting and storage and a portable fluorescence imaging setup. However, the usage of these techniques for the prognosis of sepsis can be improved by integrating the detection of multiple biomarkers with a diverse range of concentrations and that are both protein and DNA based. This would improve patient prognosis as the use of a panel consisting of multiple biomarkers has a higher accuracy in patient prognosis than any individual biomarker. This integration is feasible despite the differences in currently available detection methods for proteins and DNA as all the techniques developed in this thesis for the detection of protein C and cfDNA use nonspecific fluorescence imaging which enables simultaneous labelling of both proteins and DNA. The

integration could be realized by first developing an integrated system for the measurement of both protein C and cfDNA by

1. Extending the fluorescence camera setup developed for cfDNA detection to protein detection. This could be done in a few different ways based on the choices made for the filters and the optical system. The filters could be used in one of two ways, one possibility is the use of specific excitation lenses and a dichroic mirror that would allow two different wavelength bands to pass through. However, the filters and dichroic mirror would be specific to the dyes used and it would be time consuming to switch to a different dye. However, the cost would be lower than comparable solutions. The second possibility would use transfer cubes that is an integrated set of filters that are prepackaged. This would be more expensive but is modular and could be rapidly changed over for different dyes. Using this, a device without additional optics could be used for measurement. However, the system would require constant changes of the transfer cube to match what is being sensed. In addition, the lighting would illuminate a single region of the device and the device would need to be moved to expose the different regions of the device that are used for trapping protein C and cfDNA. An alternative that would enable simultaneous detection of both at the same time in separate areas would use two cameras attached to a multi-cam adapter for raspberry pi. A beam splitter would be used for splitting a collimated light beam from the LED and made to interact with the positioned transfer cubes. The resulting device could then be extended to as many detection windows as necessary. However, this approach would be limited by the intensity of light emitted by the LED and optimization of the layout would need to be performed.

2. The sensing platform used for the detection of protein C and cfDNA would need to be integrated together. This could be done in two ways. Integrating the currently developed xurographic protein C measurement device with the thread-silicone device using external packaging which would be a low-cost and rapid solution. However, the inhomogeneity of the two methods used would result in a device that loses some of the advantages offered by each method. The portability of the thread-silicone device is reduced, the 2D plane of the xurographic device would need to be placed in a package with the cylindrical thread device which causes wasted space and increases cost of production. The integrated of electrodes for the xurographic device would be challenging. These issues could be overcome by developing isoelectric gating and IMAT on threads for protein separation. This would reduce the cost of production of the device due to the lower cost of production and larger range of materials available, enable the possibility of storing reagents on the thread and potentially increase the sensitivity of the detection as was found with cfDNA. Preliminary tests showed that it was possible to pattern agarose gels on thread in a format similar to wax patterning with a resolution of 2mm. The volume of fluid stored in a length of thread can be controlled by varying the tpcm and knotting the thread. Optimizing the characteristics necessary to repeatably obtain reservoirs that hold a volume of fluid separated by patterned agarose would form the basis for isoelectric trapping and Ba-IMAT. The current layered xurographic structure could be replaced by a 2-D plane of threads which would simplify integration with cfDNA detection. However, the complexity of thread geometry would make the electric field less predictable and would need to be studied in detail. The thread could then be packaged to allow access to the necessary portions of the device enabling integration with cfDNA detection on the same chip.

Although the main objective of the current thesis was to develop techniques for the detection of cfDNA and protein C to aid sepsis diagnosis, the protein separation techniques, improvements in thread microfluidic techniques and low cost imaging that were developed can also be used for the detection of other biomarkers and in other sensing applications. This can be done by

1. Enhancing isoelectric gating and/or miniaturized IMAT to increase the range of proteins for which the device could be used. This could in a few different ways. One method would be to increase the resolution of isoelectric gates from the current pH 0.4 resolution. Secondly, using a closed channel device through which the sample and buffers can be pumped would increase the pH stability of the gel gates and enable the accumulation of protein over a larger volume, improving the limit of detection of the device. This would be useful for the detection of biomarkers that are present in a range of ng/mL. Thirdly, extending the use of Ba-IMAT to other metal ions which would increase the types of protein biomarkers that could be detected using a miniaturized IMAT format.

2. The use of isoelectric gates for detection is most suitable for proteins that have a unique isoelectric point at which few other proteins are present. One such set of proteins that are present in plasma only under exceptional circumstances are histones. Histones are highly basic proteins around which DNA winds to create nucleosomes. They are released into the blood stream during cellular apoptosis and are co-produced alongside cfDNA fragments. Free histones in circulation mediate cellular damage, hemostatic imbalance, and amplification of the inflammatory response in sepsis patients. Histone H4 levels in sepsis patients was found to be elevated to 0.35 – 0.4 ng/mL depending on time since onset of sepsis in comparison to an ICU control with histone concentration of 0.05 – 0.07 ng/mL [1]. Current detection methods for histones are immunoassays, which are

expensive. Immobilized pH gradient (IPG) gels were found to react with histones and could not be used for separations, because of which their isoelectric points are not well established. Histones H1, H2A, H2B, H3, H4 have been reported to have isoelectric points of around 10.5, 10.5, 11, 11 and 11 respectively [2]. As the pI's of the histones are not well established, the precise isoelectric gates that would be used for separation of H4 histones from other histones and high mobility groups (HMG) needs to be found. Following that, the stability of the gels at a high pH would need to be studied and a closed channel device fabricated that could allow a constant flow of sample to enable measurement at the low LOD needed for the detection of histones. The buffering capacities of the sample, solutions and gating buffers would need to be optimized to ensure stability over the experimental duration. The electric field and flow rate of the sample and their effects on concentration would need to be characterized to ensure that a substantial fraction of the histones are trapped. Once optimized, the ability to characterize and measure histone concentration would help in the study of the progression of cell death in sepsis and improve the utility of histones as biomarkers.

3. Extending the use of the integrated isoelectric gating – Ba-IMAT device for the measurement of other proteins containing a GLA domain. One such protein that has a high utility in understanding the progression of diseases is Factor X. It is also a part of the coagulation cascade like protein C and its activated form Factor Xa, plays as essential role in activating prothrombin to form thrombin. It is a procoagulant biomarker, and the measurement of factor X would be helpful in measuring the state of the coagulation cascade in the presence of infection. As the affinity of factor X to barium is similar to protein C, but at a higher isoelectric point of 4.9-5.2, it can be measured using the proposed two stage device with isoelectric trapping and Ba-IMAT. The isoelectric gate pH and pH of the buffer used would need to be optimized. In addition, preparatory

steps may be necessary to minimize albumin content in the sample due to the overlapping pI and resulting large nonspecific binding. However, as the concentration range is similar, the current format of the device can be used.

4. Expanding the use of fluid control using tpcm (threads-per-centimetre) for the development of multi reagent assays with threads of different diameters and tpcm's to mediate fluid intake from each thread. This would reduce the cost and improve the portability of traditional assays. Using thread as a solid-state medium for storage, transport and aliquoting would solve many of the issues faced by current colorimetric and fluorescence measurement system when transitioning to working in places with minimal infrastructural support.

The technologies developed in this thesis are aimed at improving the prognosis of sepsis through the development of low-cost detection methods for protein C and cfDNA. In the course of this, the techniques developed, and improvements made have a wide range of potential applications which can be explored over time.